THE ART AND SCIENCE IN MODELING THE PRESSURE-VELOCITY INTERACTIONS

A Dissertation

by

AASHWIN ANANDA MISHRA

Submitted to the Office of Graduate and Professional Studies of
Texas A&M University
in partial fulfillment of the requirements for the degree of

DOCTOR OF PHILOSOPHY

Chair of Committee,	Sharath Girimaji
Committee Members,	William Saric
	Suman Chakravorty
	Zenon Medina-Cetina
Head of Department,	Rodney Bowersox

August 2014

Major Subject: Aerospace Engineering

ABSTRACT

The objective of this investigation is to develop a single point model for the global effects of pressure in turbulence, while striking a judicious balance between mathematical rigor and empiricism. In this vein, we perform a linear stability analysis of planar quadratic flows to isolate and identify the action of pressure herein. This leads to the identification of the statistically most likely behavior engendered by modal ensembles. Thence, we develop a framework to augment the classical realizability constraints. Herein, we ensure that not only is the statistical state physically permissible, but the stochastic process is realizable as well. These process realizability conditions are applied a posteriori, to evaluate the dynamics predicted by established models and a priori, to develop illustrative models that maximize realizability adherence. This serves to identify the range of possible dynamics of the system. Thence, a set of studied compromises are introduced in the scope and framework of the classical modeling procedure to develop a modeling framework that ensures a high degree of fidelity along with adherence to process realizability. An illustrative model using this paradigm is constructed and its predictions are compared against numerical and experimental data, while being contrasted against established closures. The robustness of the linear analysis is tested via stochastic modeling using a Langevin equation based model. Finally, to extend this paradigm to all homogeneous flows, we carry out a linear stability analysis of general three-dimensional homogeneous flows.

TABLE OF CONTENTS

Page

LIST OF FIGURES

LIST OF TABLES

1. INTRODUCTION

The flow of fluids represents the driving physics in a multitude of occurrences all round us. These range from flows over aircraft and inside turbomachinery, atmospheric flows for weather prediction and through the heart for cardiac auscultation, from biological cases such as the flow of plasma inside a cell to galactic instances such as the Giant Red Spot over Jupiter. It is a fact that most such flows of scientific and engineering interest are turbulent. As stated in Moin and Kim (1997) “turbulence is the rule, not the exception in fluid dynamics". In this regard, the phenomenon of turbulence is omnipresent around us, as is suggested in figure 1.1.

The modern appellation of “turbulence" is derived from the Latin term *turbulentia* used in the Middle Ages colloquially, to mean “trouble". In its scientific incarnation, this term refers to a particular complex, unpredictable motion of fluids. In lieu of a definition, we state that turbulence is the manifestation of the spatio-temporal chaotic behavior of certain fluid flows at large values of destabilizing parameters. However, a categorical and unequivocal definition of this phenomenon is neither extant nor accepted. Rather, this phenomenon is defined by certain characteristics common to turbulent flows. These include, for instance,

1. Irregularity and randomness: Turbulent flows are irregular and chaotic. This complexity is present, both as erratic patterns in space and irregular fluctuations in time.

2. Unpredictability: The chaotic nature of turbulence, leads to a loss of predictability, wherein nearly identical flows soon evolve to become unrecognizably different.

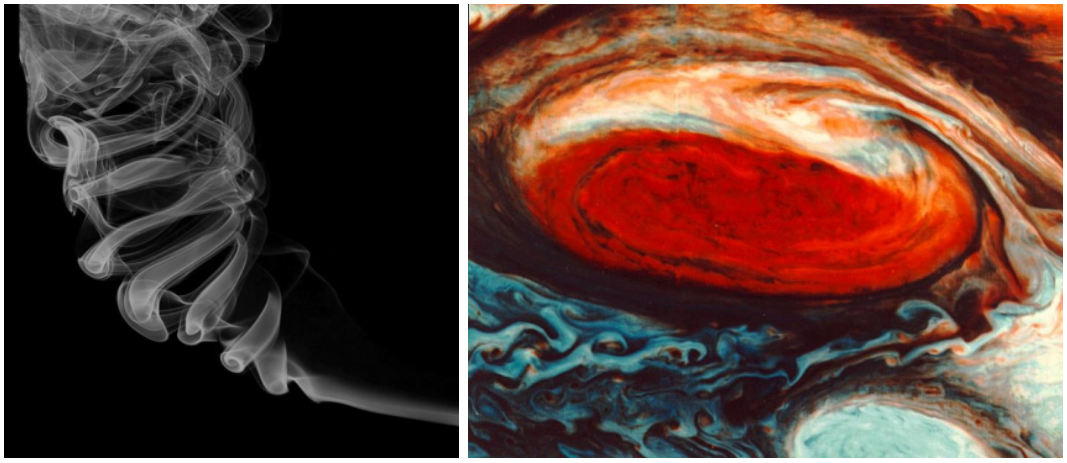

Figure 1.1: Diverse manifestations of turbulence. (a)a rising plume of smoke, (b)the Giant Red Spot on the surface of Jupiter.

3. Diffusivity: The most important aspect of turbulence as far as applications are concerned is its associated strong mixing and high rates of momentum, heat and mass transfer.

4. Dissipation: In a turbulent flow, the energy of the fluid motion is rapidly dissipated. If no energy is supplied turbulence will decay rapidly. It needs to acquire energy from its environment.

Having addressed the pertinent questions regarding the nature of turbulence and its relevance, we discuss its importance. Turbulence represents a central problem in diverse and manifold disciplines such as engineering, biomedical sciences, astrophysics, mathematics, geophysics, ad infinitum. A thorough understanding of the properties of turbulence is expected to lead to important advances in all these fields. For instance, the turbulent flow of blood in the human heart causes sclerosis leading to cardiovascular complications such as strokes and heart attacks. A resolution of the problem of turbulence would enable the Biomedical community to understand, treat and cure such disorders associated with malfunctioning heart valves. In Mete-

orology, improved prediction of turbulence occurring in the atmosphere and oceans would lead to superior forecasts of the weather and of climate change. Recently, it has been proposed that turbulence during the early stages following the Big Bang is responsible for the present form of the Universe. In this regard, an improved understanding of the phenomenon of turbulence would lead to answers involving the question of life, the universe and everything. In this vein, Richard Feynman had described turbulence as “the most important unsolved problem of classical physics". A resolution of the question of turbulence would be a momentous development in the state of human knowledge. However, in spite of over a century of focused research, no such resolution exists. The key hurdles in this are:

1. Nonlinearity: The mathematical equations governing the evolution of turbulence are nonlinear. This nonlinearity is ultimately responsible for the chaotic nature of turbulence. Additionally, the multiplicative character of this nonlineaity with respect to the velocity field leads to the so called Closure Problem in statistical approaches to turbulence.

2. Nonlocality: This addresses the presence of the long-rage interactions in turbulence, embodied in the pressure term in the governing equations. Thus, the velocity at any one point in the flow is affected by the dynamics at all other points in the domain.

In addition to these two major impediments, there are other complications such as the nonintegrability of the equations, the manifestation of intermittency, etc that further aggravate this difficulty. Thus, in spite of the focused analysis, at present there is no analytical theory explaining turbulence. Furthermore, with the present state of computational resources, a purely numerical resolution of the turbulent flows encountered in engineering problems is not viable in the near future. Consequently,

Figure 1.2: Depiction of a turbulent flow in the artwork of Leonardo Da Vinci. The different scales of motion can be correlated to the brushstrokes in the depiction, wherein the large scales have long strokes and the smaller scales have short strokes.

at present all engineering recourses to turbulence involve some degree of modeling.

In this context, the fundamental challenge to such modeling attempts lies in the inherent nature of turbulence itself. A turbulent flow can be envisaged as an amalgamation of "method" and "madness", as is suggested in the depiction in figure 1.2. Herein, the sobriquet method, refers to the large scale structures in a turbulent flow. These are highly dependent on the details of the specific flow under consideration. These structures are not amenable to modeling and should, ideally, be resolved via explicit computation. On the other hand, we have the epithet madness, referring to the small scale structures in the turbulent flow. These are apparently random and chaotic, ergo, the moniker. In spite of the appearance of complexity, these can be modeled, judiciously. A computational procedure must take both these facets into account.

The classical engineering approaches to turbulence can be broadly classified into three groups, viz.

1. Reynolds Averaged Navier Stokes models;

2. Spectral closures and multi-point models;

3. Large Eddy Simulations.

Reynolds proposed an averaging method wherein the turbulent field is decomposed into a mean and a fluctuating part. On the application of this decomposition to the governing equations, we get the Reynolds Averaged Navier Stokes equations. Models derived from this equation, attempt to predict the single-point statistics of turbulent flows up till the second order. Such RANS models include popular nominations like the mixing-length model of Prandtl and the $k - \epsilon$ model. On the other hand, multi-point models such as the Direct Interaction Approximation of Kraichnan, are statistical recourses that still subscribe to the concepts of ensemble averaging and the Reynolds decomposition. In this regard, they may be considered as advanced RANS models. However, most closures of this variety are akin to theories of turbulence. Based on some reasonable assumptions, these engender self-consistent systems that are bereft of any parameters or constants that might require empirical determination. Large Eddy Simulations involve the explicit computation for the large, energy containing scales of turbulence and utilize sub-grid-scale models to account for the dynamics of the smaller scales of motion.

Each of these methods has its respective advantages and disadvantages, along with the proponents and doubters. Due to the disparate character of turbulent flows, predictive methods must be robust, so as to be easily applicable for most of these cases, yet possessing a high degree of accuracy in each. Furthermore, as the

processes of analysis and design involve repeated iterations, the predictive method must be computationally economical. Thus, the broad criteria of evaluation can be codified as:

1. robustness of application and predictive fidelity;
2. computational costs;
3. simplicity and tractability.

Analysis of turbulent flows in inherently problematic, primarily due to two reasons:

1. the multi-scale nature of turbulent flows, arising due to the non-linearity therein;
2. the non-locality of the turbulence phenomenon, engendered by the action of pressure.

Considering the energy spectrum of turbulence, exhibited in figure 1.3, it is observed that the larger scales of motion are dominated by the linear interactions and the smaller scales are dominated by the non-linear physics. In this vein, turbulence can be described as an amalgamation of "method" (referring to the linear dynamics of the larger scales) and "madness" (referring to the chaotic dynamics of the smaller scales). Approaches such as Direct Numerical Simulation (DNS) and Large Eddy Simulation (LES) are computationally intensive. For instance, as shown in the figure, DNS attempts to compute for and resolve all the scales of turbulence. LES takes a more conservative recourse, wherein the larger scales of turbulence are explicitly computed, while the smaller scales are modeled. However, with the present state of computational resources, these are limited to very simple turbulent flows.

Spectral approaches have the potential to account for the nonlinear and, more importantly, the non-local nature of turbulence. For homogeneous turbulent flows, these

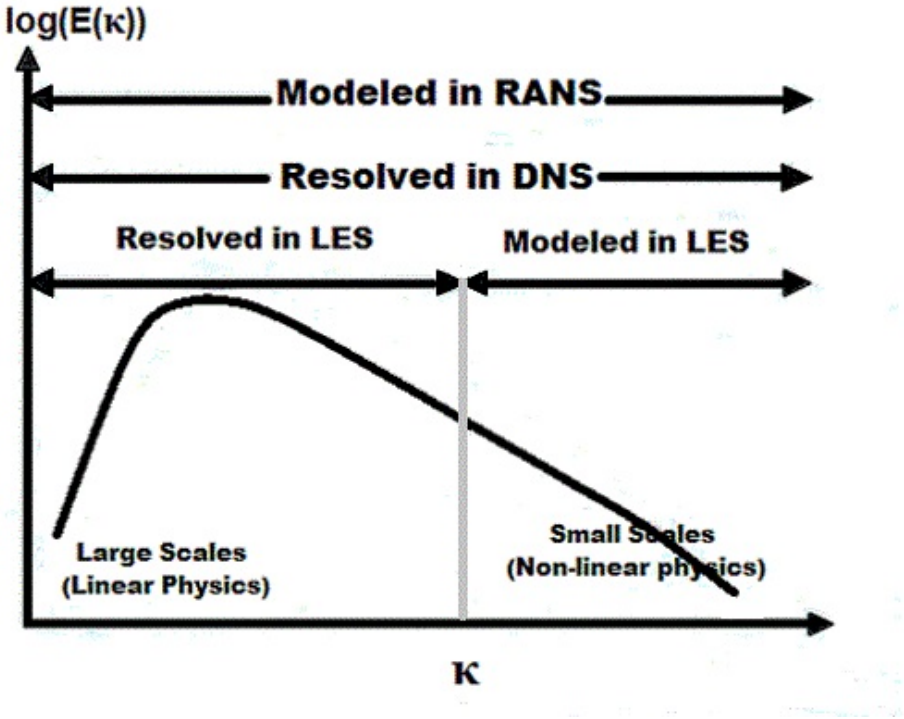

Figure 1.3: The energy spectrum of turbulence with the dominant physics therein.

have been successful in their applications to some cases. However, their extension to general problems, especially to inhomogeneous flows, represents an overwhelming hurdle. Most cases of engineering interest involve complex flows with inhomogeneity, solid boundaries and complex geometries. Thus, the robustness of this approach is very limited.

Reynolds stress models are based on the Reynolds Averaged Navier-Stokes equations and are referred to as the RANS methods. These can be broadly divided into two categories:

1. one-, or two-equation models that resort to the concept of turbulent or eddy-viscosity to provide a simple closure;

2. Second Moment Closure based models, based on the Reynolds Stress Transport

equation, that can obtain, for instance, the turbulent stresses by solving closed forms of the exact Reynolds stress equations.

Herein, Eddy-Viscosity Models (EVMs) represent the approach with the lowest computational needs. Additionally, the invocation of the eddy-viscosity hypothesis makes them relatively simple. Thus, such models, especially the two-equation models, are the norm in Computational Fluid Dynamics applications in the industry. Commercial CFD software apply such approaches to a variety of problems with high degrees of complexity, often with dubitable accuracy. While such simple relationships between the mean rate of strain and the turbulent stresses are often adequate for two-dimensional, quasi-parallel flows; in flows with streamline curvature, recirculation, impinging and three-dimensionality, these austere analogies are insufficient and more importantly, inaccurate. In the last few years, there has been a perceptible shift in modeling research, from Reynolds Averaged Navier-Stokes equations to the LES recourse. This approach proffers a significantly more detailed amount of information than the RANS paradigm and LES can potentially tackle turbulence problems beyond the other approaches. It is evident that RANS based approaches are unable to resolve the structures in a turbulent flow. However, one of the major reasons motivating this shift has been the shortcomings of the eddy viscosity based approaches.

Considering a single point closure, to overcome the shortcomings of the eddy-viscosity approach, it is completely unnecessary to resort to a method as computationally expensive as LES. Instead of applying an algebraic relationship linking stress and strain, the Reynolds stresses (and other such fluxes) can be obtained by explicit solution of closed forms of the Reynolds Stress Transport equations. This method, that seeks to close the RST equations at the level of the second moment, is aptly re-

ferred to as Second Moment Closure. Herein, the effects of the body forces, the strain field and the convective transport on the Reynolds stresses manifest explicitly in the second-moment equations. Thus, the Second Moment Closure recourse can account for these complex effects naturally, and much better than eddy-viscosity models. Additionally, the second moment level enables and aids both analysis and modeling by actualizing compliance with limiting states of turbulence. In this light, effects such as streamline curvature, swirl and recirculation, insurmountable for EVMs, are within the scope of SMC approach, in principle. The computational demands of such a scheme are typically twice that of a corresponding eddy-viscosity model. This is a small investment to ensure that the model can be applied in complex flows of engineering interest. Moreover, the computational cost of this approach is usually a few orders of magnitude less than that of the application of LES to the same scenario. For flows with large coherent structures, approaches like LES are the only recourse. However, in the context of simulation of many flows of engineering interest, single point closures are more practical and remain the norm in industrial applications.

Thus, it is argued that Second Moment Closures are tailored for many practical applications, providing a considerably higher degree of physical fidelity than two-equation closures, at a computational expense substantially lesser than those of Large Eddy Simulation. However, Second Moment Closure based approaches are not as widespread as other recourses. It has been suggested that this is because in spite of all its potential, the second moment recourse is not able to deliver upon its promises. For instance, in theory the Second Moment Closure approach is better than two-equation models as it can account for the effects of streamline curvature. However, none of the available models adhering to this paradigm are able to provide accurate predictions for closed streamline flows. Thus, there is a chasm between the capabilities of the Second Moment Closure approach and the abilities of the models

subscribing to this framework. The extant Second Moment Closure models have met with limited and qualified success. There are many important regimes of flows, wherein their performance is unsatisfactory. Two primary examples of flows where prevalent one-point closures perform inadequately are elliptic flows and, to a lesser extent, flows subject to strong system rotation. For elliptic stream-line flows, the predicted behavior is, even qualitatively, contrary to observed behavior, as exhibited in the Direct Numerical Simulations of Blaisdell and Shariff (1996). For instance, while the DNS results indicate the exponential growth of turbulent kinetic energy, the models predict that the state of turbulence decays.

This investigation seeks to address this chasm by charting a novel modeling paradigm that is precise and yet, pragmatic. In our opinion, some of the established models are quiet empirical and hence valid only over flows in which they have been calibrated. In addition to conforming to science, turbulence modeling has an artistic facet as well. As stated by Dr. Box, "All models are wrong, some are useful." In the absence of a singleton universally correct solution, different investigators espouse different approaches to the problem. The lack of any existence or uniqueness theorems engenders creative solutions to the problems therein. In this light, empiricism is an important aspect of this process, but should be minimized. The methodology developed in this investigation aims to do thus by focusing on resolving the inherent schism between the demands obligated by physics and mathematics, and the limitations of the framework.

Herein, we address one of the key hurdles in modeling under the SMC approach, that of representing the global dynamics of pressure in a local closure. The cardinal issues forestalling a better understanding of the turbulence phenomenon are the non-linearity of the inertial cascade physics and the non-local nature of the action of pressure (Tsinober 2009). In this regard, the "pressure-released" Burgers turbulence

embodies much of the non-linear character of turbulence but has been understood better (Sagaut and Cambon 2008), in contrast to its Navier-Stokes analogue. Consequently, the action of pressure may be the key challenge toward understanding turbulent flows and their subsequent closure modeling.

The Second Moment Closure methodology is based on the Reynolds Stress Transport (RST) equations:

$$\begin{aligned}
\frac{dR_{ij}}{dt} &= P_{ij} - \frac{\partial}{\partial x_k} T_{ijk} + \pi_{ij} - \epsilon_{ij}, \\
\text{where, } R_{ij} &= \sum_{\kappa} \langle u_i u_j \rangle, \\
\pi_{ij} &= \left\langle p(\frac{\partial u_i}{\partial x_j} + \frac{\partial u_j}{\partial x_i}) \right\rangle, \\
\epsilon_{ij} &= -2\nu \left\langle \frac{\partial u_i}{\partial x_k} \frac{\partial u_j}{\partial x_k} \right\rangle, \\
\text{and } P_{ij} &= -R_{jk} \frac{\partial U_i}{\partial x_k} - R_{ik} \frac{\partial U_j}{\partial x_k}.
\end{aligned} \tag{1.1}$$

The terms are arranged in groups, representing turbulent processes. Of these expressions, only the production term is closed, at the second moment level and the other terms require closure modeling. Amongst these unclosed terms, the pressure strain correlation is accepted to be the most important. At the level of the second moment, the state of turbulence is best characterized by the turbulent kinetic energy. If we analyze the evolution of the turbulent kinetic energy over a domain, the relative import of the terms comes into sharp focus. The transport term just moves energy from a spatial location to another. In the same vein, the viscous term is fairly universal in its behavior as a sink for the turbulent kinetic energy. The pressure strain correlation can have radically divergent behavior dependent on the flow regime and the initial conditions. Besides the trend of this behavior, the magnitude of the pressure effects is large enough to change the evolution of turbulence completely. Pressure

is an inherently global variable. To model it in a single-point engineering model, we have to attempt to express its global dynamics in terms of local variables. In addition to its importance, this encumbrance makes pressure strain correlation modeling a continued challenge. Linear versus nonlinear dynamics: Based on the Poisson equation governing fluctuating pressure in the incompressible flow case, pressure can be decomposed into a linear (rapid) and a non-linear (slow) part. The rapid terms refer to interaction between the mean and the fluctuating fields, and the slow terms refer to the interactions amongst the fluctuating components. Turbulence is often viewed as a sum of linear and nonlinear effects, "method" and "madness" in layperson terms. An undue modicum of import is attributed to the nonlinear dynamics in turbulence. However, in the statistical modeling recourse, it is the linear terms that are more difficult to model. In a statistical sense, the dynamics of the nonlinear terms is universal and predictable. Irrespective of the regime of flow, the slow pressure terms attempt to return the state of turbulence to an isotropic state. In this vein, bridging models have tried to model the effects of the nonlinear terms with via a white noise term and have achieved reasonable success therein. On the other hand, the effects of the linear terms are strongly dependent on the regime of mean flow and on the detailed initial conditions of the fluctuating flow field. Dependent on the regime of flow, the rapid pressure effects might stabilize the flow or destabilize it (or even do both, albeit over a cycle). In doing so, these effects can cause the decay or the growth of turbulence, dependent on the flow regime. For instance, in planar open streamline flows, rapid pressure effects mitigate the hyperbolic flow instability. However, in a planar closed streamline flow, the same terms engender the elliptic flow instability. (The dynamics of the nonlinear pressure terms is the same for both these flows, vide return to isotropy.)

At this juncture, we have established the importance of the linear pressure dy-

namics and the challenge in their modeling. Models for the pressure strain correlation should adhere to the dynamics engendered by these terms, wherever applicable. Extant nominations for the pressure strain correlation have had limited success in conforming to the behavior predicated by the linear theory, even for the simplified case of planar flows. Objectives: One of the key objectives of this research is to attempt better agreement between linear theory and pressure strain correlation models. This entails understanding the governing dynamics underlying linear physics and, at the same time, recognizing the limitations of the extant modeling framework. This research attempts to resolve the schism between the guidelines of linear theory and the inherent limitations of closure models, with a satisfactory measure of engineering utility. This is achieved by incorporating a set of studied and deliberate compromises in the structure and scope of current models. In addition to predictive fidelity, another obligation enjoined upon models is that of realizability. Herein, the predictions of the model are constrained so as to yield a Reynolds stress tensor that is positive semi-definite. However, the classical approach to realizability, in spite of its great utility, is insufficient. In this work, the realizability condition for statistical models of turbulence is enhanced and reformulated to ensure not only that the Reynolds stress tensor is positive semi-definite, but the process of its evolution is physically attainable as well. This has manifold advantages that are exhibited and discussed. This investigation consists of five sequential and systematic individual investigations. These constitute the succeeding chapters of this thesis. After an introduction in Chapter I, we address the linear physics that the model has to reproduce, for planar quadratic flows, in Chapter II. Herein one of the key phenomena to be analyzed is the Intercomponent Energy Transfer induced by pressure. This action of pressure is inherently non-local and consequently, its modeling must address multi-point physics. Yet, in Second Moment Closures, pragmatism mandates a single-point closure model for the

pressure-strain correlation that is the source of IET. We characterize the dynamics and dependence of IET and this characterization is used to examine the validity and limitations of current one point closures and propose directions for improving the fidelity of future models. Additionally, in light of this investigation into linear stability, the limitations of the single point modeling paradigm are discussed and analyzed. Chapter III develops the process realizability framework that ensures that the predicted Reynolds stress dynamics are physically permissible. Thus, the realizability condition for statistical models of turbulence is augmented to ensure not only that the Reynolds stress tensor is positive semi-definite, but the process of its evolution is physically attainable as well. The mathematical constraints due to this process realizability requirement on rapid pressure strain correlation are derived. The resulting constraints reveal important limits in the IET and the consequent flow stability characteristics as a function of the mean flow. These are applied to established models and thence, a methodology to ensure optimal process realizability adherence is outlined. Chapter IV heeds the limitations outlined earlier, along with the process realizability constraints to develop a modeling methodology. Herein, we outline a detailed recourse toward formulating a pressure strain correlation model that possesses improved agreement within the purview of single point closures. Thence, this framework is utilized to formulate an illustrative model. The predictions of this model are compared to numerical and experimental data while being contrasted against other popular modeling paradigms. Finally, as a caveat emptor, the zones of applicability of this model are clearly delineated for different mean flows.

At this juncture, in Chapter V, we investigate the robustness of the phenomena engendered by linear physics, in the presence of non-linear effects. To this end, a Langevin equation based model is utilized in lieu of DNS simulations. Having developed a satisfactory model for planar flows, in Chapter VI, we investigate the

linear stability of general three-dimensional flows. This serves as a precursor for an attempt to extend the methodology, developed earlier, to all homogeneous turbulent flows. The respective chapters along with their succinct outlines are introduced henceforth, followed by the body of the work.

2. INTERCOMPONENT ENERGY TRANSFER IN INCOMPRESSIBLE HOMOGENEOUS TURBULENCE*

2.1 Overview

Intercomponent Energy Transfer (IET) is a direct consequence of the incompressibility-preserving action of pressure. This action of pressure is inherently non-local and consequently, its modeling must address multi-point physics. Yet, in Second Moment Closures, pragmatism mandates a single-point closure model for the pressure-strain correlation, that is the source of IET. In this study, we perform a rapid distortion analysis to demonstrate that for a given mean-flow gradient, IET is strongly fluctuation-mode dependent and critically influences the flow stability, asymptotic states and their bifurcations. The inference is that multi-point physics must be characterized and appropriately incorporated into pressure-strain correlation closures. To this end, we analyze and categorize various multi-point characteristics such as: (i) the fluctuation mode wavevector dynamics, (ii) the spectral space topology of dominant modes, and (iii) the range of IET behavior and statistically most likely outcomes. Thence, this characterization is used to examine the validity and limitations of current one-point closures and propose directions for improving the fidelity of future models.

2.2 Introduction

The cardinal issues forestalling a better understanding of the turbulence phenomenon are the *non-linearity* of the inertial cascade physics and the *non-local* na-

*Reprinted with permission from Mishra, Aashwin A., and Sharath S. Girimaji. "Intercomponent energy transfer in incompressible homogeneous turbulence: multi-point physics and amenability to one-point closures." Journal of Fluid Mechanics 731 (2013): 639-681. Copyright [2013] by Cambridge University Press.

ture of the action of pressure (Tsinober, 2009). In this regard, the "pressure-released" Burgers turbulence embodies much of the non-linear character of turbulence but has been understood better (Sagaut & Cambon, 2008), in contrast to its Navier-Stokes analogue. Consequently, the action of pressure may be the key toward understanding turbulent flows and their subsequent closure modeling. In incompressible flows, the role of pressure is the enforcement of the continuity condition. To achieve this, pressure reorients the fluctuating velocity vector field leading to a redistribution of the turbulent kinetic energy amongst the spatial components. This process is referred to as Intercomponent Energy Transfer (IET). Thus, IET is the *action* of pressure through which it fulfills its *role* of maintaining continuity. To preserve incompressibility, pressure responds instantaneously to any changes in the entire velocity field. The global nature of the action of pressure is reflected in the fact that it is governed by a Poisson equation. This multi-point character is evident in a spectral representation. In the Fourier space representation, the fluctuating velocity field is expressed in terms of different modes, each characterized by a wavenumber vector and a velocity amplitude vector. The role of pressure is to maintain orthogonality between the wavenumber and amplitude vectors, so as to impose the divergence-free constraint. Clearly, this action is strongly dependent on the wavenumber vector dynamics. However, information regarding the wavenumber vector requires a multi-point description in physical space.

It is reasonable to categorize pressure effects into linear (rapid) and non-linear (slow) components. Herein, it is generally accepted that the role of slow pressure is to isotropize the velocity fluctuations. While the precise manner of return-to-isotropy is still under some debate, the general isotropizing action is established. Much of the complexity of the pressure action can be attributed to the rapid component of pressure. Under the aegis of the Rapid Distortion Theory (RDT), the action of

the rapid pressure component can be isolated from its slow counterpart. In this vein, Salhi *et al.* (1997) have pointed out the analogy between analyses based on RDT and *linear* hydrodynamic stability. Additionally, there is strong evidence that closure models consistent with linear stability theory are better equipped to capture the physics of a wide range of turbulent flows (Speziale *et al.*, 1990, 1996). In conclusion, the IET mechanism incumbent in RDT represents important physics that must be appropriately included in pressure-strain correlation models. Brasseur & Lee (1987, 1988) have studied the IET phenomenon in physical space in particular regimes of homogeneous, sheared flows. Perot & Moin (1995) have examined this phenomenon to investigate near wall turbulence. Prior studies of IET have had a predilection to investigate its importance with respect to the coherent structures in the flow. However, in this investigation, we analyze the IET mechanism with an emphasis on its multi-point characteristics and the subsequent implications to turbulence modeling.

2.2.1 Multi-point closure approaches

Multi-point closures potentially possess the means to capture the linear facets of the non-local features of turbulence. Such approaches account for the continuum of turbulent scales and are conceivably capable of adequate description of the action of pressure. Consequently, they capture the non-local nature of the turbulent flow and require closures only for the non-linear aspects thereof. Some notable approaches of this type would include the Direct Interaction Approximation (Kraichnan, 1959), the Eddy-Damped Quasi-Normal Markovian (Orszag, 1970) and the Test Field Model (Kraichnan, 1971). These were developed for the simplified case of homogeneous, isotropic turbulence. The effort to extend these to anisotropic and inhomogeneous turbulent flows is an ongoing line of research. However at present, multi-point clo-

sures are not well developed and validated for general turbulent flows. Accordingly, their use is not viable in practical computations, owing to their excessive computational burden.

A different multi-point closure paradigm is the Turbulence Structure-Based modeling framework of Reynolds and co-workers (Kassinos & Reynolds, 1994). The key element motivating this approach is the discernment between the *componentiality* and the *dimensionality* of turbulence. The one-point statistic of the Reynolds stresses, when expressed in spectral space, is the sum of the contributions of turbulent structures of different sizes and alignments. Thus, the same Reynolds stress tensor can be decomposed in a multitude of different ways in Fourier space, giving disparate spectral tensors, corresponding to different internal structuring of the turbulent flow. Consequently, an expression of the turbulent flow in terms of the Reynolds stresses only, gives information about the componentiality of the flow, but provides no insight about its internal structure. In an attempt to incorporate this missing information into the modeling framework, the Turbulence Structure-Based framework introduces additional tensors, such as Stropholysis, Circulicity, etc, into the modeling basis (Kassinos *et al.*, 2001). These tensors and the concomitant information is subsumed into the formalism of Cambon and co-investigators, wherein the anisotropy is divided into distinct contributions: isotropic, directional and polarization anisotropy (Sagaut & Cambon, 2008).

2.2.2 One-point closure approaches

Single-point closures generally omit non-local physics in favor of closure simplicity and computational viability. The level of incumbent physics strongly depends upon the specific one-point approach. The Second Moment Closure (SMC) recourse represents the lowest-level of closure in which the IET effects can be explicitly incor-

porated into the model. IET manifests itself through the pressure-strain correlation in SMC and its closure has long been identified as a major weakness in current modeling practice. Two primary examples of flows where prevalent one-point closures perform inadequately are elliptic flows and, to a lesser extent, flows subject to strong system rotation. For elliptic streamline flows, the predicted behavior is, even qualitatively, contrary to observed behavior, as exhibited in the Direct Numerical Simulations of Blaisdell & Shariff (1996). For instance, while the DNS results indicate the exponential growth of turbulent kinetic energy, the models predict that the state of turbulence decays. Consequently, the models are unable to reproduce the elliptic flow instability appropriately. In this vein, independent investigations such as Cambon (1990) and Speziale *et al.* (1996) have highlighted the inability of single-point closures to replicate the action of fluctuating pressure. In separate investigations, Jacquin *et al.* (1990) and Cambon & Jacquin (1989) have pointed out that rotating turbulence can be described much better in terms of multi-point closures. Pressure-strain correlation, in particular, and one-point closures, in general, represent ill-posed mathematical problems as the closures crucially depend upon inaccessible multi-point details of the flow field. The very simplicity that makes one-point closures useful also renders them too elementary to capture IET physics in a variety of important flows.

Thus, there is a clear impasse between different modeling approaches. Multi-point approaches that can resolve the non-local dynamics in turbulence, are computationally expensive and not robust. Single-point approaches while both robust and computationally feasible, are unable to capture the non-local phenomena manifested in turbulence. To resolve this schism, many investigations have attempted to *use the conclusions from multi-point theories to develop better single-point models.* In Godeferd *et al.* (2001), strategies for such an approach were outlined and discussed.

Additionally, newer models seek to conform with the predictions of the Rapid Distortion Theory, where applicable, as evidenced in the works of Johansson & Hallback (1994) and Mishra & Girimaji (2010). A notable example in this context is Cambon *et al.* (1992), who tried to use the information from spectral investigations to develop better closures in physical space, for rotating flows. Our investigation adheres to this paradigm. The multi-point theory of RDT is used to develop a better understanding of the system. Thence, this understanding is used to assess the capabilities of single-point closures.

In this article, we investigate the IET physics in two-dimensional homogeneous turbulent fields. These flows encompass many of the phenomena observed in redistribution physics. Furthermore, they represent benchmark cases wherein new nominations for pressure strain closures are tested and validated. Termed as planar quadratic flows (Salhi *et al.*, 1997), these flows exhibit a universal mechanism for the transfer of energy from the large scales to small scales in a turbulent flow (Pierrehumbert, 1986). For such flows, arbitrary small three-dimensional perturbations can be created by an instability of the basic two-dimensional flow. Pierrehumbert (1986) has suggested this as a mechanism for the cascade process in turbulent flows. The interested reader is referred to Pierrehumbert (1986) and Bayly (1986) for details of the mechanism and to Malkus (1989) for an experimental realization of the same. This mechanism is significant due to its role in the transition of turbulence in free-shear layers, wall-bounded shear flows, the formation of Kelvin-Helmholtz billows, etc.

2.2.3 Objectives and investigations

The objective of the present work is to investigate the multi-point characteristics of IET for the purpose of

1. establishing the scope of validity and limitations of present one-point closures;

2. examining avenues for incorporating multi-point physics into one-point closures;

3. initiating the development of a framework for uncertainty estimation in closure models.

In a Fourier decomposition of the flow field, the flow is represented via a set of wavevectors and a velocity field associated with each wavevector. Information regarding the wavevector set is inherently non-local and is not in the purview of single-point closures. As a recourse, one-point closures attempt to represent the behavior of this unknown wavevector ensemble via the evolution of a single hypothetical mode. We attempt to establish the critical characteristic features of this dynamical system and identify the statistically most likely behavior. Such a characterization would be critical for modeling, as the modeling procedure would simplify to identifying the modal alignment that replicates the dynamics of the ensemble of wavevectors. Identifying such *universal behavior* entails an analysis of the invariant sets of the wavevector (i.e. attractors, saddle nodes, limit cycles, etc) and their evolution (i.e. bifurcations, etc) along the lines of the theory of dynamical systems. Thence, we attempt to identify the dominant (most-energetic) modes. The identification of such modes would be propitious. Instead of attempting to capture the dynamics of the entire ensemble, the model can focus on replicating the behavior of this smaller set. This phase of the analysis is along the lines of hydrodynamic stability, where the focus is on the most unstable modes. Furthermore, we attempt to identify the most-likely behavior arising from this ensemble, with respect to the IET. We identify this as the statistically most likely behavior. In summation, the specific tasks undertaken in this study are:

1. to demonstrate the critical role played by IET in determining the stability of perturbation modes;

2. to establish the wavevector dynamics, specifically the fixed point behavior and the bifurcations in the system are clearly demonstrated as a function of mean velocity gradient invariants;

3. to characterize the IET for different mean velocity gradients, as a function of wavevector orientation;

4. to identify the topology of the most energetic wavevector modes for each flow regime;

5. to determine the statistically most likely (SML) IET behavior for each mean velocity-gradient and further establish the range of possible behaviors.

In light of these analyses, the article is arranged thus. The Kelvin-Moffat set of RDT equations are derived and discussed in Section II. Section III presents a preliminary examination of the contrasting IET influence on the linear stability of open and closed stream-lined flows. Building upon this, Section IV presents a more detailed RDT analysis of various features of IET: modal analysis, stability, fixed-point behavior and statistically most likely behavior. A summary of the physics of the action of pressure is also given. Section V establishes the importance of linear physics even in the presence of scrambling non-linear effects. The range of validity and limitations of one-point closures in capturing IET features is examined in Section VI. The article concludes with a reiteration of key findings and significant conclusions in Section VII.

2.3 Mathematical formulation

This investigation considers the influence of the pressure field on the evolution of the velocity perturbations, $\mathbf{u}'$, given a background velocity field, $\mathbf{U}$. We attempt to isolate the effect of the pressure field on the velocity perturbations by contrasting the evolution of said fields subject to the Euler and the Burgers equations. In this article, the investigation is restricted to a linear analysis. The linearized Euler equations (rapid distortion equations) for the velocity perturbation subject to a given mean velocity field, are given by:

$$\frac{\bar{D}u'_j}{\bar{D}t} = -u'_i \frac{\partial U_j}{\partial x_i} - \frac{1}{\rho}\frac{\partial p^{(r)}}{\partial x_j}, \tag{2.1}$$

$$\frac{1}{\rho}\nabla^2 p^{(r)} = -2\frac{\partial U_j}{\partial x_i}\frac{\partial u'_i}{\partial x_j}. \tag{2.2}$$

Here, the $\frac{\bar{D}}{\bar{D}t}$ operator represents the total derivative following a mean streamline. As per precedent, the fluctuating pressure, p, is decomposed into two components: rapid pressure, $p^{(r)}$, and slow pressure, $p^{(s)}$. Upon linearization of the Poisson equation for pressure, the slow pressure term is eliminated.

The rapid distortion equations are examined in Fourier space, via the projection:

$$u'_i(\mathbf{x},t) = \sum \hat{u}_i(\boldsymbol{\kappa},t) exp(i\boldsymbol{\kappa}\cdot\mathbf{x}), \quad p^{(r)}(\mathbf{x},t) = \sum \hat{p}(t)(\boldsymbol{\kappa},t) exp(i\boldsymbol{\kappa}\cdot\mathbf{x}). \tag{2.3}$$

In the Fourier analysis, the perturbation is characterized in terms of the wavenumber vector, $\boldsymbol{\kappa}(t)$ and $\hat{\mathbf{u}}$, $\hat{p}$, the corresponding Fourier amplitudes and pressure coefficients. As the equations (2.1) and (2.2) are linear, each Fourier mode evolves independently

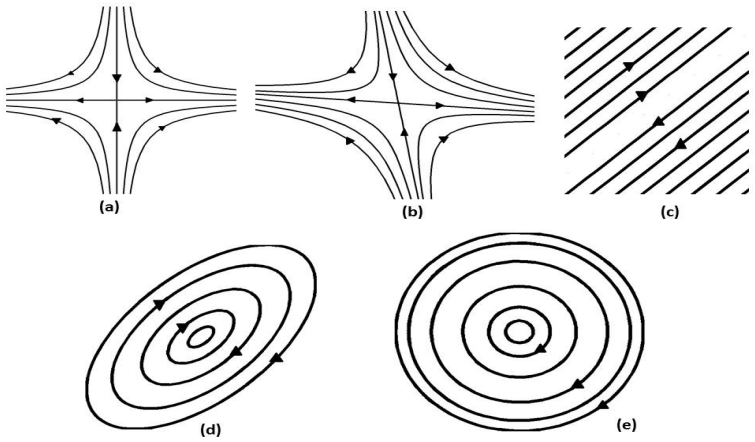

Figure 2.1: The mean flow streamlines as a function of the parameter, β. With increment in β, from zero to one over the course of the five figures, we observe the variation in the mean flow streamlines. (a) and (b) represent hyperbolic flows, where $\beta < 0.5$. (c) represents a pure shear case with β=0.5. (d) and (e) are representative of elliptic flows cases, where $\beta > 0.5$.

and hence the equations can be decomposed and written for each fluctuation mode separately. Starting from the incompressible Euler equations at the rapid distortion limit, the relevant modal equations can be derived as:

$$\frac{d\kappa_l}{dt} = -\kappa_j \frac{\partial U_j}{\partial x_l}, \tag{2.4}$$

$$\frac{d\hat{u}_j}{dt} = -\hat{u}_k \frac{\partial U_l}{\partial x_k}(\delta_{jl} - 2\frac{\kappa_j \kappa_l}{\kappa^2}), \tag{2.5}$$

and the incompressibility constraint is given by $\hat{\mathbf{u}} \cdot \boldsymbol{\kappa} = 0$. This indicates that the wavenumber vector, $\boldsymbol{\kappa}$, and Fourier amplitude vector, $\hat{\mathbf{u}}$, remain orthogonal to each other.

To characterize the applied gradient field, we introduce the ellipticity parameter,

β , defined as:

$$\beta = \frac{W_{pq}W_{pq}}{W_{ij}W_{ij} + S_{ij}S_{ij}}, S_{ij} = \frac{1}{2}(\frac{\partial U_i}{\partial x_j} + \frac{\partial U_j}{\partial x_i}), \quad W_{ij} = \frac{1}{2}(\frac{\partial U_i}{\partial x_j} - \frac{\partial U_j}{\partial x_i}). \tag{2.6}$$

Here, W_{ij} and S_{ij} refer to the rate of rotation and rate of strain tensors of the background flow. Plane quadratic flows can be uniquely characterized by the value of β, as exhibited in figure 2.1. For the purposes of the present investigation, the applied gradient field is confined to the 1-2 plane and the figures exhibit the streamlines in this plane. Quadratic flows can be divided into three classes, based on the applied gradient field: hyperbolic (strain dominated or open streamline flows), elliptic (rotation dominated or closed streamline flows) and purely sheared flows. The classification and nomenclature used to differentiate between quadratic flows are outlined in Table 2.1. The relative strengths of the rate of strain and rotation tensors can be quantified by non-dimensionalizing their norms by that of the mean velocity gradient tensor. In this regard, we define the derived parameters:

$$a = \sqrt{\frac{1-\beta}{2}}, \quad b = \sqrt{\frac{\beta}{2}}. \tag{2.7}$$

Thus, the parameter "a" measures the relative strength of the applied strain and "b", of the applied rotation. In the principal co-ordinates of strain, the requisite mean flow tensors are given as,

$$\frac{\partial U_i}{\partial x_j} = \begin{bmatrix} a & -b & 0 \\ b & -a & 0 \\ 0 & 0 & 0 \end{bmatrix}, \quad S_{ij} = \begin{bmatrix} a & 0 & 0 \\ 0 & -a & 0 \\ 0 & 0 & 0 \end{bmatrix}, \quad W_{ij} = \begin{bmatrix} 0 & -b & 0 \\ b & 0 & 0 \\ 0 & 0 & 0 \end{bmatrix}. \tag{2.8}$$

For the specific case of the two dimensional, constant mean velocity gradient

	Range of β	Nomenclature
I.	$[0, 0.5)$	Hyperbolic/Strain-dominated/Open-streamline flow
II.	0.5	Purely sheared/Homogeneous shear flow
III.	$(0.5, 1]$	Elliptic/Rotation-dominated/Closed-streamline flow

Table 2.1: The nomenclature used for the different regimes of flow and their relation to the ellipticity parameter.

fields considered in this study, the structure of the Kelvin-Moffat set (Moffatt, 1967; Sagaut & Cambon, 2008) is as follows :

$$\begin{aligned}
\frac{de_1}{dt} =& ae_1^3 - ae_1(1+e_2^2) - be_2, \\
\frac{de_2}{dt} =& -ae_2^3 + ae_2(1+e_1^2) + be_1, \\
\frac{de_3}{dt} =& ae_3(e_1^2 - e_2^2), \\
\frac{d\hat{u}_1}{dt} =& (2ae_1^2 + 2be_1e_2 - a)\hat{u}_1 - (2be_1^2 + 2ae_1e_2 - b)\hat{u}_2, \\
\frac{d\hat{u}_2}{dt} =& (2be_2^2 + 2ae_1e_2 - b)\hat{u}_1 - (2ae_2^2 + 2be_1e_2 - a)\hat{u}_2, \\
\frac{d\hat{u}_3}{dt} =& 2e_3(ae_1 + be_2)\hat{u}_1 - 2e_3(ae_2 + be_1)\hat{u}_2.
\end{aligned} \tag{2.9}$$

This represents a six-dimensional, non-linear ordinary differential equation governing the evolution of the unit wavenumber vector,$\mathbf{e}$ and the Fourier amplitude vector, $\hat{\mathbf{u}}$. With the imposed background velocity gradient field expressed as a function of the ellipticity parameter, this forms a single-parameter dynamical system.

To isolate the action of pressure, we contrast the behavior of the Euler system against its pressure-released analogue, the Burgers equations. The linearized Burgers

equation for perturbations can be expressed as:

$$\frac{\bar{D}u'_j}{\bar{D}t} = -u'_i \frac{\partial U_j}{\partial x_i}. \tag{2.10}$$

Upon projection into Fourier space, the linearized Burgers equation reduces to,

$$\begin{aligned} \frac{d\hat{u}_1}{dt} &= -a\hat{u}_1 + b\hat{u}_2, \\ \frac{d\hat{u}_2}{dt} &= -b\hat{u}_1 + a\hat{u}_2, \\ \frac{d\hat{u}_3}{dt} &= 0. \end{aligned} \tag{2.11}$$

2.3.1 Individual vs. collective behavior

In order to develop comprehensive physical understanding, it is important to examine the behavior of individual Fourier modes in addition to the investigation of the statistical behavior of the collection of Fourier modes. Under the aegis of the Rapid Distortion Theory, the magnitude of the wavevector is inconsequential and only the alignment of the mode is important. Thus, for the statistical treatment based on RDT, the initial conditions are chosen to correspond to an isotropic initial state of turbulence (unbiased initial state). To achieve an isotropic initial state, velocity fluctuations in all permissible directions are taken to be equally energetic (Girimaji *et al.*, 2003). That is, Fourier coefficients of initial velocity fluctuations in all permissible directions have equal magnitudes. For a given vector **u** all permissible wavenumber vector directions are equally probable. Consequently, the initial wavevectors are uniformly distributed on a unit sphere.

Considering a statistical ensemble as in SMC, the transport of the Reynolds stress

tensor is governed by:

$$\begin{aligned}
\frac{dR_{ij}}{dt} &= P_{ij} + \pi^r_{ij}, \\
\text{where, } R_{ij} &= \sum_{\kappa} \langle u_i u_j \rangle, \\
\pi^r_{ij} &= 2\frac{\partial U_l}{\partial x_k}(M_{kjil} + M_{ikjl}), \\
M_{ijkl} &= \sum_{\kappa} \langle \hat{u}_i \hat{u}_j e_k e_l \rangle, \\
\text{and } P_{ij} &= -R_{jk}\frac{\partial U_i}{\partial x_k} - R_{ik}\frac{\partial U_j}{\partial x_k}.
\end{aligned} \tag{2.12}$$

To understand the statistical effect of IET, it is instructive to compare the physics of the above equation with its pressure-released counterpart – Burgers turbulence or Burgulence:

$$\frac{dR_{ij}}{dt} = P_{ij}. \tag{2.13}$$

In this study, we investigate the behavior of individual modes as well as the statistics of a collection of modes. As mentioned in the Introduction, the behavior of individual modes is important to the Turbulence Structure-Based approach, as well as for SMC. While studying specific modes, the initial conditions are chosen to highlight the specific phenomenon to be studied. The investigation of the collective behavior is entirely motivated by SMC wherein the statistics of an ensemble of modes are to be determined. The challenge of one-point SMC modeling is that the modes that constitute the ensemble are not known. The best an SMC model can attempt to accomplish is to provide closure based on the statistically most likely ensemble. We propose that the SML ensemble is one wherein the wavenumber vectors are initially distributed isotropically in Fourier space. This represents an unbiased initial distribution. With such an initial choice, the most energetic wavenumbers naturally emerge from the collection to dominate the statistics (Girimaji *et al.*, 2003), leading

to the statistically most likely behavior. However, it is important to point out that the ensemble in a practical application may be very different depending on the flow conditions. Finally, a fourth-order Runge-Kutta scheme is used for time integration of all equations.

2.4 The action of pressure: overall flow stability

As pressure realigns the velocity vectors to impose the divergence-free constraint, it critically affects the flow stability. As explained in the introduction, the key challenge of one-point closures is to establish the statistical behavior of a collection of modes, bereft of any information regarding the constituents of this ensemble. The incipient step toward achieving a reasonable closure is to establish the stability characteristics of the full system. In this vein, we need to isolate the action of pressure and determine the stability characteristics engendered by pressure effects and those due to inertial effects. To categorically explicate the effect of pressure, we compare results computed from linearized (RDT based) simulations of the Euler and the Burgers equations. These are referred to as RDT-E and RDT-B, respectively. This comparison focuses on the turbulent kinetic energy, $k = \frac{\overline{u_i u_i}}{2}$, and the Reynolds stress anisotropies, $b_{ij} = \frac{\overline{u_i u_j}}{2k} - \frac{\sigma_{ij}}{3}$.

2.4.1 Burgulence

The Burgers system is governed by the production mechanism only and hence, offers an excellent platform to isolate the inertial dynamics. The linearized Burgers equations (2.11) represent a homogeneous linear differential system with the dynamics confined to the $\hat{u}_1 - \hat{u}_2$ plane, i.e. the plane of applied strain. The corresponding

solutions for the Fourier amplitude vector in the Burgers system are:

$$\begin{bmatrix} \hat{u}_1 \\ \hat{u}_2 \end{bmatrix} = c_1 \exp(\sqrt{a^2-b^2}t) \begin{bmatrix} \frac{-\sqrt{a^2-b^2}}{a-b} \\ 1 \end{bmatrix} + c_2 \exp(-\sqrt{a^2-b^2}t) \begin{bmatrix} \frac{\sqrt{a^2-b^2}}{a-b} \\ 1 \end{bmatrix}. \quad (2.14)$$

In the general case, the mean velocity gradient matrix has two non-zero eigenvalues, given by $\pm\sqrt{a^2-b^2}$. For the case of hyperbolic flows, $(a > b)$, and the eigenvalues are real. The corresponding eigenvectors represent the extensional ($\lambda > 0$) and compressional ($\lambda < 0$) directions of the background flow. With reference to the equation (2.14), the Fourier amplitude vector aligns itself with the compressional principal axis. Physically, this represents streamwise vortex stretching which is the underlying physical mechanism for the hyperbolic flow instability. For elliptic flows, the non-trivial eigenvalues are complex conjugates. Thus, the mean velocity gradient does not possess real principal axes. In this regime, production causes the fluctuating velocity vector to undergo linear oscillations in the $\hat{u}_1 - \hat{u}_2$ plane.

In summary, the scope of this production mechanism is, directly and linearly, associated with the applied gradient field and thus, the effects of production are limited to the plane of applied gradient. For RDT-B, there is a straightforward transfer of energy from the mean flow to the R_{11} and the R_{22} components and vice-versa, via positive and negative production.

2.4.2 Pressure-effects

For the case of RDT-E, pressure-strain correlation represents a mechanism to redistribute perturbation energy amongst all the components. The inclusion of the pressure effect influences the production mechanism indirectly, as it can modify the alignment of the Fourier amplitudes with the principal axes. In this vein, pressure

could cause the Fourier amplitude vector to align faster with the compressional axis, thus bolstering the instability. Conversely, the effects of pressure may counteract such an alignment and mitigate the flow instability. Conceivably, pressure effects could be negligible and not have a significant effect on the stability characteristics. As shall be proved, all of these putative actions are manifested by the system and the exact nature of the effects of pressure upon flow stability is completely dependent on the type of mean flow.

2.4.3 Flow statistics in different regimes

Figure 2.2 (a) shows the turbulent kinetic energy evolution for a representative hyperbolic flow case (Henceforth, $S = \sqrt{S_{mn}S_{mn}}$). As can be observed, in the absence of pressure (RDT-B), the kinetic energy continues to grow exponentially. In the case of RDT-E, the kinetic energy grows, exponentially, to a high value where it settles down. However, the case of RDT-E exhibits a significantly lower rate of growth for the perturbation kinetic energy, which is a manifestation of the stabilizing action of pressure. In figure 2.2 (b) and (c), the evolution of the anisotropies for hyperbolic flows in RDT-E and RDT-B are exhibited, respectively. The statistics governed by RDT-B have production as the sole turbulent process governing evolution. Consequently, the turbulent kinetic energy is contained in the compressive principal axis of the mean velocity gradient tensor, R_{cc}. However, such a state is in violation of mass conservation, as the wavevectors converge to a state of alignment along this axis as well. Thus, pressure redistributes the turbulent kinetic energy, transferring it out of the plane of applied strain. This leads to the increase of the b_{33} component, observed in the RDT-E evolution. As can be observed, the transfer of energy to the R_{33} component, exhibited in 2.2 (b), corresponds to the exact juncture when the Euler system stabilizes, exhibited in 2.2 (a).

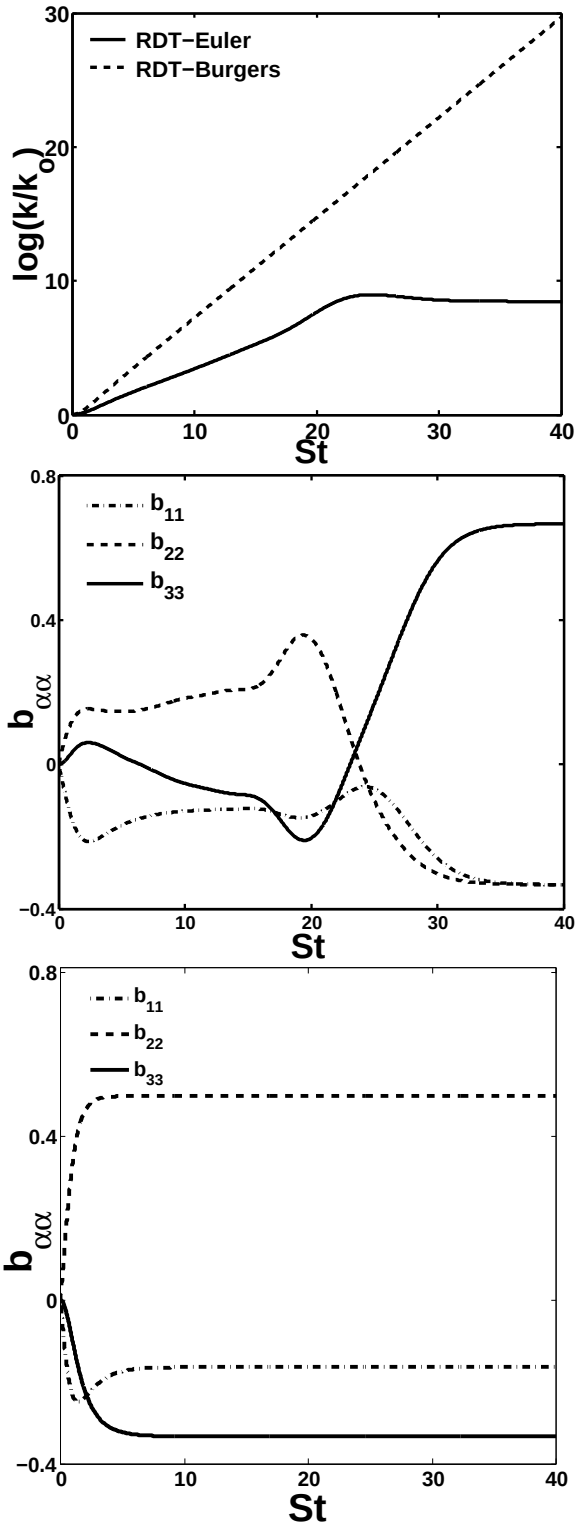

Figure 2.2: Evolution of statistics for a representative hyperbolic flow, $\beta = 0.36$. (a) Comparison of turbulent kinetic energy evolution in RDT-B and RDT-E, (b) b_{ij} evolution for RDT-E, (c) b_{ij} evolution for RDT-B.

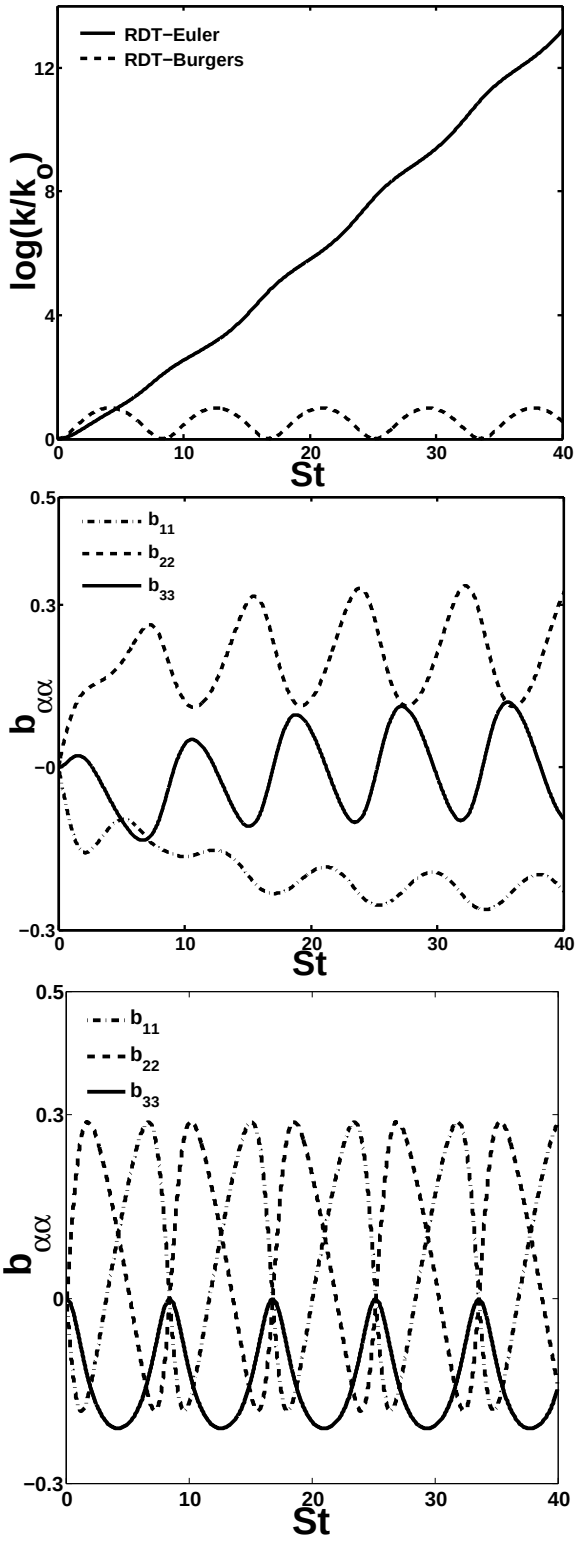

Figure 2.3: Evolution of statistics for a representative elliptic flow, $\beta = 0.64$. (a) Comparison of turbulent kinetic energy evolution, (b) b_{ij} evolution for RDT-E, (c) b_{ij} evolution for RDT-B.

Figure 2.3 (a) displays the kinetic energy evolution for a representative elliptic flow case. In this case, for RDT-E, the perturbation kinetic energy has no upper bound and keeps increasing even for the long time spans simulated in this study, exhibiting the unstable state of the flow. In contrast, for RDT-B, the kinetic energy is in a bounded, oscillatory state that has a constant amplitude and frequency of oscillation. Clearly, the pressure-less evolution is in a state of neutral stability, while the addition of the pressure term engenders the elliptic flow instability. In this context, Salhi et al. (1997) have pointed out that the elliptic flow instability is contingent upon the contribution of pressure. In figure 2.3 (b) and (c), the evolution of the anisotropies for elliptic flows in RDT-E and RDT-B are exhibited, respectively. For RDT-B, it can be observed that the anisotropy components are in a state of linear oscillation. For the case of RDT-E, pressure effects transfer energy to and from the plane of applied strain. This can be observed in the RDT-E evolution, where b_{33} oscillates about a mean of zero, representing energy transfer to and from this component.

For the case of pure shear flows, figure 2.4, it is observed that the evolution of the anisotropies and turbulent kinetic energy is very similar for both RDT-E and RDT-B. In this case, the inertial effects engender the velocity field to evolve in a manner that the continuity condition is nearly satisfied. This obviates the need for any substantial realignment of the Reynolds stress tensor and consequently, pressure has a negligible role in the evolution of the flow field. In the hyperbolic and elliptic regimes, it was observed that pressure was able to change the stability characteristic of the flow. In figure 2.4 (a), it can be observed that the kinetic energy evolution for both the Burgers and the Euler RDT simulations show unstable behavior. For the Burgers system, there is quadratic growth in kinetic energy while the Euler system exhibits linear growth. Thus, the action of pressure has a negligible effect on flow

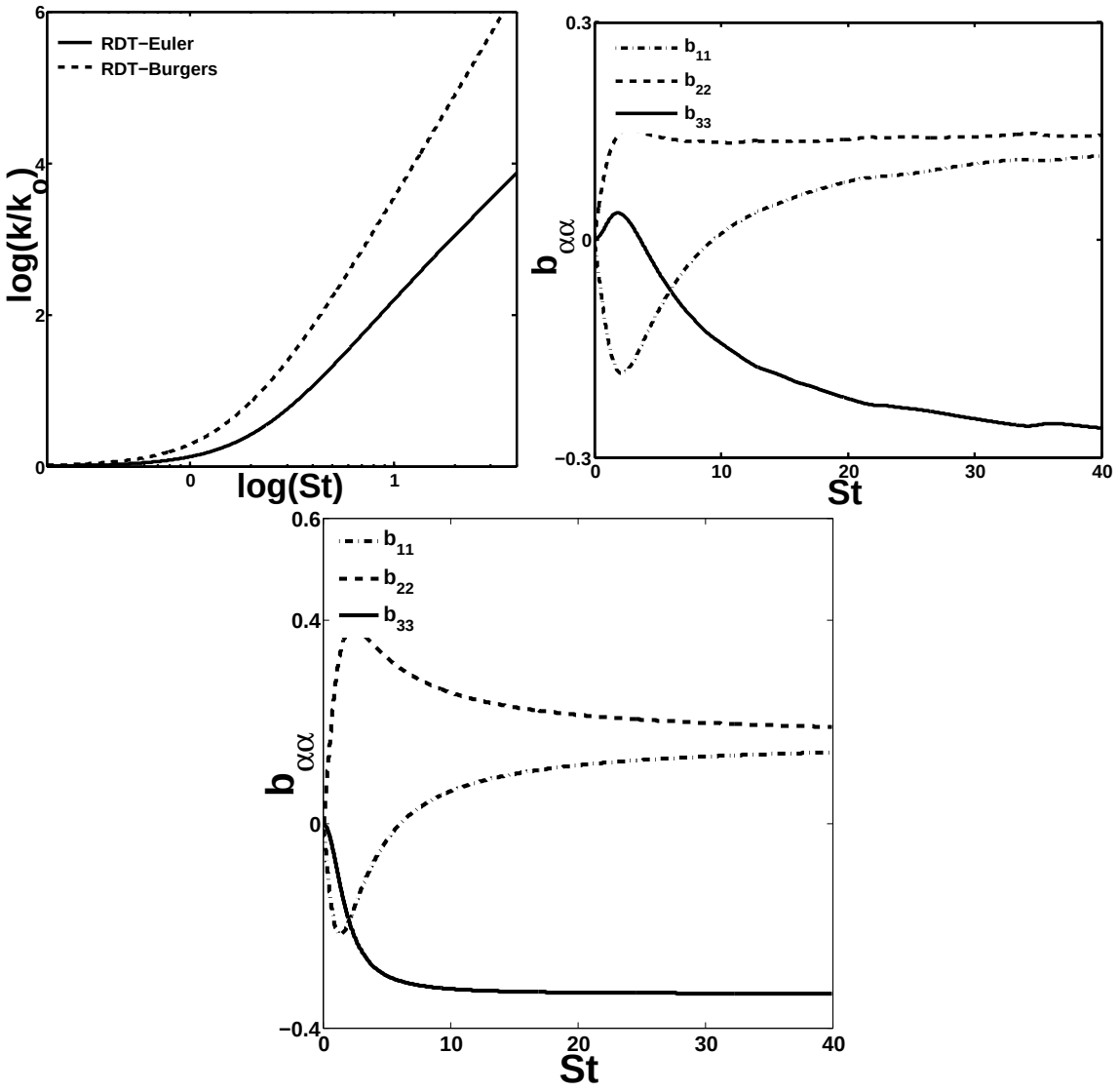

Figure 2.4: Evolution of statistics for a homogeneous shear flow, $\beta = 0.5$. (a) Comparison of turbulent kinetic energy evolution in RDT-B and RDT-E, (b) b_{ij} evolution for RDT-E, (c) b_{ij} evolution for RDT-B.

stability and is not even able to transform the nature of flow stability (polynomial, as opposed to exponential growth).

By contrasting the RDT-E and RDT-B evolution, it is observed that the effect of pressure on stability is diametric for open streamline flows and closed streamline flows. For the case of open streamline flows, pressure has a stabilizing influence and moderates the hyperbolic instability. On the contrary, for the case of closed streamline flows, pressure acts so as to initiate and sustain the elliptic flow instability. At the point of transition between these flow regimes, i.e., purely sheared flow, pressure has a minimal effect and does not even alter the nature of the flow instability.

In this section, the redistributive action of pressure and the concomitant consequences on flow stability have been established clearly. While the results illustrate the critical role of the action of pressure, further modal analysis is vital for developing the deeper insight necessary for high-fidelity closure models.

2.5 The action of pressure: modal analysis

The magnitude and nature of the action of pressure on realignment, energy redistribution and stability is highly contingent on the orientation of the perturbation mode, $\vec{e}$. This is related to the "structuring effect" of linear physics (Sagaut & Cambon, 2008). This hierarchy of dependence can be observed by decoupling the Kelvin-Moffat set of equations, wherein the wavenumber vector evolves as a function of the background gradient field only, while the modal kinetic energy evolution is dependent upon the alignment of the mode as well.

As mentioned in the introduction, the study will consist of the following four analyses for each type of flow:

1. Invariant sets and their bifurcations of the wavevector evolution.

2. IET and dynamics of Reynolds stress evolution.

3. Modal stability and the topology of unstable modes.

4. Range of IET behavior and the statistically most likely behavior.

These distinct lines of investigation can provide the insight required to incorporate multi-point features into a single-point closure, to the possible extent. Equally important, the study can identify the limitations and potential level of uncertainty in closure modeling at the single-point level.

As the wavevector evolution is central to the action of pressure, we commence our analysis with an examination of the evolution of the alignment of modes. The time-dependent solution for the wavevector evolution is,

$$\begin{bmatrix} \kappa_1 \\ \kappa_2 \end{bmatrix} = c_1 \exp(-\sqrt{a^2-b^2}t) \begin{bmatrix} \frac{-\sqrt{a^2-b^2}}{a-b} \\ 1 \end{bmatrix} + c_2 \exp(\sqrt{a^2-b^2}t) \begin{bmatrix} \frac{\sqrt{a^2-b^2}}{a-b} \\ 1 \end{bmatrix}. \quad (2.15)$$

For open streamline flows, this leads to non-trivial, stationary solutions for $\vec{e}$. For closed streamline flows, the solutions are oscillatory. In this section, we study the dynamics of the modal ensemble, with an emphasis on the wavevector. We seek a universal behavior herein and analyze the importance of the *outliers* of this distribution, that have dynamics deviating markedly from the other members of the sample.

2.5.1 Hyperbolic flows

2.5.1.1 Wavevector dynamics

For hyperbolic flows, the magnitude of S_{ij} is more than that of W_{ij}. In such strain-dominated flows, there exist stationary states for modal alignment. These correspond to the extensional and compressional principal axes of the mean velocity

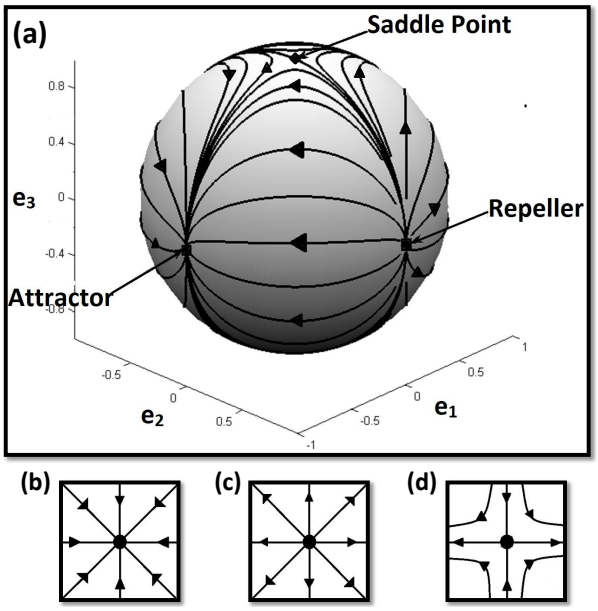

Figure 2.5: The topology of the phase space for a representative hyperbolic flow (plane strain, $\beta = 0$). The inset figures, b,c and d, delineate the topology in the neighborhood of an attractor, a repeller and a saddle-node, respectively, on a plane phase space.

gradient tensor. The mean velocity gradient has a predilection to align the modes in the flow with the compressional principal axis. Thus, in dynamical systems parlance, this state of alignment represents an *attractor*. Almost all the modes in the flow, except for a set of measure zero, have a bias to align thus. Conversely, the extensional principal axis acts as a *repeller* and modes having an alignment close to this are repelled from such a state. Furthermore, modes that are aligned perpendicular to the plane of applied velocity gradient maintain this orientation. This state of perpendicular alignment is a *saddle-node*. The saddle-nodes have the property of attracting trajectories along a specific direction and repelling trajectories along another direction. The topology of this phase space is exhibited in figure 2.5, along with the local trajectories in the vicinity of the critical points mentioned above. The attracting direction of the saddle-nodes, termed as the separatrix, is the curve joining

the repellers and the saddle-nodes along the surface of the sphere. As per definition, the separatrix demarcates the boundary separating trajectories of markedly different dynamics. In this context, it divides the basins of attraction of the two attractors. As the topology of the phase space suggests, due to the division by the seperatrix of trajectories with acutely different behaviors, the dynamics *on* the separatrix are singular. Modes that are perfectly aligned with the separatrix, are not attracted to the compressional principal axes, but instead these evolve toward a state of alignment that is perpendicular to the plane of applied gradient. As the basins of attraction cover the entire space, the asymptotic evolution of almost all modes is to either one of the two attractors. However, the *initial evolution* of the alignment of a generic mode is dependent on its proximity to the principal axes. In this regard, the modes in the flow can be classified into two categories:

1. Modes that are closer to the separatrix evolve, initially, toward a state of alignment perpendicular to the plane of the applied gradient. (This is due to the fact that their trajectories of approach to the attractor pass very close to the saddle-node.) Hereafter this set of modes is referred to as the E-modes.

2. Modes that are closer to the compressional axis evolve to a state of perfect alignment with the compressional axis. Hereafter this set of modes is referred to as the C-modes.

It will be shown that these two kinds of evolution are associated with diametric characteristics with respect to the stability of the mode.

2.5.1.2 IET dynamics

The role of pressure is to maintain the orthogonality between the Fourier amplitude vector and the wavevector. This condition is trivially satisfied if the Fourier

amplitude vector of the mode is aligned with the compressional principal axis of the applied gradient field. Consequently, for such modes, the pressure term does not affect the evolution of the modal velocities and their evolution is identical to a hypothetical Burgers mode. For all other modes, as is evident from the equations (2.15) and (2.14), to enforce continuity pressure removes turbulent kinetic energy from the plane of applied strain. This redistribution leads to a reduction in R_{11} and R_{22}, with a consequent increase in R_{33}. The hyperbolic instability is essentially due to the effects of the applied strain on the fluctuating velocity component along the compressional principal axis. Any transfer of fluctuation energy out of the plane of applied strain diminishes the magnitude of fluctuations along this direction. Thus, this out-of-plane energy transfer moderates the magnitude of production and mitigates the state of instability.

Reverting to our classification of the modes based on the initial evolution of their alignments, we find that the pressure effects are diametric for these sets.

1. C-modes: For these modes, to maintain continuity, the pressure effects project the Fourier velocity components onto the plane perpendicular to the wavevector. This reduction in R_{11} and R_{22} arrests the production mechanism and leads to modal stability within a very short span.

2. E-modes: For these modes, the pressure effects are minimal during their phase of attraction to the saddle-node. Thus, these modes can exhibit growth for prolonged periods and can possess a growth rate corresponding to a Burgers mode.

The rationale underlying this codification can be observed in the modal kinetic energy evolution in figure 2.6. The dotted line exhibits the evolution of a mode that is not influenced by pressure. This would correspond to a mode governed by the

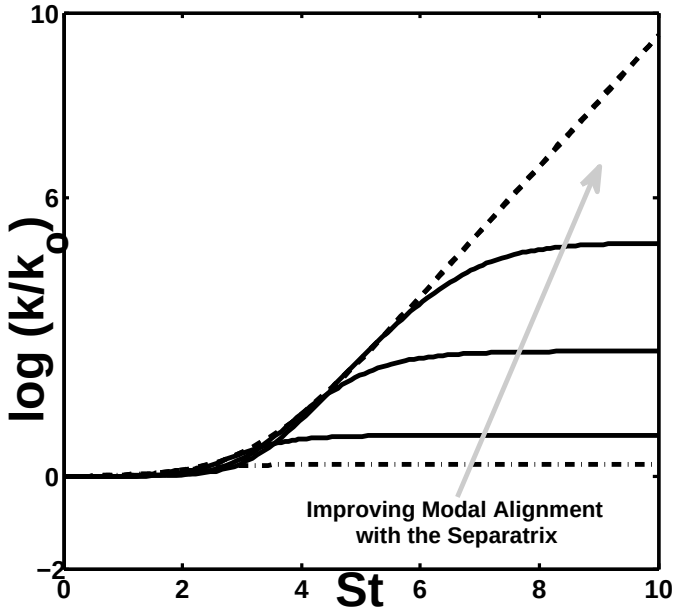

Figure 2.6: Evolution of the modal kinetic energy in a hyperbolic flow, for different modal alignments relative to the separatrix. The mode aligned with the separatrix is plotted with a dashed line, the mode aligned perpendicular to the separatrix is plotted with a dot-dash and modes in between these alignments are plotted with a solid line. As the mode's alignment with the separatrix improves, the mode becomes more unstable.

Burgers equations, or consonantly, an Euler mode whose wavevector is aligned with the separatrix perfectly. If we consider modes that are offset from such a state of alignment, the pressure effects and the consequent stabilization manifest themselves progressively. This can be observed in figure 2.6, in the solid lines representing modes that are influenced by pressure effects. As can be observed, the duration of growth and the magnitude to which the modal kinetic energy grows is dependent on the alignment of the mode with the compressive principal axis. As the mode's alignment with the axis improves, both these quantities decrease.

Due to the redistribution of kinetic energy, the C-modes reach a state of quiescence and thence, do not contribute to flow statistics. For the E-modes, the conti-

nuity is satisfied even during perturbation growth. These modes exhibit growth for prolonged periods and engender the flow instability.

2.5.1.3 Topology of the unstable modes

The dependence of modal stability on initial modal alignment is exhibited in figure 2.7, wherein this small set of outliers is evident. The instability coefficient determines the modal stability and is defined as:

$$\lambda_{mode}(t) \equiv log\left[\frac{k_{mode}(t)}{k_{mode}(0)}\right].$$

If the modal trajectories, exhibited in Figure 2.5(a), are compared to modal stability, exhibited in figure 2.7, it is observed that only a small set of modes located near the seperatrix are unstable. These are the modes that are attracted to the saddle-node and were anointed as the E-modes.

2.5.1.4 SML behavior and overall range

Figure 2.8 exhibits a schematic of the processes of the system for hyperbolic flows. The Burgers system, restricted to inertial processes, remains unstable. However, for the Euler system, the energy transfer due to pressure has a stabilizing influence. This represents the *statistically most likely* behavior. As can be observed in the schematic, the predominant energy transfer is from the compressive eigendirection to the out-of-plane component. This theme is reiterated in figure 2.9. In this figure, we present a range of IET possibilities for different wavevectors. Regarding the evolution of the products of the modal Fourier amplitudes, $\hat{u}_\alpha\hat{u}_\alpha$ (The summation convention is not applied to Greek indices.), the symbolic evolution equation is given by:

$$\frac{d\hat{u}_\alpha^2}{dt} = P_{\alpha\alpha}^{modal} + \pi_{\alpha\alpha}^{modal}. \tag{2.16}$$

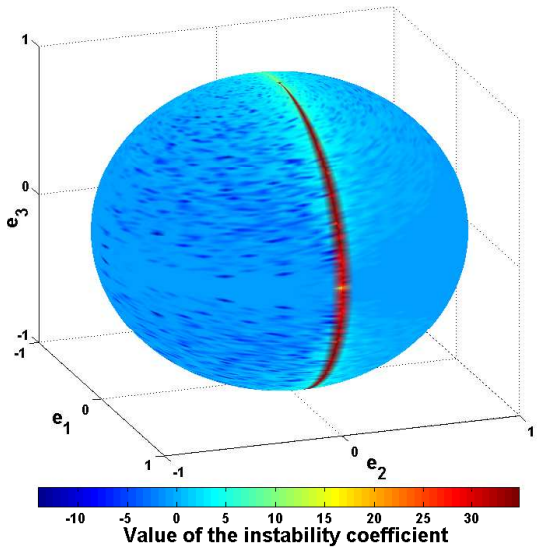

Figure 2.7: The figure illustrates the effect of initial modal alignment on modal stability for hyperbolic flows. The figure is for a plane strain case($\beta = 0$). The instability coefficient measures the growth of modal kinetic energy. Thus, a positive value indicates growth and a negative value indicates decay.

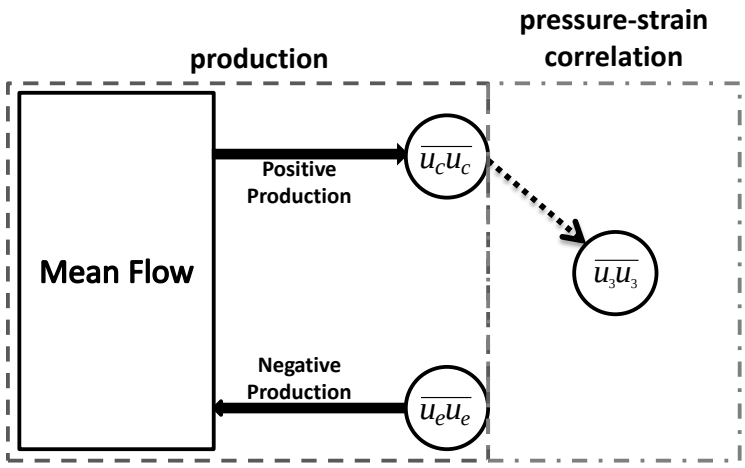

Figure 2.8: A schematic of kinetic energy exchange in a hyperbolic flow. The inertial processes are marked in filled arrows, the pressure effects via dashed arrows. The subscripts of “e" and “c" denote the extensional and compressional axes of the applied gradient.

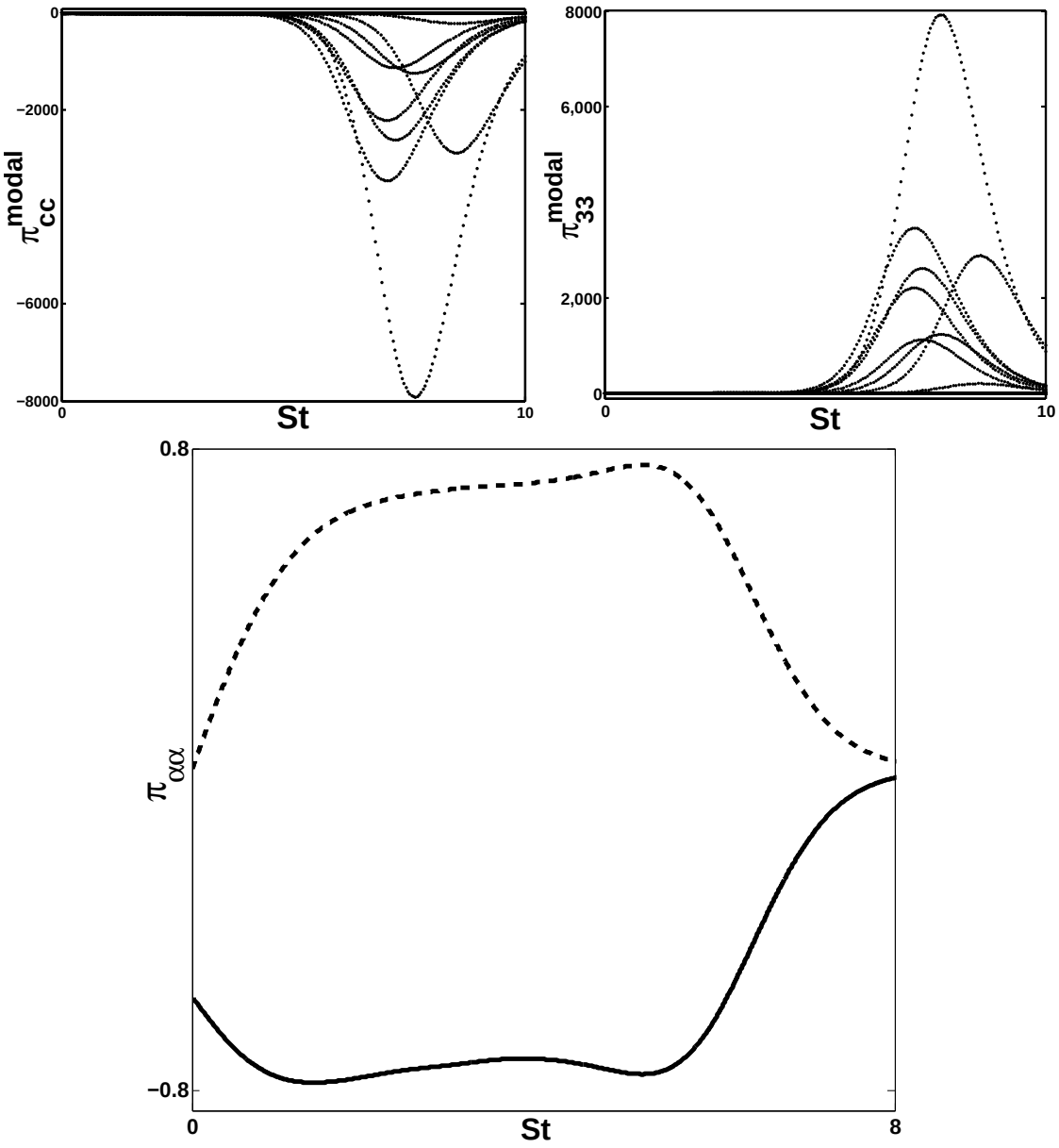

Figure 2.9: (a) The evolution of the intercomponent transfer from the compressive eigendirection for a set of randomly selected modes, (b) the evolution of the intercomponent transfer to the out of plane component for a set of randomly selected modes, (c) The evolution of the diagonal components of the rapid pressure strain correlation tensor for the case of plane strain. π_{33},− − −; π_{cc},−.

Thus, for instance, $\pi_{33}^{modal} = 4e_3[a(e_1\hat{u}_1 - e_2\hat{u}_2) + b(e_2\hat{u}_1 - e_1\hat{u}_2)]\hat{u}_3$. It is exhibited that in spite of the significant quantitative variance in the individual modal behavior, the qualitative behavior of the dominant modes is analogous to that exhibited in figure 2.8. Figure 2.9(c), shows that after a very short transient, the π_{cc} and π_{33} components balance each other exactly.

2.5.2 Purely sheared flows

In the analysis of purely sheared flows, a different co-ordinate system is utilized due to its prevalence in prior literature. Herein, the axes in the plane of applied strain are rotated by $\pi/4$ and the mean velocity gradient tensor is given by,

$$\frac{\partial U_i}{\partial x_j} = \begin{bmatrix} 0 & S' & 0 \\ 0 & 0 & 0 \\ 0 & 0 & 0 \end{bmatrix}; \textit{where } S' = \sqrt{2}S. \tag{2.17}$$

The $1, 2$ and 3 axes correspond to the established cognomen of streamwise, vertical and spanwise directions, respectively.

2.5.2.1 Wavevector dynamics

The increment in the value of the ellipticity parameter indicates an increasing influence of the rate of rotation tensor over the rate of strain tensor. This causes the principal axes of the mean velocity gradient tensor to shift toward each other, as is evident in figure 2.10. In the limit of the switch from strain dominated to rotation dominated flows, at the ellipticity parameter, β, value of 0.5, the eigenvectors of the mean velocity gradient tensor are coincident, along the “vertical" direction. The explicit solutions for the wavevector evolution is given by:

$$\kappa_1(t) = \kappa_1(0), \kappa_2(t) = \kappa_2(0) - \kappa_1(0)S't, \kappa_3(t) = \kappa_3(0). \tag{2.18}$$

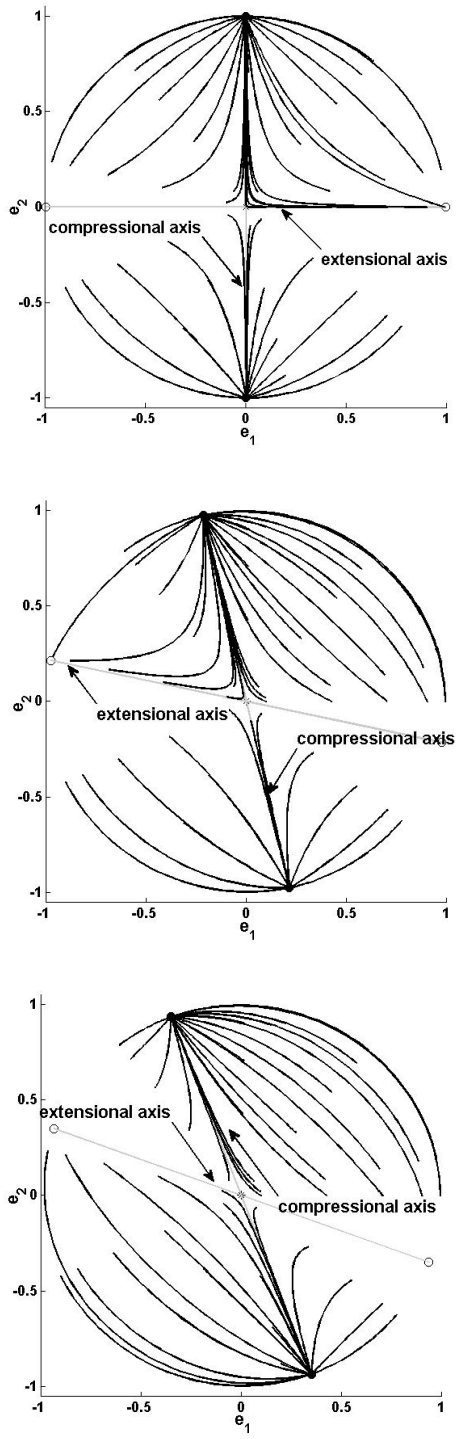

Figure 2.10: The figure illustrates the migration of the eigen-directions of the mean velocity gradient tensor, with increment in the ellipticity parameter. The specific values used are β =0, 0.19 and 0.36, respectively.

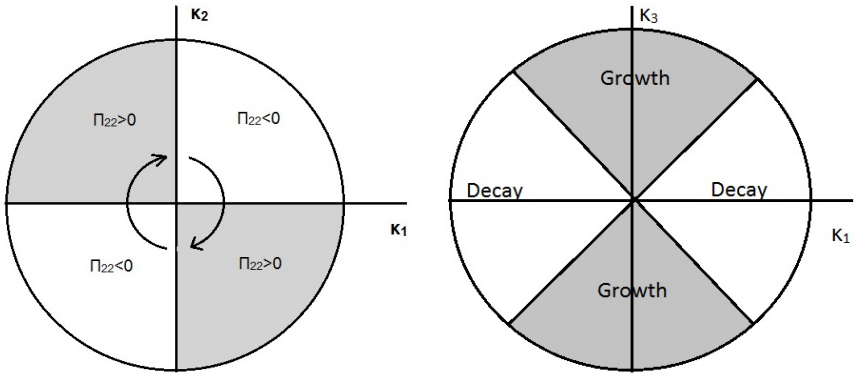

Figure 2.11: A representation of the effect of modal alignment on (a) intercomponent energy transfer (b) modal stability.

2.5.2.2 IET dynamics

For individual modes in the flow, the evolution equation for the products of the modal Fourier amplitudes, $\hat{u}_\alpha \hat{u}_\alpha$, is as follows:

$$\begin{aligned} \frac{d\hat{u}_1\hat{u}_1}{dt} &= (-2S'\hat{u}_1\hat{u}_2)(1-2e_1^2), \\ \frac{d\hat{u}_2\hat{u}_2}{dt} &= 4S'e_1e_2\hat{u}_2^2, \\ \frac{d\hat{u}_3\hat{u}_3}{dt} &= 4S'e_1e_3\hat{u}_2\hat{u}_3. \end{aligned} \tag{2.19}$$

The inertial mechanism has a predilection to inject energy along the streamwise direction and leave the fluctuations along other directions unaffected. We consider the modes where production is positive, thus $-2S'\hat{u}_1\hat{u}_2 > 0$. Examining (2.19), it is clear that for such modes, the intercomponent energy transfer takes energy from the streamwise component. Due to the motion of the wavenumber vector, after a very short span, all unit wavenumber vectors are attracted to a state of alignment with the vertical direction. Thus, the product e_1e_2 is negative. Consequently, the intercomponent energy transfer removes energy from the vertical component as well.

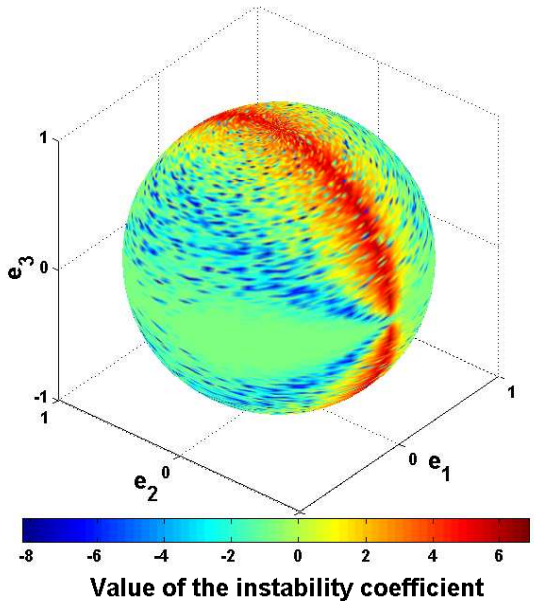

Figure 2.12: The figure illustrates the effect of initial modal alignment on modal stability for a purely sheared flow. The instability coefficient measures the growth of modal kinetic energy. Thus, a positive value indicates growth and a negative value indicates decay.

This is exhibited in figure 2.11(a). The motion of the modal alignments, marked by arrows, ensures that after a very short span, energy is removed from the vertical component for almost all modes and thus for the ensemble as well. This energy is transferred to the spanwise component. As the spanwise component is bereft of any production, transfer to this component arrests the rate of kinetic energy growth. Furthermore, the transfer from the vertical and streamwise components reduces the production of kinetic energy ($P = -2S'\hat{u}_1\hat{u}_2$). This leads to a slight mitigation of the state of instability of the Euler system, as compared to the Burgers system.

2.5.2.3 Topology of the unstable modes

Figure 2.12 exhibits the relationship between modal alignment and stability for purely sheared flows. As can be observed in the figure, the unstable modes correspond

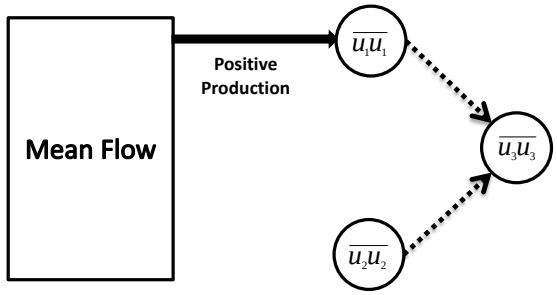

Figure 2.13: A schematic of kinetic energy exchange in a purely sheared flow. The inertial processes are marked in filled arrows, the pressure effects via dashed arrows.

to the modes with initial alignments close to κ_1=0. For almost all other modes, the redistribution of kinetic energy during the modal migration to the vertical direction causes stabilization. Thus, flow statistics are determined by a very small set of modes. The presence of this relation between the unstable modes, their alignments and such a set of measure zero has been remarked upon by Rogers (1991).

2.5.2.4 SML behavior and overall range

The motion of the modal alignments ensures that after a very short span, energy is removed from the vertical component to the spanwise component. This is exhibited in figure 2.13. This represents the *statistically most likely* behavior in this regime.

The action of pressure is constrained for the duration that the wavevector alignment is evolving to the vertical direction. Once the modes are in very close alignment with the vertical direction, the action of pressure is negligible as the production term is present for the R_{11} component, that pertains to the Fourier velocity amplitudes along the streamwise axis. This is displayed in figure 2.14(c). Thus, the action of pressure stabilizes the flow, but is substantial for a very brief duration. Consequently, the evolution of kinetic energy is qualitatively similar for RDT-B and RDT-E, as observed in figure 2.4. In figures 2.14,(a) and (b), the range of the modal

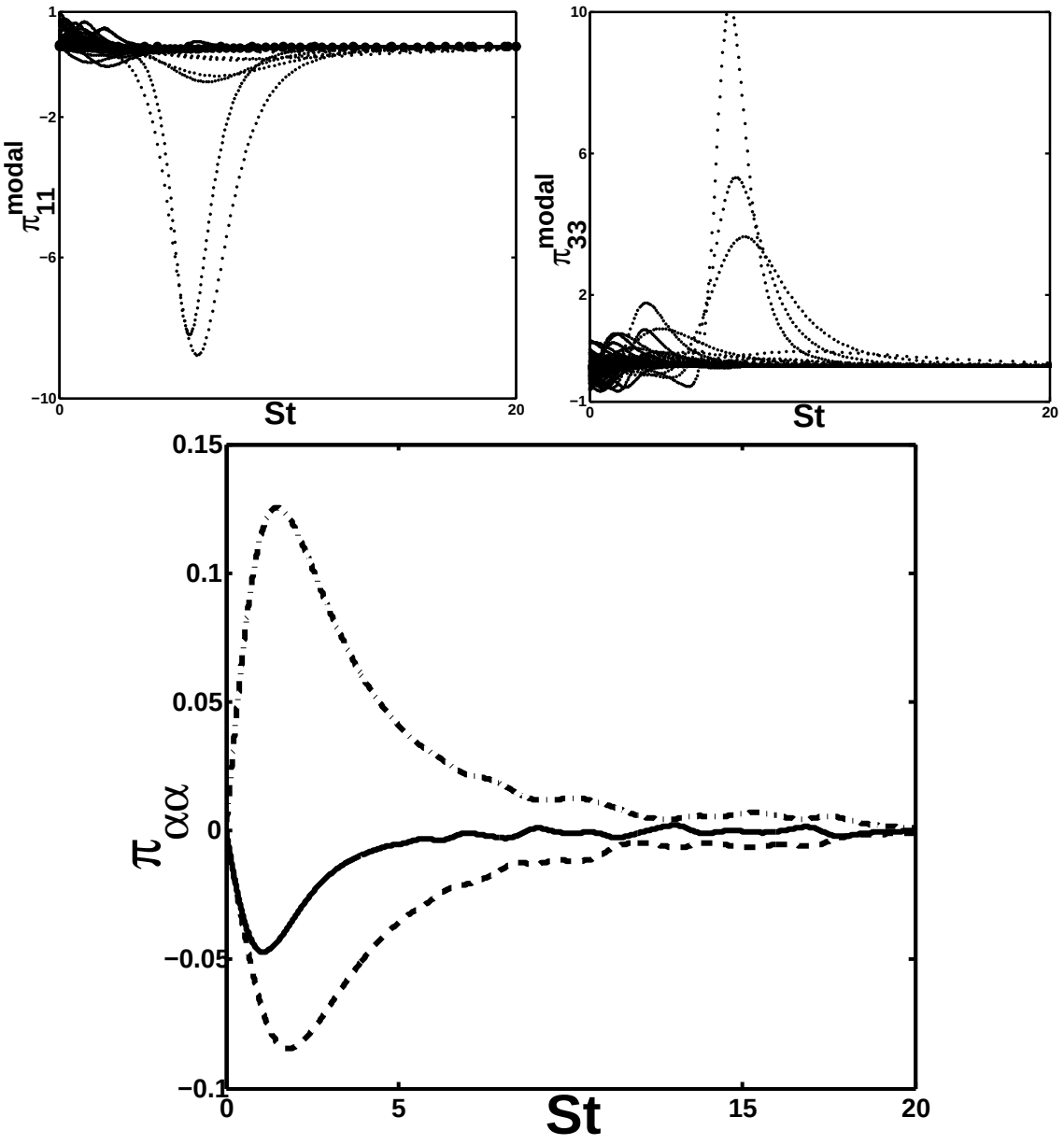

Figure 2.14: (a) The evolution of the intercomponent transfer from the streamwise direction for a set of randomly selected modes, (b) the evolution of the intercomponent transfer to the spanwise direction for a set of randomly selected modes, (c) The evolution of the diagonal components of the rapid pressure strain correlation tensor for the case of pure shear. π_{11},—; π_{22}, $--$;π_{33}, $\cdot-$.

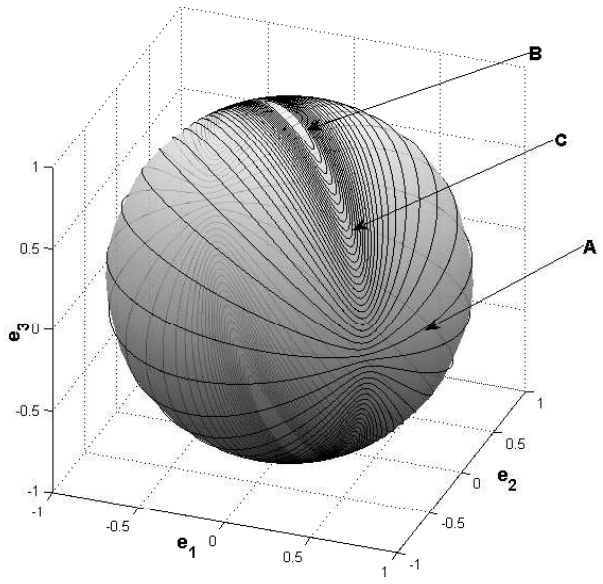

Figure 2.15: The closed orbits on the sphere at $\beta = 0.55$.

intercomponent energy transfer is exhibited. As can be observed, the variance of this distribution is significant.

2.5.3 Elliptic flows

2.5.3.1 Wavevector dynamics

For closed streamline flows, the magnitude of W_{ij} is greater than S_{ij}. Consequently, the principal axes for the mean velocity gradient are not extant and thus, the wavenumber vector exhibits periodic solutions. However, even for this regime, the rate of strain tensor has real eigendirections, associated with the stretching and squeezing of the streamlines. The wavevector trajectories are stretched along the compressive direction of the rate of strain and compressed along the extensional direction. This leads to the distortion of the periodic orbits in phase space, as can be observed in figure 2.15.The wave modes that lie proximate of the plane of applied strain undergo negligible distortion (marked as “A"). Similarly, modes that

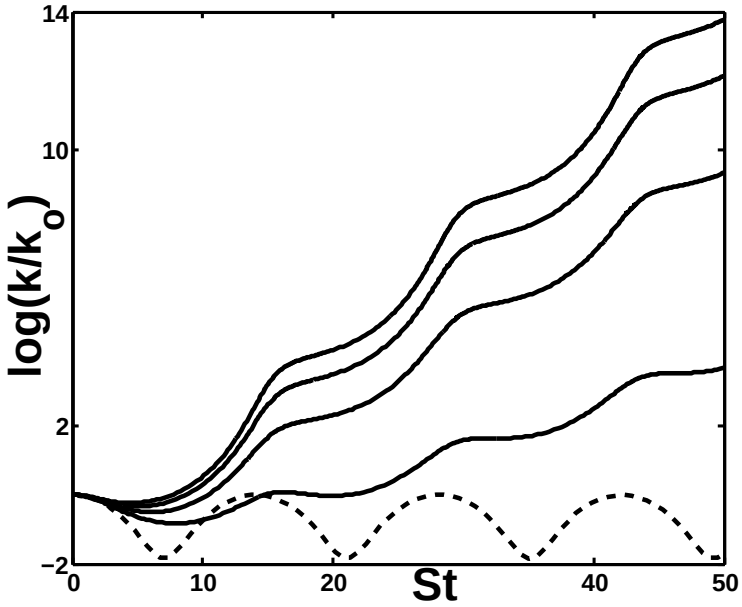

Figure 2.16: Evolution of the modal kinetic energy in an elliptic flow, for a host of initial conditions. The evolution of the mode governed by the Burgers system is plotted in a dotted line. The Euler modes are exhibited in solid lines.

are almost perpendicular to the plane of applied strain do not undergo substantial distortion (marked as "B"). It is a band of modal alignments between these extremes that shows significant distortion in the trajectories.

2.5.3.2 IET dynamics

Figure 2.16 exhibits modal kinetic energy evolution for elliptic flows. The mode governed by the Burgers equations, exhibited by a dashed line in the figure, is neutrally stable. The behavior of Euler modes that are aligned perfectly perpendicular to the plane of applied strain, or, completely in the plane of applied strain is identical to this. For all other modes the effects of pressure manifest themselves in the modal kinetic energy evolution. For elliptic flows, as can be seen from figure 2.16, this effect is predominantly destabilizing.

For the Burgers system in the elliptic regime, both the wavenumber vector and

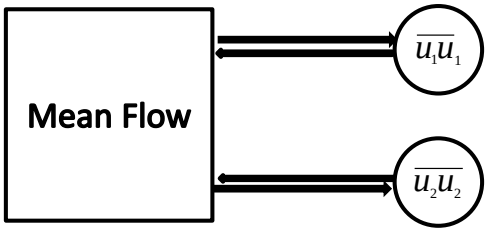

Figure 2.17: A schematic of kinetic energy exchange in an elliptic flow, as per the Burgers equations. The inertial processes are marked in filled arrows, their directions establish positive and negative states of production.

the Fourier velocity amplitudes undergo linear oscillations, with a constant phase difference and amplitude. Thus, the consequent velocity gradients are in a state of linear oscillation. The mode is stretched and compressed, alternately, along the axes in the plane of applied strain. The flow governed by the Burgers equations is in a state of neutral stability. There is a cyclic exchange of energy to and from the external source, representing negative and positive production, respectively. This is exhibited, schematically, in figure 2.17.

For the unstable modes, the out-of-plane transfer to and from R_{33} causes the Fourier amplitude vector to stay in a state of positive production. This mechanism occurs in two stages. In the first stage, the wavevector is being stretched due to the effect of the rate of strain tensor while the Fourier amplitude vector is in a state of positive production. Consequently, the components of the Fourier amplitude vector and the wavevector along the compressive eigen-direction of the rate of strain tensor are increasing. This would cause the fluctuating velocity gradients in this plane to increase to very high magnitudes. Such a mode would be stretched along this direction to very high dimensions and would be in violation of the divergence-free constraint. Thus, during this period pressure transfers fluctuating kinetic energy out of this direction to alleviate this conceivable stretching. Explicitly, when the

wavevector is being stretched, there is a large change in the e_3 component. Such motion of the unit wavenumber vector “pulls" the Fourier amplitude vector along with it causing the modal velocity vector to remain in the zone of positive production. The second phase occurs when the mode is being compressed due to the effects of the rate of strain tensor. This squeezing would cause the velocity gradients along this direction to decrease to very low magnitudes. Such a mode would be compressed to very small dimensions and would violate continuity. Thus, during this period pressure transfers fluctuating kinetic energy to the plane of applied strain to curtail this contraction. This re-alignment of the Reynolds stress ellipsoid re-aligns the fluctuating velocity toward the region of positive production.

This mechanism can be observed in figure 2.18, where the rising production for the mode is arrested by the out of plane energy transfer. As the modal production reduces, there is a transfer of energy to the plane of applied strain. Due to this mechanism, the production of turbulent kinetic energy for the mode remains positive through the cycle, leading to a state of instability.

2.5.3.3 SML behavior and overall range

Figure 2.19 exhibits the energy transfer during the aforementioned stages. These two stages represent the *statistically most likely* behavior, to be incorporated into models.

In figures 2.20,(a) and (b), the range of the modal intercomponent energy transfer is exhibited. Out of the hundreds of modes plotted, relatively few show significant growth. When contrasted to the corresponding figure for hyperbolic flows, figure 2.9, the number of unstable modes is much higher for this case. This is due to the banded nature of the elliptic flow instability (Pierrehumbert, 1986; Cambon *et al.*, 1994*b*), as opposed to the zero measure set of unstable modes for hyperbolic flows. Irrespective

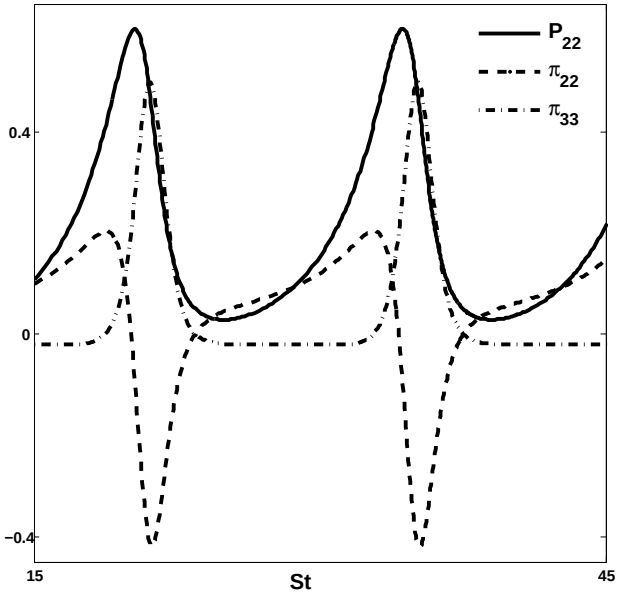

Figure 2.18: The evolution of flow statistics for a representative elliptic mode. The statistics have been scaled with the modal kinetic energy.

of these nuances, as can be observed, this distribution has a very significant degree of variance.

2.5.3.4 Topology of the unstable modes

As can be observed in figure 2.21, the stability of a mode in an elliptic flow is highly dependent on the modal alignment. Herein, the Floquet multipliers refer to the eigenvalues of the Monodromy matrix. The figure is motivated by a congruous illustration in Cambon *et al.* (1994*b*). The unstable modes form a band of instability, when viewed in wavevector space. Furthermore, with a change in the ellipticity parameter, the shape of this band changes, corresponding to the closed orbits of the unit wavevector trajectories. With an increment in the ellipticity parameter, this band shrinks and, in the limit of pure rotation, no unstable modes are extant.

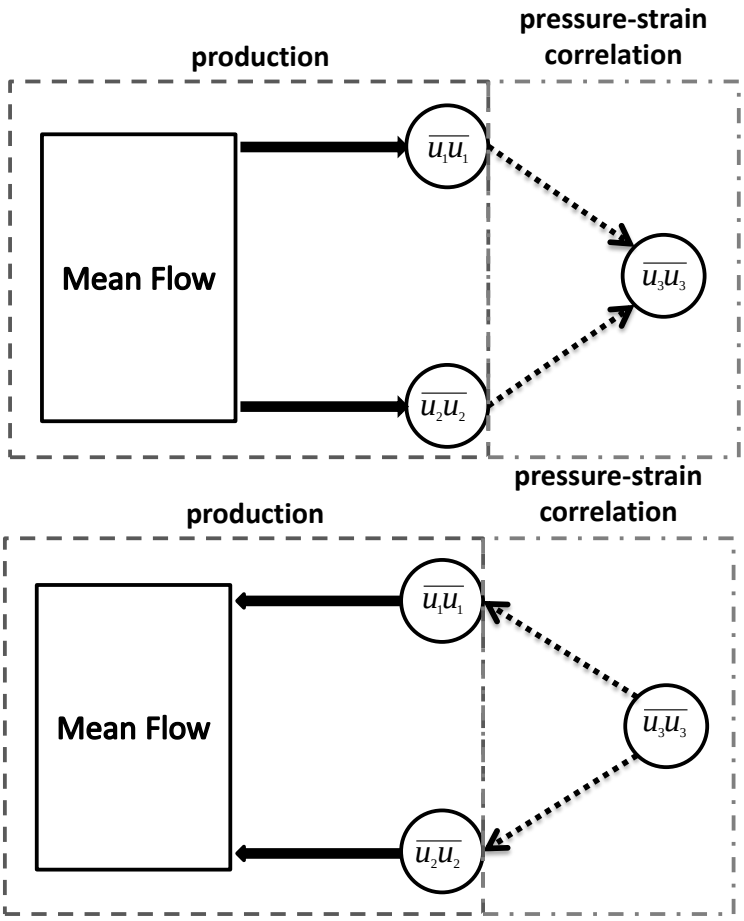

Figure 2.19: A schematic of kinetic energy exchange in an elliptic flow, (a) while the wavevector is being stretched and (b) while the wavevector is being compressed.

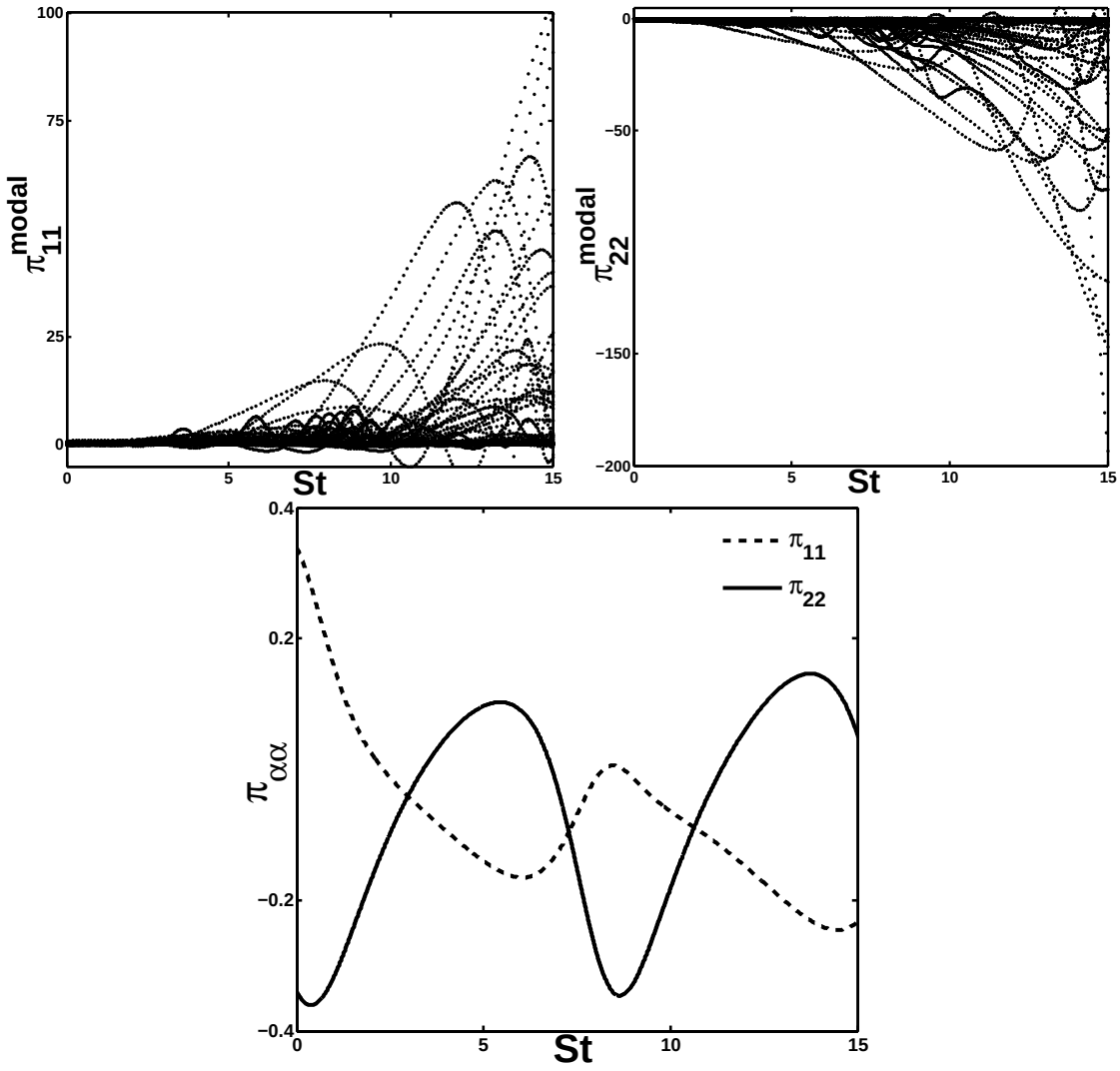

Figure 2.20: (a) The evolution of π_{11} for a set of randomly selected modes, (b) the evolution of π_{22} for a set of randomly selected modes, (c) The evolution of the diagonal components of the rapid pressure strain correlation tensor for the case of a representative elliptic flow.

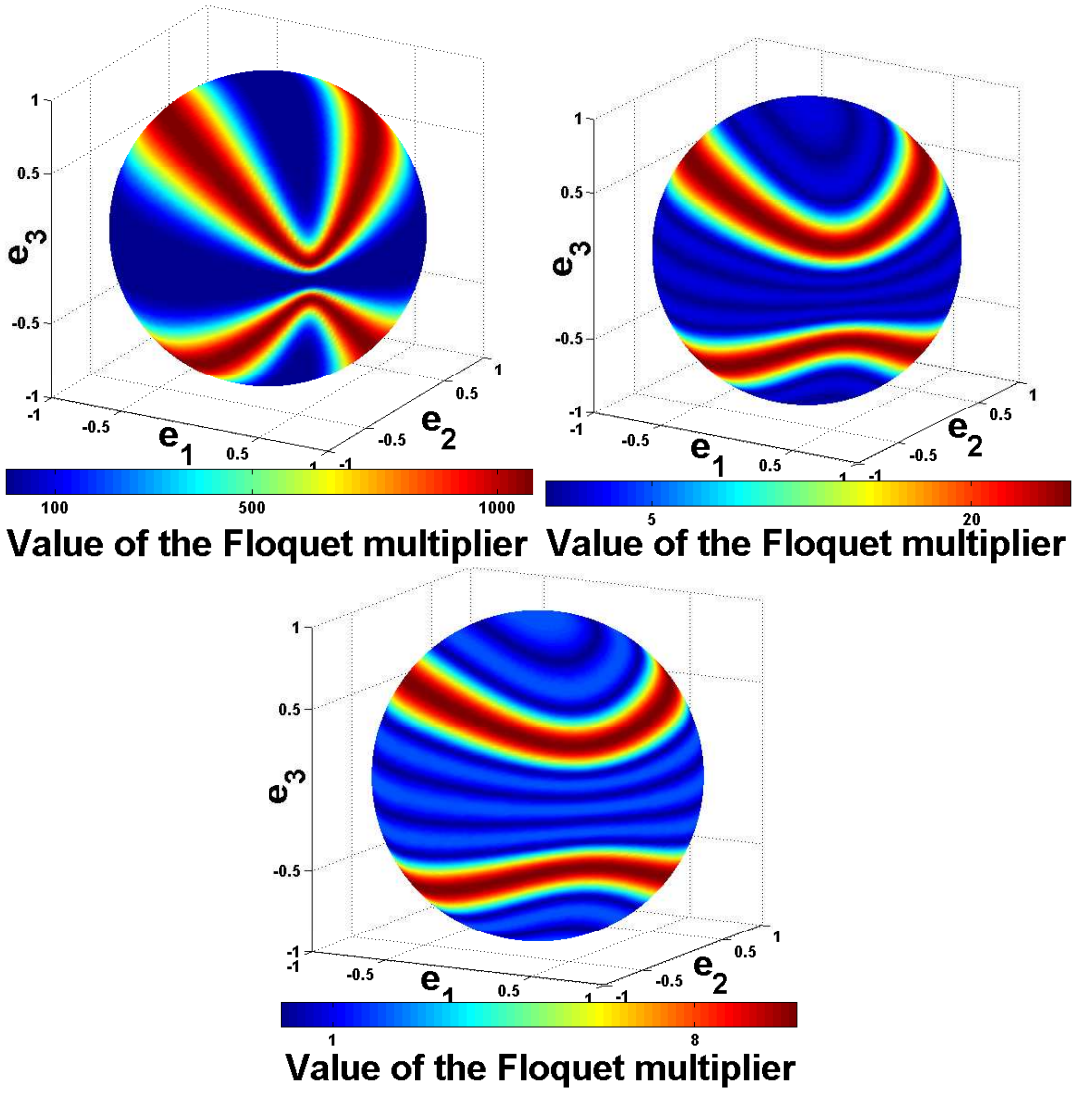

Figure 2.21: The zones of instability in unit wavenumber space at β=0.51, 0.65 and 0.75, respectively.

2.6 Importance of linear physics

In turbulence modeling, it is accepted that the linear physics provide a qualitative representation for many features of turbulent flows. Linear theories such as RDT omit the interaction of the fluctuating flow field with itself. This is justified via assumptions regarding the times scales (of mean and fluctuating distortions), a weak turbulence assumption, etc. However, the linear instabilities manifested in RDT obviate these assumptions. With the increase in the turbulent kinetic energy, the non-linear effects become more important and thus, linear theory cannot suffice beyond a limited time period. Thus, any conclusions derived in a purely linear limit may be equivocal when transferred to general turbulent flows. This ambiguity would be with respect to the validity of these RDT-based conclusions and the duration of their applicability. Cambon & Scott (1999) observe that for unstable flows, RDT contains the seeds of its own invalidity, thus limiting the duration of its applicability.

Before we present any closure modeling inferences based on our linear analysis, their pertinence to real turbulence is examined in the presence of non-linear effects. Key RDT results are contrasted against similar data from simulations at smaller values of $\frac{Sk}{\epsilon}$ (Here, ϵ refers to the turbulent energy dissipation rate and $S = \sqrt{S_{mn}S_{mn}}$). For such an investigation, we would require DNS data for *a range of values of* $\frac{Sk}{\epsilon}$, as well as *different values of the ellipticity parameter,* β. DNS results of such a wide and varied nature are not available as of now. Consequently, in lieu of DNS, the Langevin equation based stochastic model of Slooten & Pope (1997) is utilized to generate the required data for comparison. The Langevin model accounts for the phase scrambling effects of non-linear interactions using the Wiener process. Herein, we provide the germane model equations and their salient points.

The set of model equations is as follows:

$$\begin{aligned} d\hat{u}_i = &- \hat{u}_k \frac{\partial U_l}{\partial x_k}(\delta_{il} - 2e_i e_l)dt - \frac{1}{2}\frac{\epsilon}{k}(1 + \frac{3}{2}a_u)\hat{u}_i dt \\ &+ \frac{\gamma\epsilon}{k}(b_{ij} - II_b\delta_{ij})\hat{u}_j dt - \sqrt{a_u\epsilon}dW_i. \end{aligned} \tag{2.20}$$

$$\begin{aligned} de_i = &- \frac{\partial U_m}{\partial x_l}e_m(\delta_{il} - e_i e_l)dt - \frac{1}{2}\frac{\epsilon}{k}(a_e + a_u\frac{k}{u_s u_s})e_i dt \\ &- \frac{\gamma\epsilon}{k}(\delta_{ij} - 2e_i e_j)b_{jl}e_l - \sqrt{a_u\epsilon}\frac{u_i e_l}{u_s u_s}dW_l + \\ &\sqrt{\frac{a_e\epsilon}{k}}(\delta_{il} - e_i e_l - \frac{\hat{u}_i\hat{u}_l}{\hat{u}_s\hat{u}_s})dW'_l, \end{aligned} \tag{2.21}$$

where dW is an isotropic Wiener process and a_u, a_e and γ are coefficients of the model. For the formulation and benchmarking of the aforementioned, the reader is referred to Slooten & Pope (1997). For the solution of this set of Ito-stochastic differential equations, the Milstein method was utilized.

The performance of this Langevin model is exhibited in figure 2.22, where the results of the Langevin equation representation are compared to those from RDT based simulations.

Figures 2.6 and 2.21 exhibit the unstable modes, in a representative hyperbolic and an elliptic flow, with respect to their alignment. As can be observed, the unstable modes in an elliptic flow form a continuous band, of finite and sizable measure. However, the unstable modes in a hyperbolic flow lie on a set of almost zero measure. In the hyperbolic case, all other modes are either stable or can undergo limited transient growth. Furthermore, this state of alignment for the growing modes is in itself unstable and these modes can be forced off this alignment by any perturbations. This is evident in figure 2.2, wherein the hyperbolic flow instability is arrested by the pressure effects. This occurs via the transfer of turbulent kinetic energy out of the

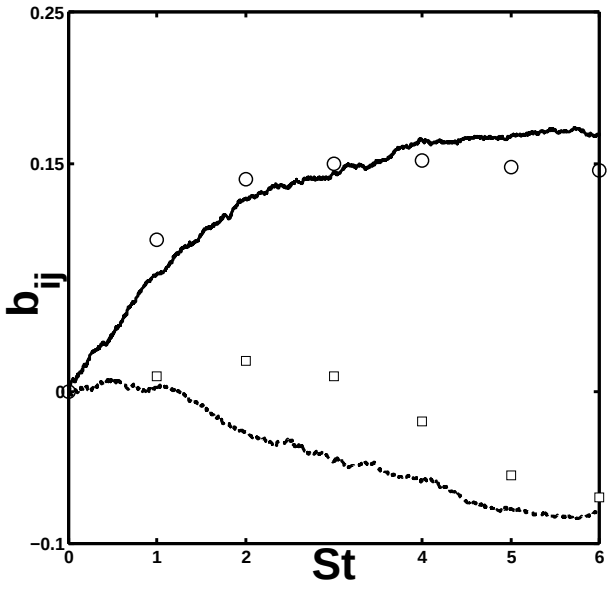

Figure 2.22: Comparison of the evolution of Reynolds stress anisotropies in a purely sheared flow. The lines correspond to a Langevin representation with $\frac{Sk}{\epsilon} = 2.36$, b_{33},− − −; b_{22},−.

plane of applied strain via the pressure strain correlation. In this vein, it is pertinent to question the exactitude of the hyperbolic instability, caused by this very small set of modes, in regimes where the non-linear effects become more and more significant.

Figure 2.23 compares the evolution of flow statistics for elliptic flows in the presence and absence of non-linear effects. As can be observed, the results are very similar in the absence of non-linear effects or at moderately high values of $\frac{Sk}{\epsilon}$. This is due to the finite measure of the set of unstable modes. However, this scenario does not persist for all elliptic flows. For instance, in purely rotating flows, it is known that linear theory is inconsistent with DNS results (Cambon & Scott (1999)).

Figure 2.24 compares the evolution of Reynolds stress anisotropies in a hyperbolic flow, for $\beta = 0.19$, as the non-linear effects become more important. The shifts in the dominant anisotropy component, from b_{22} to b_{33}, correspond to the migration

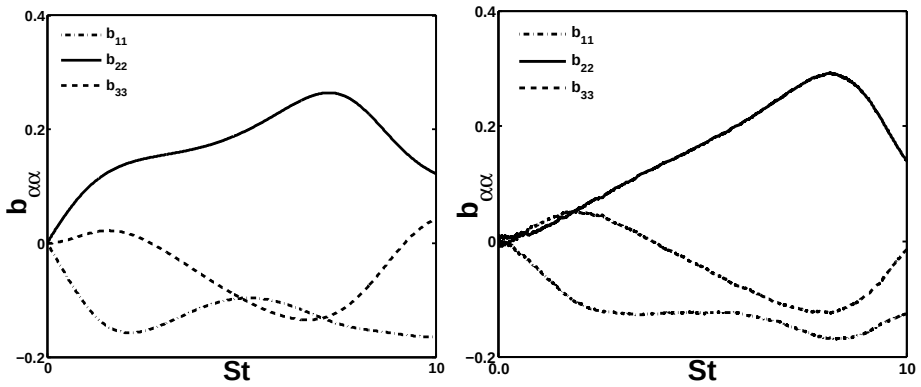

Figure 2.23: Comparison of the evolution of Reynolds stress anisotropies in a representative elliptic flow $\beta = 0.61$ (a) RDT results, (b) Langevin representation with $\frac{Sk}{\epsilon} = 50$.

of energetic modes from the seperatrix to the attractor, with the ensuing energy transfer from R_{22} to R_{33}. Due to the high number of such modes and their disparate initial locations, there are more than one of these shifts in the RDT simulation. This causes the transfer of energy between $\overline{u_c u_c}$ and the $\overline{u_3 u_3}$, as observed in figure 2.8. As is exhibited in figures 2.24, (a) and (b), the evolution of Reynolds stress anisotropies is very similar in the RDT limit and a moderately high $\frac{Sk}{\epsilon} = 25$. At a $\frac{Sk}{\epsilon} = 5$, exhibited in figure 2.24(c), the nonlinear effects are significant. Nevertheless, the dynamics determined by the linear physics, wherein the energy transfer is between $\overline{u_c u_c}$ and $\overline{u_3 u_3}$, are still reflected, qualitatively.

In summary, it is shown that the key phenomena observed in RDT based simulations, are *qualitatively relevant* even in the presence of moderate non-linear effects, for different regimes of flow. Thus, conclusions derived from the linear analysis *may be* pertinent for the development of pressure strain correlation models. Obligating pressure strain correlation models to retain the RDT physics is not just reasonable, but may be desirable (Speziale *et al.*, 1990, 1996).

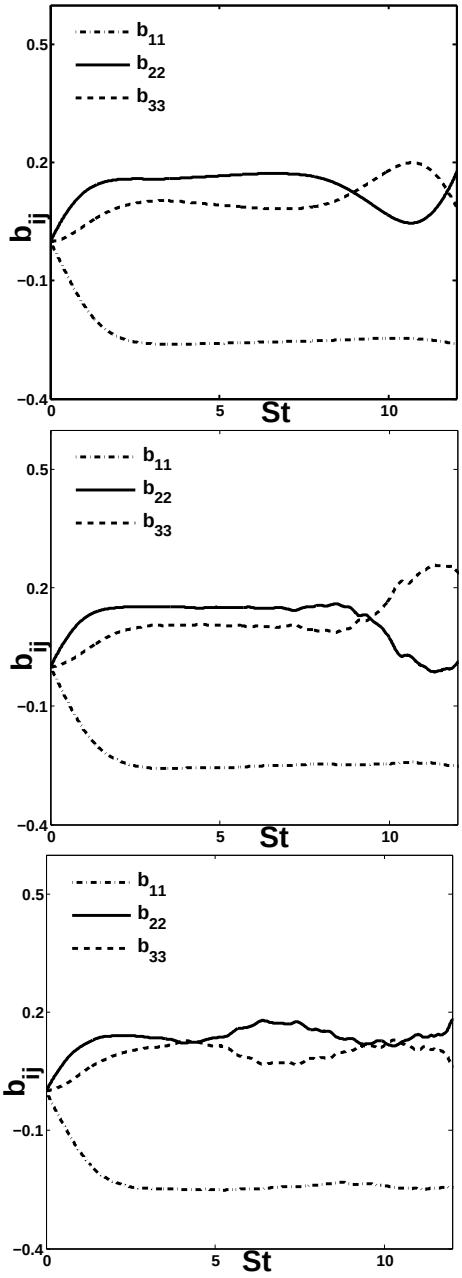

Figure 2.24: Comparison of the evolution of Reynolds stress anisotropies in a representative hyperbolic flow ($\beta = 0.19$) (a) RDT results, (b) Langevin representation with initial $\frac{Sk}{\epsilon} = 25$, (c) Langevin representation with initial $\frac{Sk}{\epsilon} = 5$.

2.7 Implications to closure modeling

It is reasonable to demand that, in the Rapid Distortion Limit, models for the pressure strain correlation reflect the dynamics determined by linear physics(Kassinos & Reynolds, 1994; Pope, 2000). Accordingly, in this section, while comparing RDT simulations to model predictions, we have restricted the models to terms that scale with the mean velocity gradient. Consequently, the observations made in this section pertain to the rapid part of the pressure strain correlation models.

The primary challenge in the single-point closure modeling of the pressure strain correlation is the representation of the non-local behavior of pressure in terms local tensors. According to RDT, we must have:

$$\pi_{ij}^{RDT} = \pi(S_{ij}, W_{ij}, e_i e_j \hat{u}_k \hat{u}_l), \tag{2.22}$$

wherein, the summation of $e_i e_j \hat{u}_k \hat{u}_l$ over wavenumber space would result in the M_{ijkl} tensor. The M_{ijkl} tensor contains both the dimensionality ($e_i e_j$) and the componentiality ($\hat{u}_i \hat{u}_j$) contributions. While componentiality information may be included in a single-point closure, the information in wavenumber space is non-local and consequently, not available in the one-point closure paradigm. Thus, in single-point closures π_{ij} is modeled in terms of local tensors:

$$\pi_{ij}^{model} = \pi(S_{ij}, W_{ij}, \hat{u}_k \hat{u}_l). \tag{2.23}$$

Herein, the summation of $\hat{u}_k \hat{u}_l$ over wavenumber space would result in the Reynolds stress tensor. Consequently, the pressure strain correlation has to be modeled with an incomplete basis, wherein the M_{ijkl} tensor is supplanted by the R_{kl} tensor. From a statistical perspective, this is tantamount to representing the dimensionality of an

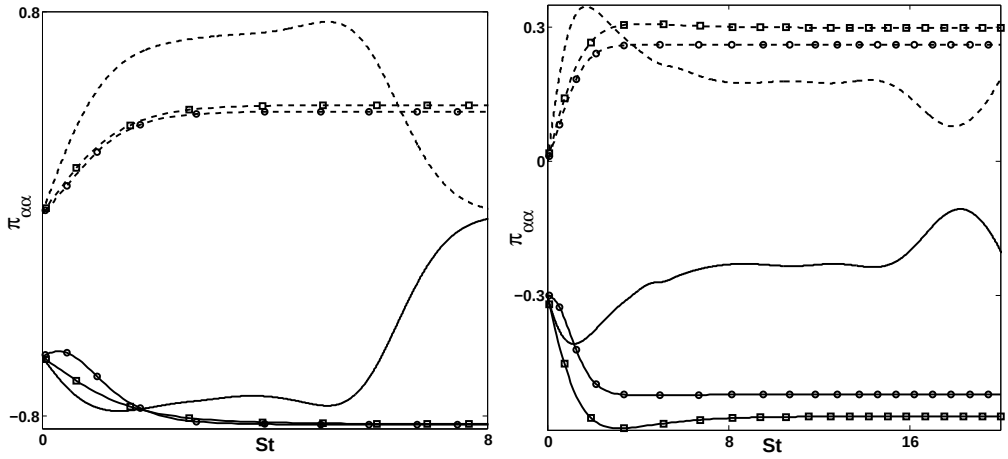

Figure 2.25: A comparison of the energy transfer predicted in the Rapid Distortion Limit by established models contrasted against linear physics for hyperbolic flows. (a) Plane strain, (b) $\beta = 0.36$. π_{33},− − −; π_{cc},—; SSG, circles; LRR, squares.

unknown ensemble of modes with a hypothetical single mode. This severely limits the features of the action of pressure that such models can replicate. As was mentioned in the Introduction, this truncated representation precipitates a closure modeling problem, wherein this system is ill-posed. As the preeminent action of pressure is the intercomponent energy transfer, to ensure any degree of fidelity the models must be qualitatively consistent with this redistribution. This energy transfer affects various aspects of the turbulent flow: stability, invariant sets and their bifurcation, and the holistic nature of dynamics. The manifestation of each of these features depends on the regime of flow. To evaluate the measure of adherence to IET physics afforded by models, henceforth, the components of the π_{ij} tensor are contrasted in different regimes. For these comparisons, the models are evaluated in the Rapid Distortion Limit.

2.7.1 Closure modeling: different flow regimes

Hyperbolic flows: As exhibited in figure 2.8, the predominant energy transfer for hyperbolic flows is from the compressional eigendirection to the R_{33} component. As can be seen in figure 2.25, after a very short transient, π_{cc} and π_{33} balance each other. The established models are not sentient of this and for the case of plane strain, under predict the out of plane energy transfer. Consequently, they transfer a large part of the turbulent kinetic energy from the compressional eigendirection to the extensional. Ignoring this characteristic causes the models to generate inaccurate predictions. Furthermore, the eigendirections of the mean velocity gradient tensor do not remain stationary. With increment in the ellipticity parameter, β, the eigendirections shift toward each other, as exhibited in figure 2.10. The established models do not heed this shift and thus, even their transfer from the compressive eigendirection becomes exorbitant. This progressively impairs their ability to mimic the system's behavior in the Rapid Distortion Limit.

Pure shear flows: Pure shear flow represents the point of bifurcation of quadratic flows and therefore, the evolution of flow statistics is asymptotic. As can be observed in figure 2.26, the energy redistribution is significant for a very short duration, while the modes in the flow are aligning with the eigenaxes. Subsequently, the transfer abates quickly. Established models are not cognizant of this transient nature arising due to the evolution of the wavevector alignment. Such models continue to predict stationary states for the energy transfer in the Rapid Distortion Limit. Consequently, their predictions of flow statistics are incorrect, quantitatively and qualitatively.

Elliptic flows: As outlined in the figure 2.19, the energy transfer is cyclic, to and from the plane of applied strain. With just a local basis, the established models cannot capture this oscillatory behavior. This is evident in the figures 2.27, wherein

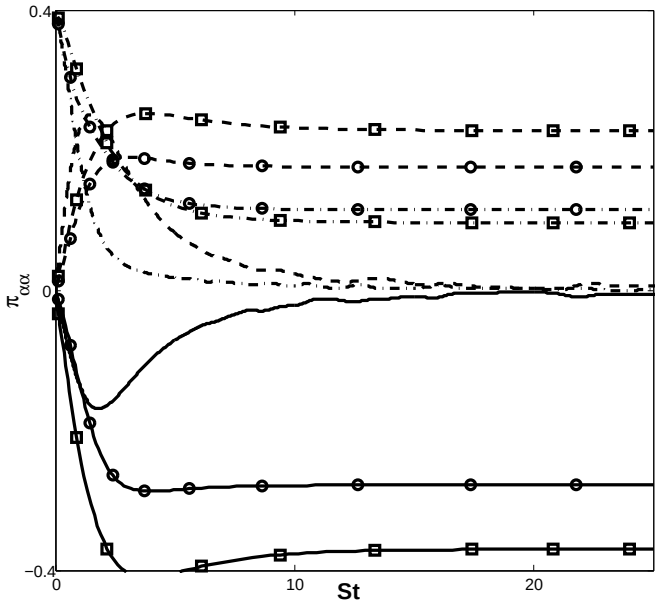

Figure 2.26: A comparison of the energy transfer predicted in the Rapid Distortion Limit by established models contrasted against linear physics, for pure shear flows. π_{33},− − −; π_{11},—; π_{22},•−; SSG, circle ; LRR, squares.

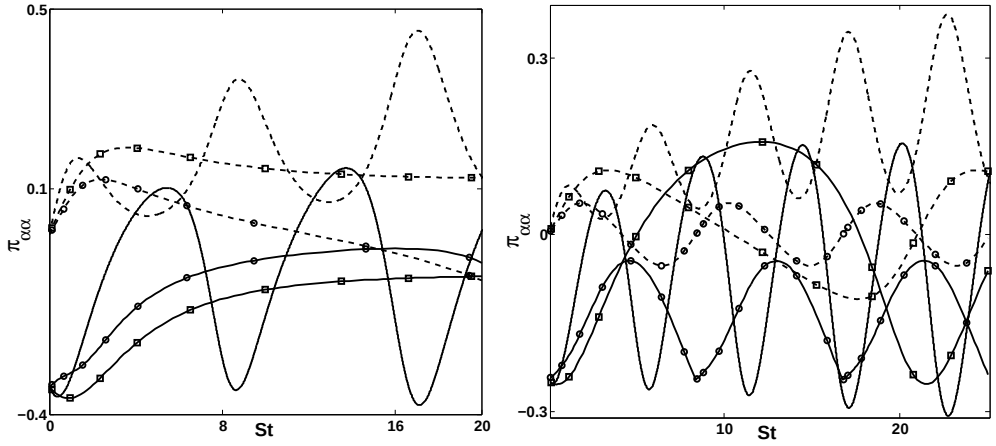

Figure 2.27: A comparison of the energy transfer predicted in the Rapid Distortion Limit by established models contrasted against linear physics for elliptic flows. (a) $\beta = 0.64$, (b) $\beta = 0.81$. π_{33},− − −; π_{cc},—; SSG, circles; LRR, squares.

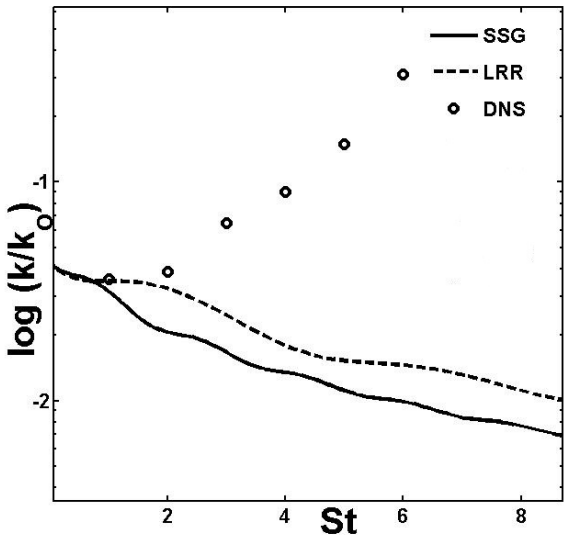

Figure 2.28: A comparison of the turbulent kinetic evolution predicted by established models contrasted against DNS, for an elliptic flow with β =0.87.

the established models predict oscillatory transfer but these oscillations have no congruence with the RDT dynamics. Accordingly, the predicted evolution of the flow field is not in conformity with linear physics.

2.7.2 Closure modeling: different flow features

Now, we address the various flow features that are affected by IET and the tractability of each of these to single-point closure modeling. Illustrative calculations from current single-point closures, in the Rapid Distortion Limit, are provided to further bolster the arguments presented hereupon.

Flow instabilities: Both the elliptic flow instability and the hyperbolic instability, are induced due to the alignment of specific modes. This is exhibited in figures 2.7 and 2.21, where we exhibit the relationship between initial modal alignment in wavenumber space and modal stability. For the hyperbolic flow, only a very small

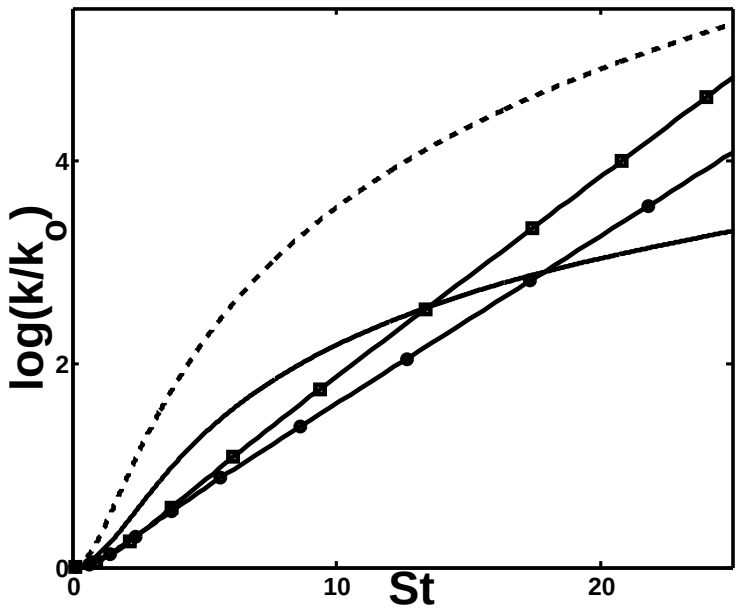

Figure 2.29: A comparison of the turbulent kinetic evolution predicted by established models in the Rapid Distortion Limit contrasted against linear physics, for a purely sheared flow. Euler RDT,—; Burgers RDT,– – –; SSG, circles; LRR, squares.

set of modes, aligned with the extensional eigendirection, exhibit prolonged unstable behavior. For pure shear flows, the set of unstable modes is relatively larger. However, only the modes aligned with the “vertical" direction, show significant growth. This scenario is further exacerbated in the case of the elliptic flow instability wherein only a narrow “band" of oscillatory modes exhibit unstable behavior. Additionally, the shape of this instability band is dependent on the ellipticity parameter. In this light, it is not surprising that the predictions from one-point closures are contrary to linear physics. This can be observed in figure 2.28 where established models predict that the state of turbulence will decay for an elliptic flow with β =0.87, while DNS (Blaisdell & Shariff, 1996) exhibits unstable behavior. In the same vein, a key feature of pure shear flows is the non-modal nature of their instability. This results in the linear growth of the turbulent kinetic energy. As can be seen in figure 2.29,

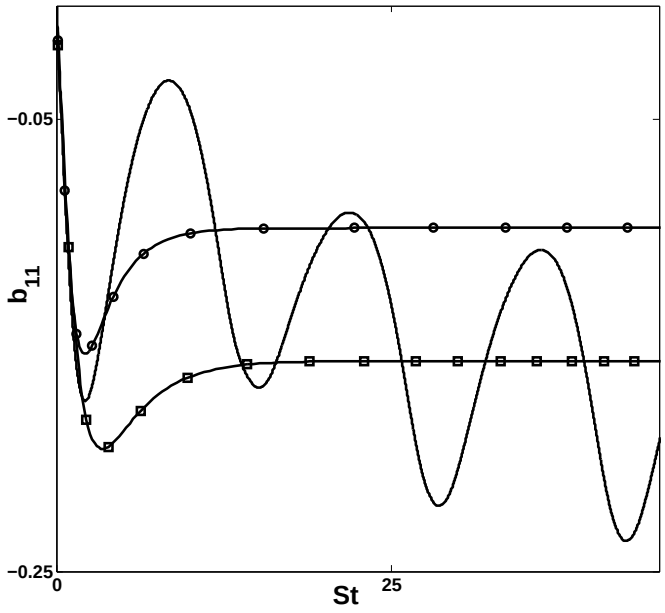

Figure 2.30: A comparison of the anisotropy evolution predicted by established models in the Rapid Distortion Limit contrasted against linear physics, at $\beta = 0.55$. Euler RDT,—; SSG, circles; LRR, squares.

established models are unable to replicate this fundamental attribute and predict exponential growth, which is not even achieved in the "pressure-released" Burgers system.

In summary, linear physics has a structuring effect on the flow, wherein select modes are stabilized or destabilized contingent upon their alignment. This information about modal alignments is not contained in the basis of single-point closures. Thus, *faithful replication of these flow instabilities is not within the purview of single-point closures.*

The bifurcation in the system: In transitioning from hyperbolic to elliptic flows, the system undergoes a saddle-node bifurcation. Consequently, the evolution of the Reynolds stress anisotropies changes from stationary states to oscillatory solutions. This has been addressed in Girimaji (2000). However, this bifurcation is engendered

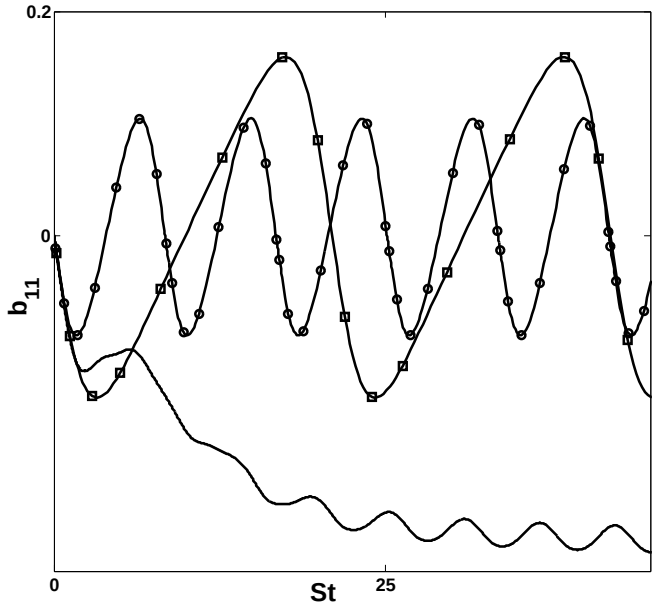

Figure 2.31: A comparison of the anisotropy evolution predicted by established models in the Rapid Distortion Limit contrasted against linear physics, at $\beta = 0.81$. Euler RDT,—; SSG, circles; LRR, squares.

in the wavevector evolution equation. Thus, popular *one-point closure models are not able to capture the location or the nature of this change in the system's dynamics*. This is exhibited in figure 2.30, where the RDT calculations reveal oscillatory behavior while models continue to predict stationary states.

The oscillatory behavior in elliptic flows: In this regime, RDT indicates that flow statistics (such as the Reynolds stress anisotropies) exhibit bilinear oscillations. Herein, the oscillations have a varying amplitude about a time dependent mean. On the contrary, the models predict linear oscillations, exhibiting a constant mean and amplitude, as observed in figure 2.31. To reproduce a time dependent mean and amplitude with an incomplete basis, the models would have to resort to limit cycle oscillations to mimic bilinear phenomena. This would require a rapid pressure strain correlation that is non-linear in the Reynolds stress anisotropies, that would violate

guidelines obligated by physics. Prior investigations, such as Sjogren & Johansson (2000), have employed models that are non-linear in the mean velocity gradients to capture said oscillatory behavior. In turbulent flows, the oscillations of flow statistics are caused, primarily, due to the dynamics of the wavevector and are thus, outside the scope of one-point modeling. *No permutations of such local tensors can enable one-point closures to replicate this behavior faithfully.*

Uncertainty Quantification: The Reynolds stresses express the componentiality of the turbulent flow field and do not provide a complete description of the internal structure of the flow. For the rapid distortion equations, the specification of the Reynolds stresses does not lead to a unique evolution trajectory. Instead of a single unique solution once the Reynolds stress tensor has been specified, there is a range of permissible solutions. In figure 2.32 this range is shown for a representative hyperbolic flow (plane strain) and an elliptic flow (β =0.64). The well distributed ensemble mimics the statistically most likely behavior. In practical flows, the distribution can be far from such a well distributed ensemble, due to forcing, initial and boundary conditions. In essence, the distribution of the modes accounts for the history of the particular flow. It can be observed that even for a purely irrotational case of plane strain, the wavenumber information is still essential. This is at odds with Kassinos & Reynolds (1994), wherein the requirement of additional tensors is restricted to strongly rotational mean flows. For the closed streamline flow, we observe that the behavior of popular models corresponds to periodic behavior with a frequency that can't be replicated via any ensemble of modes. Thus, the predictions are not just incorrect for this ensemble; they are incorrect for all possible ensembles. For both these flow regimes, the turbulent kinetic energy evolution is not universal and is notably dependent on the alignments of the modes in the flow. Bereft of wavevector information, *high fidelity modeling of such behavior by one-point closures remains*

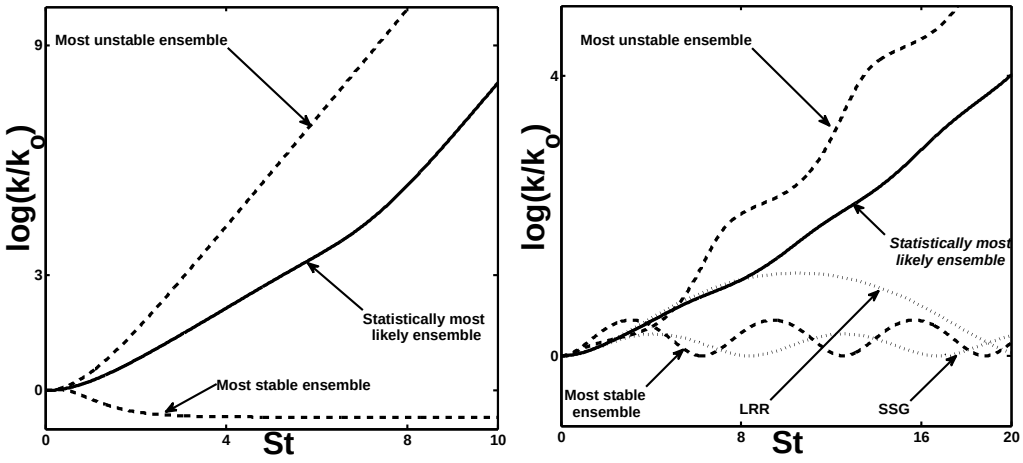

Figure 2.32: The range of permissible behavior for a representative hyperbolic flow, β =0, and an elliptic flow, β =0.64.

infeasible. Consequently, modeling the statistically most likely behavior, depicted in Section IV, is an expedient recourse. Even with a model based on the SML behavior, variations in behavior must be considered as a possible uncertainty in the model. Further study must address the issue of Uncertainty Quantification for such closures.

Tables 2.2 and 2.3 contrast the behavior of flow statistics according to linear physics against that predicted by established models. It is observed that in spite of the attempts of one-point closures to capture the dynamics of elliptic flows faithfully, the results are disappointing. For a large measure of the elliptic regime, the models are not even cognizant of any oscillations. When the models manage to predict oscillatory dynamics, these have no correspondence to the cyclic behavior of the system, qualitatively or quantitatively. With respect to the evolution of the Reynolds stress anisotropies and the turbulent kinetic energy in elliptic flows, the amplitudes of these oscillations are typically small when compared to the overall trend of their evolution. This has been exhibited in RDT based simulations (Mishra & Girimaji, 2010) and DNS (Blaisdell & Shariff, 1994). In this light, it may be expedient to focus

Regime	Burgers RDT	Euler RDT	Established models	Nonlinear turbulence
Hyperbolic	exponential growth	exponential growth	exponential growth	exponential growth
Pure shear	quadratic growth	linear growth	exponential growth	growth
Elliptic	neutrally stable	exponential growth	decay	exponential growth

Table 2.2: A comparison of the linear stability behavior governed by physics, contrasted against established models.

on capturing the mean of these oscillations. As the amplitude of the oscillations is much smaller than said mean, such a prediction would still have engineering utility. Furthermore, the energy transfer in hyperbolic flows can be replicated by tuning the models to transfer energy out of the plane of applied strain from the compressive eigendirection. Such a model would have to be cognizant of the migration of the eigen-axes with changes in the mean flow. To achieve this would require models to utilize the linear physics regarding the structure of turbulence. Accommodation of this degree of information would require the model coefficients to vary. Except for a few notable exceptions, such as Ristorcelli *et al.* (1995), Girimaji (2000) these coefficients have been considered constants, whose values are assigned from algebraic relations and numerical simulations. Such a model would be non-linear in the mean velocity gradients and thus, would violate one of the conditions obligated upon an ideal model. However, this might represent the optimal substitute for wavevector information as the wavevector evolution is contingent upon the mean velocity gradients.

2.8 Conclusions

In the field of turbulence modeling, pressure-strain correlation poses a unique set of closure challenges. This is primarily due to the fact that pressure is inherently

Regime	Burgers RDT	Euler RDT	Established models	Nonlinear turbulence
Hyperbolic	attracting fixed point	saddle nodes	fixed points	fixed points
Pure shear	asymptotic fixed points	asymptotic fixed points	fixed points	asymptotic fixed points
Elliptic	linear oscillations	bilinear oscillations	linear oscillations	limit cycle

Table 2.3: A comparison of the asymptotic behavior governed by physics, contrasted against established models.

non-local in character and yet, due to pragmatic considerations, one is constrained to model its effects with a one-point (local) model. From a statistical view-point, this difficulty can be expressed as modeling the statistics of an unknown ensemble of fluctuation wavevector modes with a hypothetical singleton mode. The loss of wavevector information is particularly detrimental as it plays a key role in determining the manner of Intercomponent Energy Transfer and ultimately, the stability of the perturbation mode. In the classical one-point modeling approach, the lack of the wavevector details is compensated by performing an empirical calibration of the coefficients leading to the closure. While such an approach has served reasonably well over the decades, serious deficiencies remain. First and foremost, the wavevector ensemble in the calibration flow can be very different from that in the test flow resulting in poor predictions. More importantly, owing to the lack of physical basis, the empirical approach does not allow for:

1. clear avenues for improvement and

2. reasonable basis for estimating the uncertainty involved.

We propose that both improvement in prediction fidelity and uncertainty estimation can be accomplished within the one-point closure framework if and only if wavevector dynamics and IET can be characterized in terms of mean velocity gra-

dients. If such characterization can be accomplished, then the coefficients in the one-point closure model can be rendered functions of velocity-gradient invariants to bring about the requisite IET dynamics. Thus motivated, we perform the following sequence of studies in the RDT limit of turbulence for two-dimensional mean flows:

1. First we demonstrate the critical role played by IET in determining the stability of perturbation modes. It is established that pressure-driven wavevector-dependent IET generally stabilizes perturbations in hyperbolic flows but destabilizes them in elliptic flows.

2. The wavevector dynamics, specifically the fixed point behavior and its bifurcation, are clearly established as a function of mean velocity gradient invariant.

3. For different mean velocity gradients, the IET is characterized as a function of wavevector orientation. The resulting effect on anisotropy is also established.

4. The topology of the most energetic wavevector modes that dominate the turbulence statistics is categorized for each mean-velocity type.

5. Finally, we identify the statistically most likely IET behavior for each mean velocity-gradient and further establish the range of possible behavior.

Future work will address incorporation of the SML behavior into traditional one-point closures by rendering model coefficients as functions of mean velocity-gradient invariants. Further research is also underway into developing a framework for quantifying the possible uncertainty in the SML closure utilizing the range of possible IET behavior investigated in study (e), outlined above. Another future research direction is to characterize wavevector dynamics in general three-dimensional mean flows.

3. ON THE REALIZABILITY OF PRESSURE-STRAIN CLOSURES

3.1 Overview

The realizability condition for statistical models of turbulence is augmented to ensure not only that the Reynolds stress tensor is positive semi-definite, but the process of its evolution is physically attainable as well. The mathematical constraints due to this process realizability requirement on rapid pressure strain correlation are derived. The resulting constraints reveal important limits in the intercomponent energy transfer and the consequent flow stability characteristics as a function of the mean flow. Unexpectedly, the realizability constraints are most stringent for the case of purely sheared flows rather than elliptic flows. The relationship between the constraints and flow stability is explained. Process realizability leads to closure model guidance not only at the two-component limit of turbulence (as in the classical realizability approach) but throughout the anisotropy space. Consequently, the domain of validity and applicability of current models can be clearly identified for different mean flows. A simple framework for formulating a rapid pressure-strain correlation model without resorting to nonlinear expressions in the Reynolds stresses is identified.

3.2 Introduction and overview

Statistical models of turbulence draw heavily from mathematical precepts for closure expression form and on physical concepts for function. The realizability principle holds a crucial place in the model development process as it constrains the model system behavior to be within mathematically permissible limits. Schumann (1977) was the first to articulate the realizability constraint in the context of turbulence closures, requiring models to yield a Reynolds stress tensor that is positive semi-definite. The

utility of Schumann realizability constraints is well established in second moment closure literature. The strong (Lumley, 1978) and weak (Pope, 1985a) realizability techniques are the two prominent approaches for implementing classical realizability constraints. Unrealizable models can lead to problems in numerical convergence and even numerical instability (Hanjalic & Launder, 2011). Realizability considerations allow for the inclusion of additional closure features yielding better overall fidelity, for instance, as observed in Shih *et al.* (1987). Many advanced modeling approaches, such as Johansson & Hallback (1994) and Sjogren & Johansson (2000) use realizability adherence to mandate the entire closure framework and the formulation of the models.

While the realizability principle as currently formulated is useful, it is not complete or sufficient to ensure that the Reynolds stress evolution is physical. For example, evolution of Reynolds stress from one physically permissible state to another is permitted even if the ensuing Reynolds stress dynamics are non-physical. Another crucial deficiency of classical realizability lies in its applicability only at the two-component (2C) limit of turbulence (Schumann, 1977) and its inability to provide modeling guidance elsewhere in the Reynolds stress anisotropy space. Rubinstein & Girimaji (2006) point out that 2C limit represents a closure singularity as the correspondence between the Reynolds Stress Transport equations and the underlying equation for the fluctuating field is not unique. Therefore, any realizability constraint applied on the Reynolds stress equation in this limit does not accurately represent the dynamics of the underlying fluctuating field evolution. Furthermore, adherence to classical realizability necessitates closure expressions to be complex nonlinear functions of the Reynolds stress tensor. Not only is this physically inconsistent for the rapid pressure-strain correlation but it also leads to spurious oscillations in the vicinity of the 2C state. Even models satisfying the classical realizability condi-

tions can transition to unrealizable zones near the 1C state (Speziale *et al.*, 1994). Additionally, classical realizability conditions lack robustness. For instance, under the rotation of the principal axes of the Reynolds stress tensor, they can lead to singularities (Speziale & Durbin, 1994).

It has been exhibited in Girimaji (2004) that unrealizable Reynolds stress dynamics precede and lead to unrealizable Reynolds stresses. Evidently, classical realizability constraints are insufficient as they address the *effect* and not the *cause* of realizability violations. Thus, there exists a clear need to expand the formulation of realizability constraints to ensure that the process of evolution from one Reynolds stress state to another is also mandated to be physical. Classical realizability focuses in the *statistical state* of the flow and not the *statistical process* underlying its evolution. Concordantly, in this article the classical realizability framework is appellated as *state realizability*. Necessitating the evolution path to be realizable addresses the statistical process and hence, it is named *process realizability*.

The first investigation addressing the realizability of Reynolds stress dynamics was reported in Shih *et al.* (1990). Using a simplified representation of the spectrum tensor in very weakly anisotropic turbulence, the authors derived a linear model for the rapid pressure strain correlation and postulated its range of validity. Speziale & Durbin (1994) and Pope (1985) also address process realizability, albeit indirectly using stochastic analysis. Girimaji (2004) proposed the concept of comprehensive realizability and instituted constraints for the rapid pressure strain correlation in order to satisfy the Cauchy's inequality. The objective of this investigation is to extend realizability considerations to include the Reynolds stress evolution dynamics; derive precise constraints that can be employed in closure model development and evaluation; and establish a framework to extract physical insight therefrom. The realizability analysis is presented in the context of Reynolds averaged statistics in

this article. However, the implications can be extended to filtered statistics as well, using the averaging invariance principle (Germano, 1992).

After a brief overview, we derive and discuss the process realizability constraints in Section II. In Section III, the insight afforded by the process realizability framework is explicated. Specific discussions in Section III include the broader applicability of process realizability, their ability to highlight energy redistribution features and provide more precise model development guidance. Section IV deals with the application of the process realizability constraints to popular pressure strain correlation models and examining the validity of these closures. In Section V, we present a simple procedure to formulate a prototypical linear model heeding process realizability and contrast the new closure against well-established counterparts. The article concludes with a summary and discussion of results in Section VI.

3.3 Mathematical formulation of process realizability

Realizability is an important concept in the statistical modeling of any physical process and is applicable to closure representations of all statistics. Ideally, it would be expedient to have not just the Reynolds stresses, but their derivatives to be realizable as well. This would ensure that the complete evolution of the Reynolds stress is physically permissible at all orders. However, the requirement of all higher order derivatives being realizable is difficult to implement. As a practical closure modeling requirement, it is reasonable to mandate that the substantiative derivative of the Reynolds stresses, that is, the Reynolds stress dynamics be realizable.

The Second Moment Closure approach entails solving the Reynolds Stress Trans-

port equations:

$$\begin{aligned}
\frac{dR_{ij}}{dt} &= P_{ij} - \frac{\partial}{\partial x_k} T_{ijk} + \pi_{ij} - \epsilon_{ij}, \\
\text{where, } R_{ij} &= \langle u_i u_j \rangle, \pi_{ij} = \left\langle p(\frac{\partial u_i}{\partial x_j} + \frac{\partial u_j}{\partial x_i}) \right\rangle, \\
\epsilon_{ij} &= -2\nu \left\langle \frac{\partial u_i}{\partial x_k} \frac{\partial u_j}{\partial x_k} \right\rangle \text{ and } P_{ij} = -R_{jk} \frac{\partial U_i}{\partial x_k} - R_{ik} \frac{\partial U_j}{\partial x_k}, \\
\text{and } T_{kij} &= -\nu \frac{\partial \langle u_i u_j \rangle}{\partial x_k} + \frac{2}{3} \delta_{ij} \langle u_k p \rangle + \langle u_i u_j u_k \rangle.
\end{aligned} \tag{3.1}$$

wherein U represents the mean flow field; lowercase variables represent the fluctuating field and $\langle . \rangle$ represents the Reynolds averaging operator. The fluctuating pressure, p is governed by a Poisson equation, explicitly:

$$\frac{1}{\rho} \nabla^2 p = -2 \frac{\partial U_i}{\partial x_j} \frac{\partial u_j}{\partial x_i} - \frac{\partial^2}{\partial x_i \partial x_j} (u_i u_j - \langle u_i u_j \rangle). \tag{3.2}$$

On this basis, the pressure field is decomposed into its linear (rapid) and non-linear (slow) components: $p = p^{(r)} + p^{(s)}$. Concordantly, the pressure strain correlation is divided as $\pi_{ij} = \pi_{ij}^{(r)} + \pi_{ij}^{(s)}$.

Of the turbulence processes delineated above, the production term, P_{ij}, does not require closure and thus, is consistent with realizability. The other turbulence processes are unclosed and require models for their closure. Realizability violations are engendered by unphysical or inconsistent aspects in these closure. Consequently, process realizability entails the investigation of the model expressions for the unclosed terms.

In this paper we will restrict our attention to the realizability issues pertaining to rapid pressure strain correlation closures. While models for the other processes can potentially lead to violations as well, their transgressions are expected to be less severe. For instance, the turbulent transport term, T_{ijk}, is often modeled using

a gradient-diffusion paradigm. This is deemed physically achievable as it has the same functional form as a molecular transport term, except with an enhanced (turbulent) diffusivity coefficient. The combination of isotropic dissipation and linear slow pressure-strain correlation models leads to exponential decay of the Reynolds anisotropy. For example, with reference to the model presented by Rotta (1951), the evolution equation of the Reynolds stress anisotropies reduces to

$$\dot{b}_{ij} = \frac{\epsilon}{k}(1 - C_R)b_{ij}, \tag{3.3}$$

where $b_{ij} = \frac{\overline{u_i u_j}}{2k} - \frac{\sigma_{ij}}{3}$ denotes the Reynolds stress anisotropy; k, the turbulent kinetic energy and ϵ, the dissipation. Clearly, this model combination leads the anisotropy evolution trajectory away from the troubling 2C limit for all anisotropic initial states of turbulence. Consequently, this process of sequential exclusion indicates the key transgressor for the realizability violations to be the rapid pressure term. In this regard, it has been exhibited that the primary cause for realizability violations is the rapid component of the pressure strain correlation Sambasivam *et al.* (2004) and in this investigation, we focus on its dynamics.

The correlation between the rapid pressure and the fluctuating velocity gradient is given by (Pope, 2000):

$$\left\langle \frac{p^{(r)}}{\rho}\frac{\partial u_i}{\partial x_j} \right\rangle = -\frac{1}{2\pi}\frac{\partial U_k}{\partial x_l}\iiint \frac{1}{|r|}\frac{\partial^2 R_{il}^{+}}{\partial x_k \partial x_j} d\vec{r}, \tag{3.4}$$

where R^{+} is the two-point correlation and r is the separation vector. The forth order $\mathbf{M}$ tensor is defined as an integral of the two-point correlation (Pope, 2000):

$$M_{iljk} = -\frac{1}{4\pi}\int \frac{1}{|r|}\frac{\partial^2 R_{il}^{+}}{\partial r_j \partial r_k} d\vec{r}. \tag{3.5}$$

The concordant relationship between the **M** tensor and the rapid pressure strain correlation is given by:

$$\pi_{ij}^{(r)} = 2\frac{\partial U_l}{\partial x_k}(M_{kjil} + M_{ikjl}). \tag{3.6}$$

In homogeneous flows, the turbulence processes can be examined in Fourier space. In the Fourier analysis, the fluctuation is characterized in terms of the wavenumber vector, $\boldsymbol{\kappa}(t)$ and $\hat{\mathbf{u}}$, $\hat{p}$, the corresponding Fourier amplitudes and pressure coefficients.

$$u_i(\mathbf{x},t) = \sum \hat{u}_i(\boldsymbol{\kappa},t)exp(i\boldsymbol{\kappa}\cdot\mathbf{x}), \quad p^{(r)}(\mathbf{x},t) = \sum \hat{p}(t)(\boldsymbol{\kappa},t)exp(i\boldsymbol{\kappa}\cdot\mathbf{x}). \tag{3.7}$$

In this representation, the **M** tensor is expressed as

$$M_{ijkl} = \sum \frac{\hat{u_i}^* \hat{u_j} \kappa_k \kappa_l}{\kappa^2}. \tag{3.8}$$

Modeling the rapid pressure strain correlation is tantamount to modeling the **M** tensor. Thus, a realizable closure model for the M tensor is critical for a realizable rapid pressure strain correlation. In the following section, we introduce the process realizability constraints, along with their underlying mathematical and physical rationale. The key consideration underlying these conditions is the positive semi-definite nature of the spectrum tensor, Φ_{ij}, and consequently the Fourier coefficients of the two-point velocity correlation,$\hat{R}_{ij}$. The requisite tensors are defined in Fourier space as

$$\Phi_{ij} = \frac{1}{(2\pi)^3}\iiint_{-\infty}^{\infty} e^{-i\vec{\kappa}.\vec{x}} R_{ij}^{+}(\vec{r},t)d\vec{r}, \quad \hat{R}_{ij} = \hat{u_i}^* \hat{u_j}, \tag{3.9}$$

where R_{ij}^{+} denotes the two-point velocity correlation. The relationship between the

aforementioned is denoted by

$$\Phi_{ij}(\bar{\kappa}, t) = \sum_{\kappa} \delta(\bar{\kappa} - \kappa)\hat{R}_{ij}(\vec{\kappa}, t), \tag{3.10}$$

where $\bar{\kappa}$ is the continuous wavenumber, κ is the discrete wavenumber and δ is the delta function.

3.3.1 Prior process realizability constraints

We review the constraints on the **M** tensor that have been introduced heretofore. Pursuant to the paradigm in Shih *et al.* (1990), the spectrum tensor *induced by the closure for the pressure strain correlation* must be positive semi-definite. Since process realizability does not consider higher order derivatives, it must be emphasized that it is only possible to formulate necessary conditions for realizability and not sufficient conditions. Girimaji(2004) expressed this via two necessary (but not sufficient) conditions on the **M** tensor.

First lower bound on the M tensor: *The **M** tensor must be positive semi-definite.* The Poisson equation for the rapid component is:

$$\nabla^2 p^{(r)} = -2\frac{\partial U_i}{\partial x_j}\frac{\partial u_j}{\partial x_i}. \tag{3.11}$$

Multiplying this by the rapid pressure term and averaging, we get:

$$\left\langle p^{(r)}\nabla^2 p^{(r)} \right\rangle = -2\frac{\partial U_i}{\partial x_j}\left\langle p^{(r)}\frac{\partial u_j}{\partial x_i}\right\rangle. \tag{3.12}$$

For homogeneous turbulence, this reduces to:

$$\left\langle \frac{\partial p^{(r)}}{\partial x_m}\frac{\partial p^{(r)}}{\partial x_m} \right\rangle = 2\frac{\partial U_i}{\partial x_j}\left\langle p^{(r)}\frac{\partial u_j}{\partial x_i}\right\rangle. \tag{3.13}$$

Utilizing the definition of the **M** tensor, this can be expressed as:

$$\left\langle \frac{\partial p^{(r)}}{\partial x_m} \frac{\partial p^{(r)}}{\partial x_m} \right\rangle = 4 \frac{\partial U_j}{\partial x_i} \frac{\partial U_k}{\partial x_l} M_{iljk}. \tag{3.14}$$

Herein, the rapid pressure gradient variance must be non-negative. Thus, the condition reduces to the *First lower bound on the M tensor*, explicitly:

$$\frac{\partial U_j}{\partial x_i} \frac{\partial U_k}{\partial x_l} M_{iljk} \geq 0. \tag{3.15}$$

This condition ensures that the pressure gradient variance is non-negative for all mean gradients or equivalently, that the pressure gradient is real. The constraint acts as a lower bound on the expression for the **M** tensor.

Second lower bound on the M tensor: *The rapid pressure-strain correlation must adhere to Cauchy's Inequality.* Expressing the pressure strain correlation in physical space (here, the Greek indices are independent of the summation convention)

$$|\pi_{\alpha\beta}| = \left| u_\alpha \frac{\partial p}{\partial x_\beta} + u_\beta \frac{\partial p}{\partial x_\alpha} \right|. \tag{3.16}$$

Applying the Triangle Inequality, this reduces to:

$$|\pi_{\alpha\beta}| \leq \left| u_\alpha \frac{\partial p}{\partial x_\beta} \right| + \left| u_\beta \frac{\partial p}{\partial x_\alpha} \right|. \tag{3.17}$$

Using the Cauchy's Condition, we get

$$|\pi_{\alpha\beta}| \leq \sqrt{R_{\alpha\alpha} \left\langle \frac{\partial p}{\partial x_\beta} \frac{\partial p}{\partial x_\beta} \right\rangle} + \sqrt{R_{\beta\beta} \left\langle \frac{\partial p}{\partial x_\alpha} \frac{\partial p}{\partial x_\alpha} \right\rangle} \leq \left(\sqrt{R_{\alpha\alpha}} + \sqrt{R_{\beta\beta}} \right) \sqrt{\left\langle \frac{\partial p}{\partial x_k} \frac{\partial p}{\partial x_k} \right\rangle}. \tag{3.18}$$

Re-expressing the pressure gradient variance in terms of the **M** tensor, this reduces

to the *Second lower bound on the M tensor*, explicitly:

$$\frac{|\pi_{\alpha\beta}|}{\sqrt{\frac{\partial U_j}{\partial x_i}\frac{\partial U_k}{\partial x_l}M_{iljk}}} \leq 2(\sqrt{R_{\alpha\alpha}} + \sqrt{R_{\beta\beta}}). \tag{3.19}$$

This obliges the pressure gradient variance (equivalent to $4\frac{\partial U_j}{\partial x_i}\frac{\partial U_k}{\partial x_l}M_{iljk}$) to not just be positive semi-definite, but be large enough to satisfy the Cauchy's inequality applied to the pressure-strain correlation. As can be observed, this is a more stringent condition on the **M** tensor. In this investigation, these conditions are examined to yield meaningful guidance for closure formulation.

3.3.2 Supplementary process realizability constraints

In this section, we introduce additional constraints on the pressure strain correlation that may be more suitable for closure model development. These utilize the stronger condition of the semi-definite nature of the spectrum tensor in Fourier space. These include bounds on the **M** tensor and on the the π_{ij} tensor. Furthermore, these incorporate both upper and lower bounds for the closure expressions of the aforementioned. For any given mean gradient, *these engender the* $\boldsymbol{M}$ *tensor and the the* π_{ij} *tensor to become completely bounded quantities.*

Expressing the pressure strain correlation tensor in Fourier space, we get

$$\pi_{ij} = \sum_{\kappa} \frac{\partial U_l}{\partial x_m}\left[\hat{R}_{im}e_l e_j + \hat{R}_{jm}e_l e_i\right]. \tag{3.20}$$

Using this representation and considering the contraction between the rapid pressure

strain correlation and the mean gradient tensor

$$\frac{\partial U_j}{\partial x_i}\pi_{ij} \equiv \left\{\frac{\partial U}{\partial x}, \pi\right\} = \sum_{\kappa}\left[\hat{R}_{im}(\frac{\partial U_l}{\partial x_m}e_l)(\frac{\partial U_j}{\partial x_i}e_j) + \hat{R}_{jm}(\frac{\partial U_l}{\partial x_m}e_l)(\frac{\partial U_j}{\partial x_i}e_i)\right]. \quad (3.21)$$

Due to the positive semi-definite nature of the spectrum tensor,

$$\hat{R}_{ij}f_i f_j \geq 0, \quad (3.22)$$

where f is any real vector. Without loss of generality, we consider vectors of the from $G_{ij}e_i$ to be members of this vector space, wherein G is an arbitrary tensor of the second order, with real entries, and $\vec{e}$ represents the unit wavevector. Consequently, in the term $\hat{R}_{jm}(\frac{\partial U_l}{\partial x_m}e_l)(\frac{\partial U_j}{\partial x_i}e_i)$, the mean gradient is decomposed into its symmetric and anti-symmetric components to ensure a uniform formulation, given by $S_{ij} = \frac{1}{2}(\frac{\partial U_i}{\partial x_j} + \frac{\partial U_j}{\partial x_i}), W_{ij} = \frac{1}{2}(\frac{\partial U_i}{\partial x_j} - \frac{\partial U_j}{\partial x_i})$, respectively.

$$\left\{\frac{\partial U}{\partial x}, \pi\right\} = \sum_{\kappa}\left[\hat{R}_{im}(\frac{\partial U_l}{\partial x_m}e_l)(\frac{\partial U_j}{\partial x_i}e_j) + \hat{R}_{mj}(S_{lm}e_l)(S_{ij}e_i) - \hat{R}_{mj}(W_{lm}e_l)(W_{ij}e_i)\right]. \quad (3.23)$$

Our objective is to determine the extrema of the contraction $\left\{\frac{\partial U}{\partial x}, \pi\right\}$. To this end, we examine the ranges of each of the three discrete terms on the R.H.S. of equation (3.23). Considering the term $\hat{R}_{mj}(S_{lm}e_l)(S_{ij}e_i)$. Since $\hat{R}_{ij}$ positive semi-definite,equation (3.22), and $S_{ij}e_i$ defines a real vector v_j, we conclude

$$\hat{R}_{mj}(S_{lm}e_l)(S_{ij}e_i) \geq 0. \quad (3.24)$$

Consequently, the term $\hat{R}_{mj}(S_{lm}e_l)(S_{ij}e_i)$ is strictly non-negative. To determine the upper bound, we restrict the analysis to induced norms possessing the sub-

multiplicative property (Meyer, 2001), such that

$$\hat{R}_{ij} v_i v_j \leq \left|\hat{R}\right| |v \otimes v| \,, \tag{3.25}$$

where v_j represents the vector $S_{ij} e_i$ and $\otimes$, the tensor product. Since e is the unit wavenumber vector ($e_i = \frac{\kappa_i}{|\kappa|}$), we obtain

$$|v \otimes v| \leq |S \otimes S| \,. \tag{3.26}$$

Additionally, $\left|\hat{R}\right|$ possesses the upper bound $2k_{modal}$, where, k_{modal} is the modal kinetic energy. Consequently, the limits on the term under consideration can be expressed as:

$$0 \leq \hat{R}_{mj} (S_{lm} e_l)(S_{ij} e_i) \leq 2k_{modal} |S \otimes S| \,. \tag{3.27}$$

Similarly, the other terms in the expression can be bounded as

$$0 \leq \hat{R}_{mj} (W_{lm} e_l)(W_{ij} e_i) \leq 2k_{modal} |W \otimes W| \,, \tag{3.28}$$

$$0 \leq \hat{R}_{im} (\frac{\partial U_l}{\partial x_m} e_l)(\frac{\partial U_j}{\partial x_i} e_i) \leq 2k_{modal} \left|\frac{\partial U}{\partial x} \otimes \frac{\partial U}{\partial x}\right| . \tag{3.29}$$

As the matrix representations of the tensors under consideration is of rank two, we utilize the respective Spectral norms. Additionally, this is an induced norm and thus, has the *sub-multiplicative property* over the vector space composed of real matrices of rank two. Using this,

$$\left|\frac{\partial U}{\partial x} \otimes \frac{\partial U}{\partial x}\right| \leq (S + W)^2, \quad |S \otimes S| \leq S^2, \quad |W \otimes W| \leq W^2. \tag{3.30}$$

Here, the symbols S and W represent the magnitudes of the rate of strain and the rate of rotation tensors, respectively. Utilizing equation (3.22), we can express the contraction symbolically as

$$\left\{\frac{\partial U}{\partial x}, \pi\right\} = A + B - C, \tag{3.31}$$

where $\{A, B, C\}$ are strictly non-negative. Using the norms of $\{A, B, C\}$ and the summation over all the modes, the limits of this contraction can be stated as:

$$-4kW^2 \leq \left\{\frac{\partial U}{\partial x}, \pi\right\} \leq 4k\left(2S^2 + W^2 + 2SW\right). \tag{3.32}$$

The aforesaid constitute *the lower and the upper bounds on the rapid pressure strain correlation*, respectively.

Lower bound on the pressure strain correlation: This is a less stringent constraint than equation (3.15). However, it can be expressed directly in terms of the π_{ij} tensor, utilizing the positive semi-definite nature of the spectrum in Fourier space:

$$-4kW^2 \leq \left\{\frac{\partial U}{\partial x}, \pi^{(r)}\right\}. \tag{3.33}$$

Herein, W represents the norm of the rate of rotation tensor. This constraint is not as stringent as the First Lower Bound in terms of the $\mathbf{M}$ tensor, equation (3.15), but is more amenable to application in cases where the $\mathbf{M}$ tensor may be ambiguous.

Upper bound on the pressure strain correlation: Utilizing the positive semi-definite nature of the spectrum tensor in Fourier space, this is expressed as:

$$\left\{\frac{\partial U}{\partial x}, \pi^{(r)}\right\} \leq 4k(2S^2 + W^2 + 2SW). \tag{3.34}$$

This constraint sets a limit for the maximum rate of energy redistribution that a given mean gradient field can support.

For an upper bound on the pressure gradient variance, we consider the projection in Fourier space

$$\frac{\partial U_j}{\partial x_i}\frac{\partial U_k}{\partial x_l}M_{iljk} = \frac{\partial U_j}{\partial x_i}\frac{\partial U_k}{\partial x_l}\sum_{\kappa}\hat{R}_{il}e_j e_k. \tag{3.35}$$

Using homogeneity, we get

$$\frac{\partial U_j}{\partial x_i}\frac{\partial U_k}{\partial x_l}M_{iljk} \leq \left|\sum_{\kappa}\frac{\partial U_j}{\partial x_i}\frac{\partial U_k}{\partial x_l}\hat{R}_{il}e_j e_k\right|. \tag{3.36}$$

If said norm is an operator, this reduces to

$$\frac{\partial U_j}{\partial x_i}\frac{\partial U_k}{\partial x_l}M_{iljk} \leq \sum_{\kappa}\left|\frac{\partial U}{\partial x}\otimes\frac{\partial U}{\partial x}\right|\left|\hat{R}\right|. \tag{3.37}$$

Using the inequalities derived earlier, this reduces to *the Upper bound on the M tensor*, explicitly

$$\frac{\partial U_j}{\partial x_i}\frac{\partial U_k}{\partial x_l}M_{iljk} \leq 2k(S+W)^2. \tag{3.38}$$

This acts as an upper bound for the rapid pressure-strain variance, and concordantly, the $\mathbf{M}$ tensor. It circumscribes the pressure gradient that a given mean velocity gradient field can support.

3.4 Process realizability constraints and stability implications

In the analysis of explicating the physics incumbent in the process realizability constraints, for each case of a specific mean flow, a particular constraint is chosen. The explicit expression for the constraint is examined. The traits of the intercomponent energy transfer obligated by this inequality are simplified and isolated. The ramifications of such energy redistribution on the flow stability (and the concordant

effect of pressure) are established and discussed.

We commence the analysis with the evolution equation for turbulent kinetic energy:

$$\frac{dk}{dt} = -2aR_{12}. \tag{3.39}$$

Here, a is a non-negative norm associated with the mean gradient, thus more negative values of R_{12} lead to higher growth of turbulent kinetic energy. Concordantly, any agency that increases R_{12} to higher positive values will decrease the growth rate of kinetic energy and consequently, will have a stabilizing effect. To further examine the implications of kinetic energy growth, we present the evolution equation for R_{12}:

$$\frac{dR_{12}}{dt} = P_{12} + \pi_{12}. \tag{3.40}$$

Thus, positive values of π_{12} engender an increment in the value of R_{12}, leading to a lower growth for turbulent kinetic energy and consequently, having a stabilizing effect.

Considering the first lower bound, equation (3.15), for a planar quadratic flow the inequality reduces to:

$$\frac{\partial U_j}{\partial x_i}\frac{\partial U_k}{\partial x_l}M_{iljk} \geq 0 \Rightarrow (a-b)^2 M_{1122} + (a+b)^2 M_{2211} + 2(a^2-b^2)M_{1221} \geq 0. \tag{3.41}$$

Evidently, the process realizability expression is strongly dependent upon the mean gradient field. This is in clear contrast to the state realizability framework wherein the implementation of the constraints does not take the mean gradient field into account. Since production and pressure strain correlation are strong functions of the mean gradient field, it is natural that process realizability is also contingent upon the mean gradient. Contrary to state realizability, process realizability fulfills this

natural requirement. To glean the physical insight afforded by the process realizability constraints for a given mean gradient field, we specify the value of the ellipticity parameter, β, in equation (3.41).

For the case of plane strain, $\beta = 0$ (thus, $b = 0$). The relationship between the components of the M tensor and π_{12} is explicitly given by:

$$\pi_{12} = 2\frac{\partial U_k}{\partial x_l}\left(M_{1l2k} + M_{2l1k}\right). \tag{3.42}$$

This can be simplified further to:

$$\pi_{12} = 2a\left(M_{1122} + M_{1221}\right) + 2a\left(M_{2211} + M_{1221}\right). \tag{3.43}$$

In this case, the requirement that the $\mathbf{M}$ tensor be positive semi-definite, equation (3.41), reduces to:

$$\begin{aligned} &\frac{\partial U_j}{\partial x_i}\frac{\partial U_k}{\partial x_l}M_{iljk} \geq 0 \\ \Rightarrow &(a-b)^2 M_{1122} + (a+b)^2 M_{2211} + 2(a^2-b^2)M_{1221} \geq 0 \\ \Rightarrow &a\left(M_{1122} + M_{1221}\right) + a\left(M_{2211} + M_{1221}\right) \geq 0 \\ \Rightarrow &\qquad\qquad \pi_{12} \geq 0, \end{aligned} \tag{3.44}$$

where, $\Rightarrow$ denotes the material implication. Thus, for this case, the action of pressure is stabilizing. This predisposition of the intercomponent energy transfer has been observed in Mishra & Girimaji (2013), where the investigation considered the dominant energy redistribution and its relationship with predictive fidelity. Evidently, for the case of plane strain, such a trend in the energy redistribution is not only expedient to ensure predictive fidelity but is essential to maintain process realizability. Furthermore, such limits on the energy redistribution hold for the ensemble and for

each mode separately. Process realizability necessitates the action of pressure to be stabilizing in this case, irrespective of the state of turbulence.

Considering an general elliptic flow, the inertial effects engender a state of neutral stability (Salhi *et al.*, 1997). It is known that the action of pressure initiates and maintains the elliptic flow instability (Cambon, 1982). As the inertial effects conserve the neutral stability of the system, it is expected that the action of pressure is destabilizing. Applying the upper and lower bounds on the pressure strain correlation, equations (3.33) and (3.34) respectively:

$$\begin{aligned} -4kW^2 \leq \left\{ \frac{\partial U}{\partial x}, \pi^{(r)} \right\} \leq 4k(2S^2 + W^2 + 2SW) \\ \Rightarrow -4b^2 \leq 2a\pi_{12}/k \leq 4(2a^2 + b^2 + 2ab) \end{aligned} \tag{3.45}$$

Clearly, process realizability permits π_{12} to be both positive and negative. Concordantly, the *action of pressure can be both stabilizing or destabilizing.* This is bolstered by numerical investigations(Mishra & Girimaji, 2013). The energy redistribution due to pressure in elliptic flows is not a straightforward destabilizing effect. As is observed in numerical simulations, over every cycle of growth during the elliptical instability, pressure transfers energy both from and to the the plane of applied shear for distinct intervals. Thus, over the cycle, the action of pressure destabilizes and stabilizes the flow for distinct intervals.

For the case of a mean flow corresponding to pure shear in a plane, $a = b$. Herein, applying equation (3.7),

$$4a^2 M_{2211} \geq 0 \Rightarrow M_{2211} \geq 0. \tag{3.46}$$

This condition prepossess the π_{12} term to favor positive values. However, this does not lead to π_{12} being non-negative for all cases. Thus, this condition is not sufficient to establish the effect of pressure on flow stability in this case.

Considering mean gradients that are non-planar, we analyze the benchmark case of axisymmetric contraction, wherein the requisite mean gradient is given by:

$$\frac{\partial U_i}{\partial x_j} = \begin{bmatrix} -S/2 & 0 & 0 \\ 0 & -S/2 & 0 \\ 0 & 0 & S \end{bmatrix}. \tag{3.47}$$

In this configuration, the Reynolds stress components R_{11} and R_{22} have positive production, while R_{33} has negative production. Thus, the inertial effects destabilize the fluctuations along the 1 and 2 axes while engendering decay of the fluctuations along the 3 axis. In this scenario, the only manner by which pressure can keep the fluctuating velocity gradients bounded (that is, maintain continuity), is by redistributing the energy from R_{11} and R_{22} to R_{33}. The first lower bound, equation (3.15), is mathematically stated as:

$$\begin{aligned} & S^2\left(\frac{M_{1111}}{4} + \frac{M_{2222}}{4} + M_{3333} + \frac{M_{1221}}{2} - M_{1331} - M_{2332}\right) \geq 0 \\ \Rightarrow \quad & (M_{1111} + M_{1221} - 2M_{1331}) + (M_{1221} + M_{2222} - 2M_{2332}) + (M_{3113} + M_{3223} - 2M_{3333}) \\ & -3(M_{3113} + M_{3223} - 2M_{3333}) \geq 0 \\ \Rightarrow \quad & (-\pi_{11} - \pi_{22} - \pi_{33}) + 3\pi_{33} \geq 0 \\ \Rightarrow \quad & \pi_{33} \geq 0. \end{aligned} \tag{3.48}$$

In agreement with process realizability, this predicated energy transfer is observed in DNS studies(Mishra & Girimaji, 2013). Thus, process realizability obliges the

closure model to *counter the inertial effects and stabilize the system.*

Similarly, for axisymmetric expansion, R_{11} and R_{22} have negative production, while R_{33} has positive production. In this case, the first lower bound is mathematically stated as $\pi_{33} \leq 0$. This is in congruence with physical precepts wherein pressure must redistribute energy thus, to ensure that the fluctuating velocity gradients do not become unbounded along the 3-axis. Consequently process realizability states that the action of pressure *counters the inertial effects and stabilizes the system.*

In this section, the implications of the process realizability constraints on flow physics and stability were discussed. Most notably, process realizability is able to identify the directions and chief trends of energy redistribution. It is shown that process realizability constrains the pressure-strain correlation to yield the observed stabilizing influence on the turbulent kinetic energy evolution.

3.5 Conformity of various models with process realizability

We commence with a conspectus of the classical pressure strain correlation modeling framework. The most general closure expression for the M_{ijpq} tensor, satisfying the innate symmetries is (Johansson & Hallback, 1994):

$$\begin{aligned}
M_{ijpq} = {} & A_1\delta_{ij}\delta_{pq} + A_2(\delta_{ip}\delta_{jq} + \delta_{iq}\delta_{jp}) + A_3\delta_{ij}b_{pq} + A_4\delta_{pq}b_{ij} \\
& + A_5(\delta_{ip}b_{jq} + \delta_{iq}b_{jp} + \delta_{jp}b_{iq} + \delta_{jq}b_{ip}) + A_6 b_{ij}b_{pq} \\
& + A_7(b_{ip}b_{jq} + b_{iq}b_{jp}) + A_8 b_{pk}b_{qk}\delta_{ij} + A_9 b_{ik}b_{jk}\delta_{pq} \\
& + A_{10}(b_{ik}b_{pk}\delta_{jq} + b_{jk}b_{pk}\delta_{iq} + b_{ik}b_{qk}\delta_{jp} + b_{jk}b_{qk}\delta_{ip}) \\
& + A_{11}b_{ij}b_{pk}b_{qk} + A_{12}b_{pq}b_{ik}b_{jk} + A_{13}(b_{ik}b_{pk}b_{jq} + b_{jk}b_{pk}b_{iq} + b_{ik}b_{qk}b_{jp} + b_{jk}b_{qk}b_{ip}) \\
& + A_{14}b_{ik}b_{jk}b_{pl}b_{ql} + A_{15}b_{ik}b_{jl}(b_{pk}b_{ql} + b_{qk}b_{pl}).
\end{aligned} \tag{3.49}$$

The corresponding general ansatz for the Rapid Pressure Strain Correlation is:

$$\begin{aligned}\frac{\pi_{ij}^{(r)}}{k} = S_{pq}\Big(&Q_1\delta_{ip}\delta_{jq} + Q_2(b_{ip}\delta_{jq} + \delta_{iq}b_{jp} - \frac{2}{3}b_{pq}\delta_{ij}) \\ &+Q_3 b_{pq}b_{ij} + Q_4(b_{iq}b_{jp} - \frac{1}{3}b_{pk}b_{qk}\delta_{ij}) \\ &+Q_5 b_{pl}b_{ql}b_{ij} + (Q_5 b_{pq} + Q_6 b_{pl}b_{ql})(b_{ik}b_{jk} - \frac{1}{3}II_a\delta_{ij})\Big) \\ +W_{pq}\Big(&Q_7(b_{ip}\delta_{jq} + b_{jp}\delta_{iq}) + Q_8 b_{pk}(b_{jk}\delta_{iq} + b_{ik}\delta_{jq}) + Q_9 b_{pk}(b_{jk}b_{iq} + b_{ik}b_{jq})\Big).\end{aligned} \tag{3.50}$$

Herein, the Reynolds stress anisotropies are defined as $b_{ij} = \frac{\overline{u_i u_j}}{2k} - \frac{\sigma_{ij}}{3}$ and the model coefficients, A_i, are scalar functions of the anisotropy invariants. These are chosen so as to satisfy continuity, the normalization condition and the Crow Constraint (Crow, 1968); and calibrated to yield good agreement over a set of benchmark flows (Johansson & Hallback, 1994).

Closure modeling of the rapid pressure strain correlation is tantamount to determining the coefficients A_i, subject to mathematical constraints and physical fidelity. As elaborated in Pope (2000), the notable mathematical constraints are

1. realizability;
2. linearity in the Reynolds stresses;
3. linearity in the mean gradient tensor.

It has been established that closures that are linear in the Reynolds stresses are unable to adhere to the state realizability condition at the 2C limit (Lumley, 1978). Consequently, many closure nominations forgo linearity in the Reynolds stresses and incorporate non-linear terms in the closure expression. Adopting nonlinear expressions for the M tensor, allows the model to be realizable in the neighborhood of the

	Closure Model	M_{ijkl} Coefficients	π_{ij} Coefficients
I.	Launder *et al.* (1975)	A_1-A_5	Q_1,Q_2 & Q_7
II.	Speziale *et al.* (1991)	A_1-A_7	Q_1-Q_3 & Q_7
III.	Johansson & Hallback (1994), 2^{nd} order	A_1-A_{10}	Q_1-Q_4 & Q_7-Q_8
IV.	Johansson & Hallback (1994), 3^{rd} order	A_1-A_{13}	Q_1-Q_5 & Q_7-Q_9
V.	Johansson & Hallback (1994), 4^{th} order	A_1-A_{15}	Q_1-Q_9

Table 3.1: Specifics of the $\mathbf{M}$ and π tensor expressions in closure models.

2C limit. Higher degrees of nonlinearity provide additional degrees of freedom in the formulation. This enables the model coefficients to be calibrated for accuracy in certain flows while still adhering to state realizability.

Hereon, we evaluate the nature of the Reynolds stress dynamics engendered by popular closure models, for different mean flow gradients. The closures analyzed correspond to the models introduced in Launder *et al.* (1975), Speziale *et al.* (1991) and Johansson & Hallback (1994). In addition to representing the most widely tested, verified and applied closures in the field, this set provides a cross-section of the modeling paradigms vis-à-vis the nonlinearity in the Reynolds stress tensor in the closure expression and the adherence of the closure to state realizability. The model of Launder *et al.* (1975) is linear in the Reynolds stresses and the coefficients therein are constants. The model of Speziale *et al.* (1991) is quadratic and the coefficients are functions of the Reynolds stress anisotropies. The family of models introduced in Johansson & Hallback (1994) are up to the fourth order in Reynolds stresses and the coefficients are quadratic bilinear forms in the Reynolds stress anisotropies. Additionally, the model of Launder *et al.* (1975) was not explicitly formulated to satisfy any form of state realizability. The model of Speziale *et al.* (1991) adheres to weak realizability and those of Johansson & Hallback (1994) satisfy the strong form of the realizability constraint. These closure expressions are detailed and contrasted in table 3.1. In addition to the aforementioned closures subscribing to the classical

Closure Model	**Closure expression**	**Closure coefficients**	**Realizability adherence**
Launder *et al.* (1975)	Linear in Reynolds stresses	Constants	None
Speziale *et al.* (1991)	Quadratic	Linear in anisotropies	Weak realizability
Johansson & Hallback (1994)	Up to the $4th$ order	Quadratic bilinear forms	Strong realizability
Kassinos & Reynolds (1994)	Linear in R_{ij} and D_{ij}	Constants	None

Table 3.2: Comparison and contrast of the set of models considered

framework, we consider alternative modeling approaches that counsel the inclusion of additional tensors to the modeling basis, in form of the model of Kassinos & Reynolds (1994). These modeling paradigms are contrasted in table 3.2.

In the Second Moment Closure approach, the evolution of the Reynolds stresses is calculated via a modeled equation. Any unphysical behavior of the Reynolds stresses has to originate due to unphysical features of the closure models. Nonlinear models forgo the important superposition requirement (Reynolds, 1976) pertaining to Reynolds stress evolution in favor of state realizability adherence. Thus, it is important to examine if these closures satisfy the process realizability constraints. Explicitly, do higher degrees of nonlinearity lead to improved or diminished consistency with of Reynolds stress dynamics.

We perform a phenomenological investigation of the relationship between linearity, state realizability and process realizability. We examine if adherence to state realizability leads to better process realizability characteristics. Furthermore, in light of the arguments given in Speziale *et al.* (1994), it is important to consider if adherence to the weak realizability condition leads to better replication of Reynolds stress dynamics than the strong realizability condition.

The process realizability violation for each model is examined as follows. The anisotropy space is discretized into several nodes for the case of each mean velocity gradient. The modeled M_{ijkl} tensor is constructed at each node. Then, the compliance of the model expression at each node with each of the process realizability

constraints, equations (3.15), (3.33) and (3.38), is determined. If any of the constraints is violated, the model is deemed unrealizable at that location. Herein, the requisite grid independence is duly carried out. This manner of realizability evolution is different from that followed by Sambasivam *et al.* (2004).

3.5.1 The linear closure of Launder et al. *(1975)*

The linear representation for the M tensor can be expressed as:

$$\begin{aligned} M_{ijpq}^{linear} = & A_1\delta_{ij}\delta_{pq} + A_2(\delta_{ip}\delta_{jq} + \delta_{iq}\delta_{jp}) + A_3\delta_{ij}b_{pq} + A_4\delta_{pq}b_{ij} \\ & + A_5(\delta_{ip}b_{jq} + \delta_{iq}b_{jp} + \delta_{jp}b_{iq} + \delta_{jq}b_{ip}). \end{aligned} \tag{3.51}$$

Of the coefficients in the expansion, A_1 and A_2 are determined from the Crow Constraint. The latter set of coefficients, A_3 to A_5 are constrained by continuity and the normalization condition. These are co-dependent and have only one degree of freedom. Without loss of generality, this is considered to be A_5. In the closure presented in Launder *et al.* (1975), the value of A_5 is taken to be a constant and is calibrated for performance in a set of benchmark flows, leading to the parameter value of $A_5 = -0.286$. The entire set of parameters is given by $\{A_1, A_2, A_3, A_4, A_5\} = \left\{\frac{4}{15}, -\frac{1}{15}, -\frac{1}{3}(2 + 11A_5), \frac{2}{3}(1 - 2A_5), -0.286\right\}$.

Figure 3.1 exhibits the zones of process realizability adherence for this model. The shaded region of the anisotropy invariant map signifies the zones where the closure is unable to ensure a $\mathbf{M}$ tensor that is positive semi-definite. As can be observed, the constraints are violated for significant regions of the anisotropy invariant map. The 2C limit is not attainable with realizable dynamics, for any quadratic flow. Contrary to expectations, it is not the elliptic flows wherein the realizability violations are most severe. Purely sheared flows have the largest zone of violation. For hyperbolic and elliptic flows, pressure counters the inertial effects, stabilizing and destabilizing

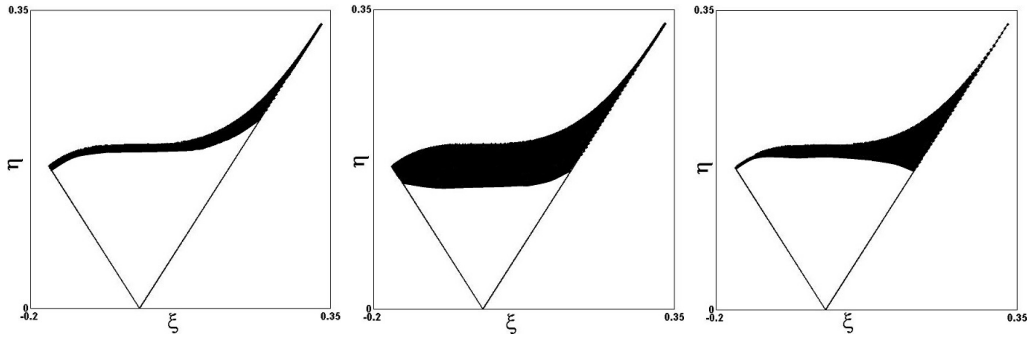

Figure 3.1: Zones of unrealizable dynamics for the model of Launder *et al.* (1975). (a)Plane strain, (b)purely sheared, (c)Pure rotation.

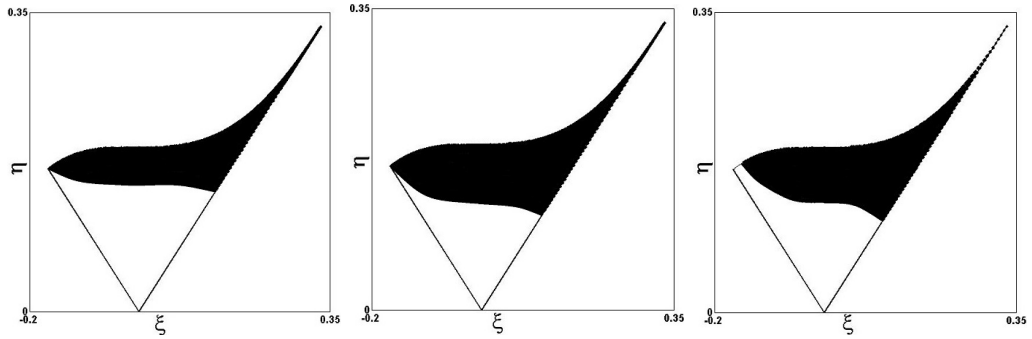

Figure 3.2: Zones of unrealizable dynamics for the model of Speziale *et al.* (1991). (a)Plane strain, (b)pure shear, (c)Pure rotation.

the flow, respectively. For purely sheared flows, pressure has a modest effect and does not even affect the nature of the instability (Mishra & Girimaji, 2013). Paradoxically, the case of a purely sheared mean flow leads to the largest area of violation, in spite of having a nominal action of pressure.

3.5.2 The quadratic model of Speziale et al. *(1991)*

The zones of process realizability adherence for the quadratic model of Speziale *et al.* (1991) are exhibited in figure 3.2. The coefficients for this model, with reference to the notation used in Speziale *et al.* (1991), are $\{A_1, A_2, A_3, A_4, A_5, A_6, A_7\}$

are given by $\left\{\frac{C_3-C_3^*\sqrt{II}}{3}, -\frac{C_3-C_3^*\sqrt{II}}{12}, \frac{101}{240}, \frac{149}{240}, -\frac{5}{24}, -1.8, 1.8\right\}$. Although satisfying the weak form of state realizability, the model is unable to ensure realizable Reynolds stress dynamics beyond moderate degrees of anisotropy. The 2C limit and its neighborhood, wherein weak realizability is applied, are not amenable to realizable dynamics for any quadratic flow. Thus, even before the weak realizability condition would be actuated, the predicted Reynolds stress dynamics would become unphysical. Additionally, in comparison to the results for the LRR model, notwithstanding the nonlinearity of the SSG model it exhibits larger zones of process realizability violation.

3.5.3 The nonlinear models of Johansson & Hallback (1994)

Johansson & Hallback (1994) have formulated a family of closures for the rapid pressure strain correlation, of the forth, third and second order in anisotropies. All these proposed closures satisfy the strong form of state realizability. The details of the closures for the $\mathbf{M}$ tensor can be found in Johansson & Hallback (1994) and Sjogren & Johansson (2000). To evaluate the process realizability for these individual closures, we appraise their ability to ensure a $\mathbf{M}$ tensor that is positive semi-definite for the case of a plane strain mean flow gradient. The second order model is able to do thus for the entire Lumely's Triangle. However, the third and forth order models exhibit substantial regions where the predicted $\mathbf{M}$ tensor is unrealizable, as exhibited in figure 3.3. Moreover, the zones of violation increase with a corresponding increment in the order of the model. This trend is observed for all quadratic mean flows. Consequently, we restrict this investigation to the quadratic model, having the best process realizability adherence amongst these.

The zones of process realizability adherence for the quadratic model of Johansson & Hallback (1994) are exhibited in figure 3.4. As can be observed, the process realiz-

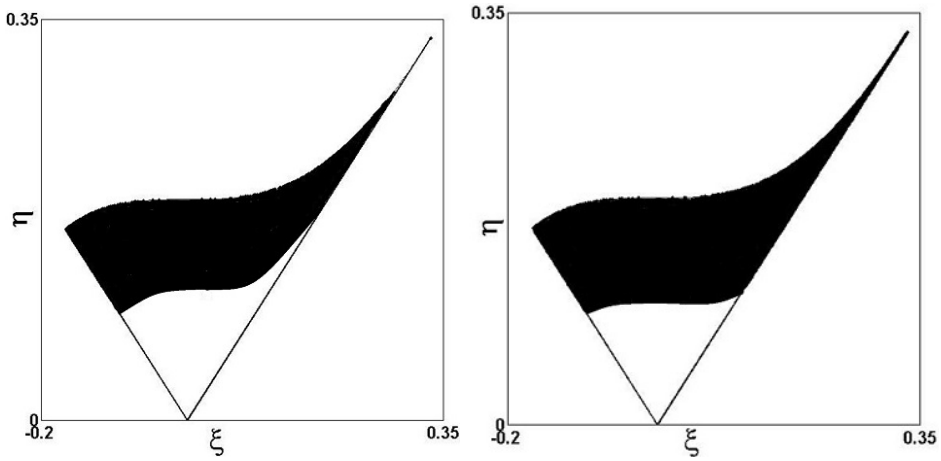

Figure 3.3: Zones of adherence to the first lower bound for the models of Johansson & Hallback (1994) for the case of a plane strain mean flow. (a)Third order, (b)Forth order.

ability adherence of the model is far superior to all other closures considered in this section. However, in spite of its adherence to the strong form of state realizability, the model is unable to ensure realizable dynamics at the 2C limit or its neighborhood. Consequently, the predicted Reynolds stress dynamics would have become unsubstantiable well before the required application of the strong realizability condition. It must be observed that the second order model of Johansson & Hallback (1994) is completely constrained by the conditions of consistency and strong realizability. Thus, it does not allow for the tuning of the coefficients in the expression to ensure any degree of predictive fidelity.

3.5.4 Process realizability and intercomponent energy transfer

At this juncture, we address the relationship between closure expressions, of different orders in the anisotropy tensor, and their amenability at replicating the Reynolds stress dynamics. Considering the case axisymmetric contraction, the linear model of Launder, Reece and Rodi complies with the first lower bound on the M tensor,

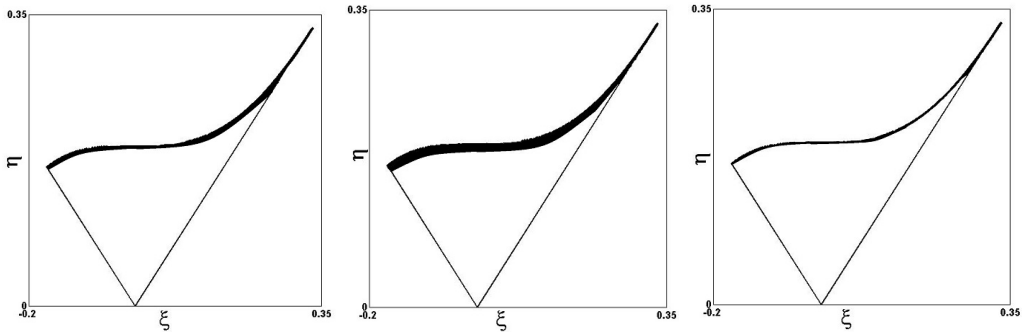

Figure 3.4: Zones of unrealizable dynamics for the second order model of Johansson & Hallback (1994). (a)Plane strain, (b)Purely sheared, (c)Pure rotation.

equation (3.15), for all states of turbulence. However, as exhibited in figure 3.5, the non-linear models of Speziale *et al.* (1991) and Johansson & Hallback (1994) have significant regions of violation. Furthermore, the region of violation increases substantially with the order of the modeling expression. On manifesting such violations, the model transfers energy from R_{33} to R_{11} and R_{22}. This trend of redistribution is clearly unphysical as it leads to unbounded velocity gradients along the 1 and 2-axes. However, more importantly, for such a violation of the process realizability constraints, R_{33} will be acted upon by *negative production and a negative pressure strain correlation*. This will drive the system toward the 2C limit, where such violations are even more severe. This will rapidly lead to a negative value for R_{33} and thus, a violation of State Realizability. This illustration exemplifies the manner in which *realizability violations of the Reynolds stress dynamics precede and lead to realizability violations of the Reynolds stresses*. In the case that the closure complies with the strong realizability constraint, the value of the pressure strain correlation will be artificially and unphysically reset at the 2C limit. This would displace the evolution off the 2C limit whence the process realizability violation would cause it to proceed toward the 2C limit again and this cycle would repeat interminably. In

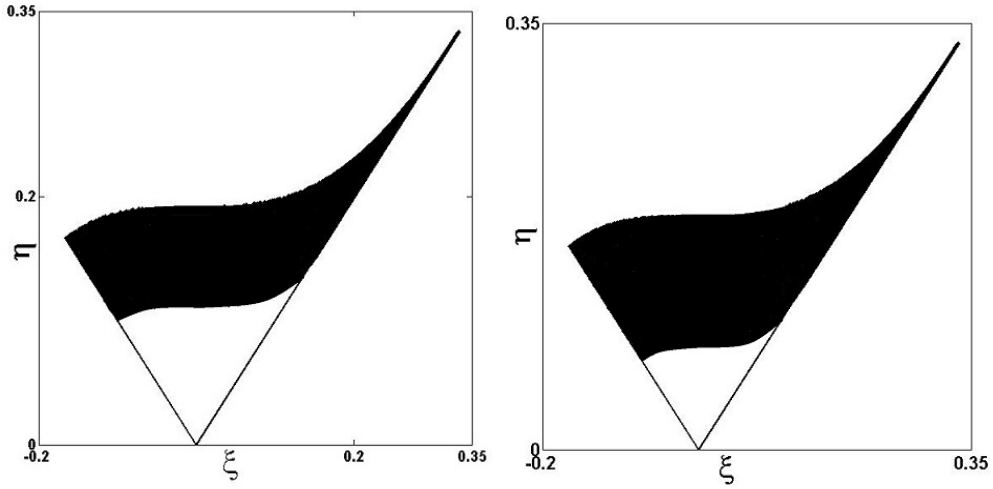

Figure 3.5: Zones of adherence to the first lower bound for the case of axisymmetric contraction for the model of (a)Speziale *et al.* (1991), (b)Johansson & Hallback (1994).(LRR satisfies this constraint everywhere.)

this light, it is not surprising that such models exhibit spurious oscillations in the vicinity of the 2C limit (Speziale *et al.*, 1994). This explication serves to underline the fact that State Realizability constraints are insufficient as they *address the effect of realizability violation and not the cause thereof.*

This theme, of unphysical energy redistribution to satisfy state realizability, is repeated in other varieties of flows as well. For instance, this can be observed in figure 3.6, where the zones of adherence to the first lower bound, equation (3.15), are exhibited for the closures of Launder *et al.* (1975) and Speziale *et al.* (1991). These figures indicate that closure expressions of higher orders do not lead to a better representation of the Reynolds stress dynamics.

3.5.5 Models with extended bases: Kassinos & Reynolds (1994)

Due to the unsatisfactory performance of classical pressure strain correlation models in certain classes of flows, Kassinos & Reynolds (1994); and Cambon and co-workers(Cambon *et al.*, 1992) have attempted to use additional tensors in their

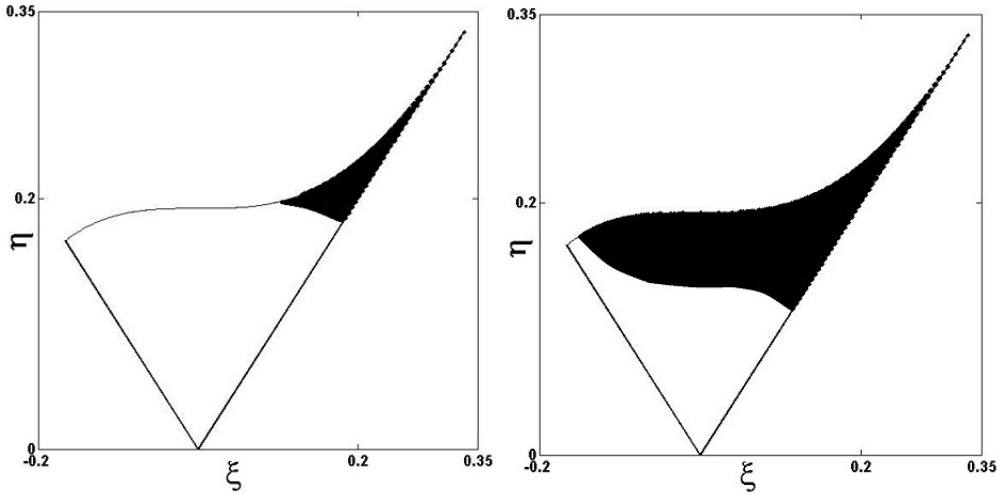

Figure 3.6: Zones of adherence to First Lower Bound for a plane strain flow for (a)Launder *et al.* (1975), (b)Speziale *et al.* (1991).

modeling attempts. Such attempts have very credible arguments, both physical and mathematical, in their favor. It is accepted that the Reynolds stresses and the mean gradients do not constitute a complete basis to model the pressure strain correlation, even in homogeneous flows. Thus, additional tensors are required to provide the missing information. Kassinos & Reynolds (1994) have averred that single-point modeling of the dynamics of pressure requires supplementary tensors, such as Dimensionality, D_{ij}, Circulicity, F_{ij} and Stropholysis, Q_{ijk}. For homogeneous turbulence, these can be defined as:

$$R_{ij} = M_{ijkk}, D_{ij} = M_{kkij}, F_{ij} = \epsilon_{imp}\epsilon_{jrs}M_{psrm}, Q_{ijk} = \epsilon_{ipq}M_{jqpk}. \tag{3.52}$$

The authors then proceed to proffer and test models utilizing this basis. For rotation dominated flows, these models exhibit improved fidelity and capture significantly more flow features. However, the process realizability adherence of these models is unsatisfactory, as exhibited in figure 3.7. For quadratic mean flows, these models

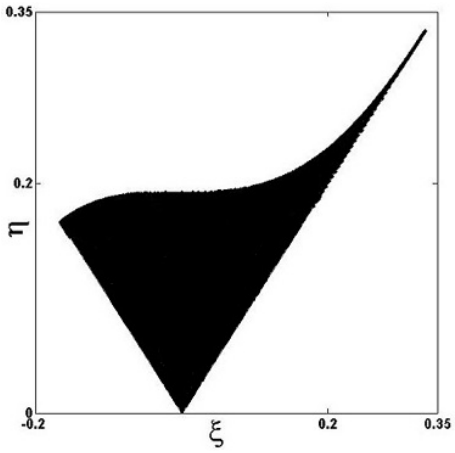

Figure 3.7: Zone of process realizability violation for the model of Kassinos & Reynolds (1994), for a purely sheared mean flow.

could not ensure realizable Reynolds stress dynamics for any state of turbulence, including isotropic turbulence. The details of the closures used can be found in Kassinos & Reynolds (1994) (equations (3.3.5), (3.3.6) and (3.7.2) therein).

3.5.6 Summary

The incomplete basis used in pressure strain correlation modeling leads to the inapplicability of closure expressions to higher values of anisotropy(Cambon & Rubinstein, 2006; Sagaut & Cambon, 2008). This feature is evident in the results of the process realizability constraints, wherein it is shown that most models can ensure realizable predictions only for low to moderate levels of anisotropy. All models have *significantly large regions on the anisotropy invariant map where they are unable to ensure realizable Reynolds stress dynamics.* This has consequential ramifications in the application of such models to engineering problems. This is exacerbated in the case of strain dominated flows, wherein the state of turbulence evolves to a moderately high level of anisotropy. For instance, figure 3.8 exhibits the evolution of the anisotropy invariants for the case of a purely sheared mean flow. In spite of com-

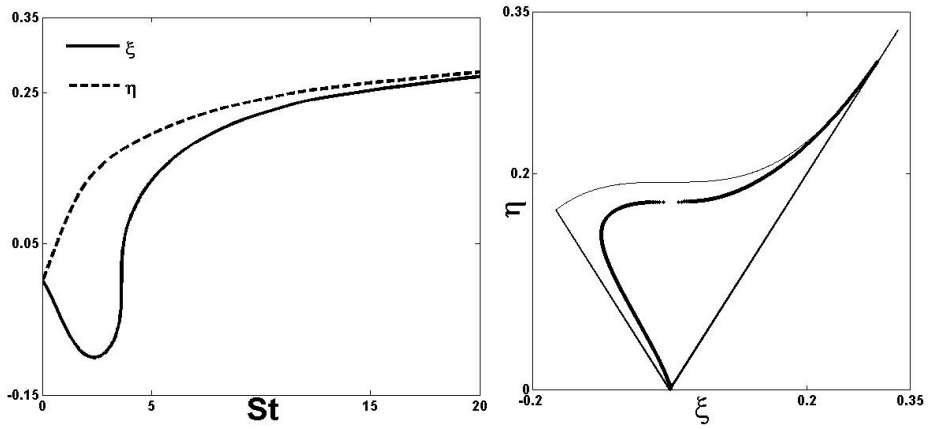

Figure 3.8: Evolution of the anisotropy invariants for the case of a Purely sheared mean flow. (a)Temporal evolution, (b)evolution on the anisotropy invariant map.

mencing from an isotropic initial state, no model can ensure realizable prediction after a span of two shear time units.

It was observed that *compliance with state realizability has no direct correlation with the process realizability characteristics* of the model. One of the primary reasons to resort to non-linear models for the Rapid Pressure Strain Correlation is to ensure compliance with state realizability. In this investigation, we have exhibited that *non-linear models do not guarantee better process realizability characteristics.*

3.6 A realizability-based linear M_{ijkl} closure

The classical modeling formulation seeks to model this with a basis comprising of the Reynolds stresses and the mean gradient. However, the Reynolds stresses do not provide an adequate description of the turbulent flow field (Cambon & Scott, 1999). Concordantly, the M_{ijkl} tensor, describing the action of pressure, depends on the *componentiality* and *dimensionality* of the turbulent flow field. As discussed in Mishra & Girimaji (2013), the dimensionality information is unavailable in the classical modeling formulation. The challenge inherent to pressure strain correlation

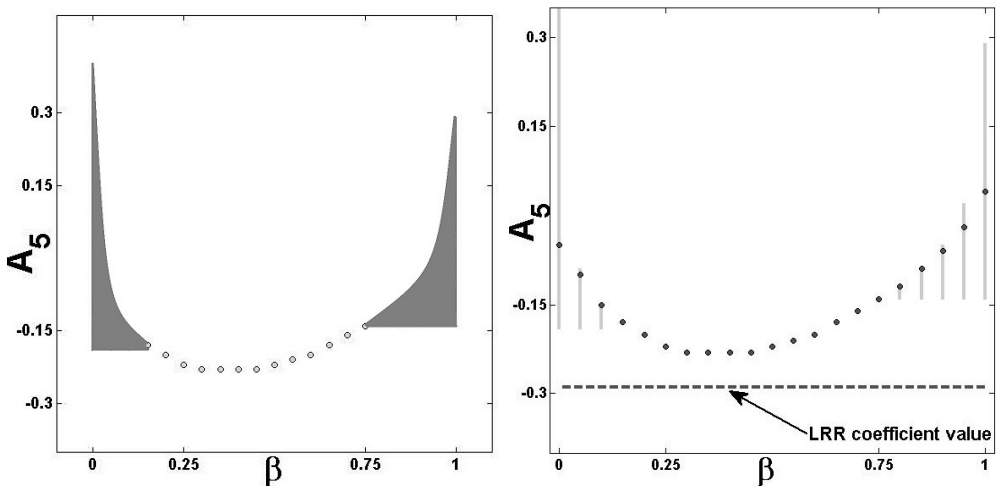

Figure 3.9: (a)Formulation of a archetypal linear model, vis a vis process realizability, for planar quadratic flows,(b)The explicit values of the new model, the value of the LRR coefficient is notated.

modeling is to presuppose a latent dimensionality, leading to a consistent closure expression.

Compliance with process realizability is contingent on the mean gradient, for instance as exhibited in equation (3.53). Consequently, in lieu of the Dimensionality information, using the mean gradient information is more physical (Mishra & Girimaji, 2013) and would enable better process realizability characteristics. Thus, we propose a simple recourse of making the coefficients of the closure expression functions of the mean flow invariants. Lee (1990), Girimaji (2000) and Sjogren & Johansson (2000) represent the few investigations that have considered such an approach. Both these models exhibited considerable improvements in predictions. Our thesis recommends this surrogate procedure, not only for predictive fidelity but also for realizability.

In this section, we outline an *a priori* application of the process realizability constraints to formulate a rapid pressure strain correlation model. Thus, the di-

mensionality information is inferred from the process realizability constraints. These constraints are used to develop a model that is linear in the anisotropies but uses model coefficients that are functions of the mean gradient. As mentioned in the previous section, the most general form of the M tensor that is linear in the anisotropies can be expressed as equation (3.51). We substitute this expression for the **M** tensor in equation (3.41). For a quadratic flow this reduces the constraint to:

$$\begin{aligned}\left[\frac{1}{5}-\frac{3}{2}A_5(b_{11}+b_{22})\right]-\sqrt{\beta(1-\beta)}\left[\frac{4+7A_5}{3}(b_{11}-b_{22})\right]\\ -2\beta\left[\frac{-1}{15}+A_5(b_{11}+b_{22})\right]\geq 0.\end{aligned} \tag{3.53}$$

This inequality is used to determine the admissible values for A_5 for a given value of β. Figure 3.9 exhibits the adherence to the first lower bound for a linear model, as a function of its coefficient, A_5, and the ellipticity parameter, β. The shaded intervals exhibit values of β where this constraint can be fulfilled for a range of A_5. The singleton circles represent values where this constraint cannot be fulfilled for any value of A_5. This indicates that the value of the coefficient for these flows depends strongly on the underlying dimensionality. For these values of β no single values of A_5 can lead to realizable results for all the permissible values of the dimensionality tensor. In such a case, we choose the value of A_5 that minimizes the zone of process realizability violation. Based on the extension of this smooth curve, as exhibited in figure 3.9(b), an archetypal linear closure can be obtained. The distribution underscores that process realizability constraints are most stringent for flows where the magnitudes of the mean rate of strain and rate of rotation are similar. Furthermore, as exhibited, the stringency of the constraints is similar for both elliptic and hyperbolic flows.

The degree of process realizability adherence for this model is exhibited in fig-

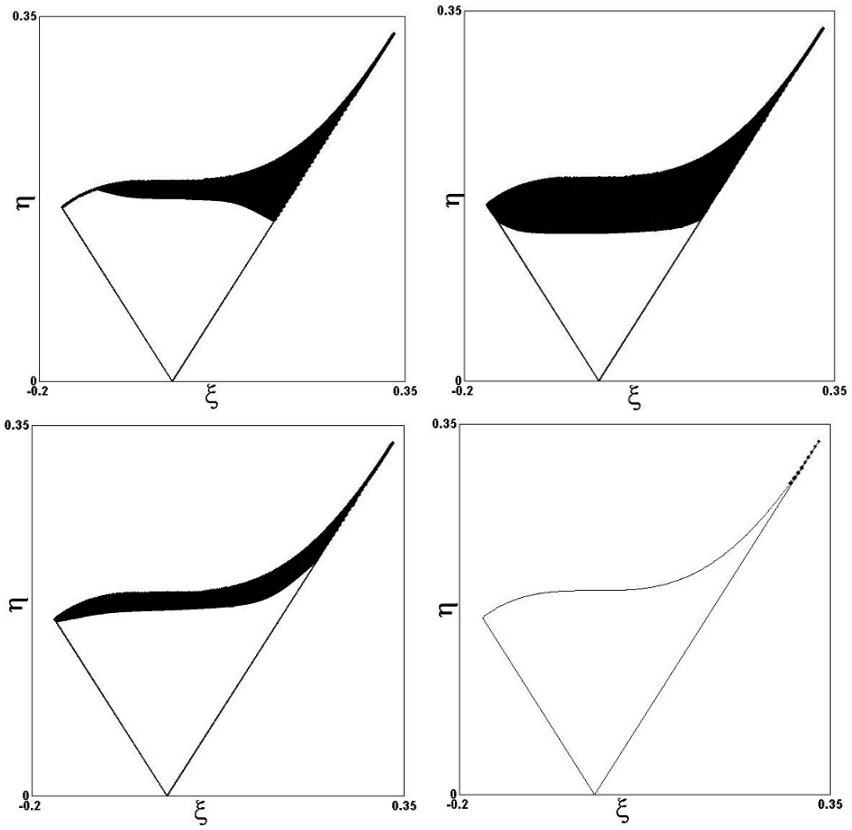

Figure 3.10: Realizability adherence of the process realizability based model for a quadratic flows with β=0, 0.5, 0.75 and 1.

ure 3.10 for different types of mean flows. As can be observed, process realizability adherence of this model is comparable to the linear and non-linear closures evaluated earlier. Furthermore, the closure gives adequate compliance with the constraints for elliptic flows. For instance, for a purely rotating mean flow, the model is able to satisfy process realizability everywhere on the anisotropy invariant map except for a very small region in the vicinity of the 1C state.

It should be pointed out that the focus of this exercise is to demonstrate process realizability and not predictive fidelity. We seek to outline the general procedure by which models can be formulated to ensure physically permissible Reynolds stress dynamics for the maximal possible states of turbulent flow, at any order of expression. While developing a new closure model, an acceptable compromise can be arrived at between predictive fidelity for benchmark flows and process realizability adherence. Such an effort will be carried out in a subsequent investigation.

3.7 Summary and conclusions

In this investigation, we formulate a set of realizability constraints that behoove the Reynolds stress dynamics to be physically permissible. It is exhibited that unlike classical realizability, these constraints are applicable at all states of turbulence. Thereby, the process realizability framework provides a *caveat emptor* by clearly demarcating zones where extant models are inapplicable. Furthermore, process realizability constraints provide better guidance for model development as they indicate permissible ranges for closure coefficients. Most importantly, with specific examples, it is shown that the process realizability framework gives unequivocal physical insight into the process of energy redistribution. The differences between the process realizability and the state realizability approaches are highlighted in table 3.3.

Popular closures are evaluated under the purview of these conditions, indicating

Issue	**Process Realizability**	**State Realizability**
Focus	Statistical Process. (Reynolds stress dynamics)	Statistical state. (Reynolds stress tensor)
Applicability	All states of turbulence.	Restricted to the 2C limit.
Hierarchy	Address *cause* of violation.	Address the *effect*.
Physics	Lead to insight into energy redistribution.	—-
Modeling	More amenable to modeling. (Provide ranges for coefficients)	—-
Utility	As a *caveat emptor*. (Clearly indicate zones of inapplicability.)	Incapable of doing so.

Table 3.3: Contrasting the different approaches to realizability.

regions of realizability adherence for each model and for each mean flow. It is shown that all the models considered could not ensure realizable Reynolds stress dynamics for significant regions of the anisotropy invariant map. Furthermore, it is exhibited that adherence to state realizability in any form does not lead to better process realizability compliance. The primary reason to resort to non-linear models for the rapid pressure strain correlation is to ensure compliance with state realizability. We exhibit that non-linear models do not guarantee better representation of the Reynolds stress dynamics. In fact, in many cases as the degree of non-linearity increases, the process realizability characteristics of the closure are progressively undermined. Finally, we develop an archetypal closure expression, linear in the Reynolds stress, that gives process realizability adherence at par with highly non-linear closures.

4. A DYNAMICAL SYSTEMS APPROACH TOWARD MODELING THE PRESSURE STRAIN CORRELATION

4.1 Overview

A key hurdle in turbulence modeling is the representation of the non-local dynamics of pressure within the framework of a single point closure, as manifested in the pressure strain correlation. In this article, we outline a detailed recourse toward formulating a pressure strain correlation model that exhibits improved agreement within the purview of single point closures. Different aspects of the dynamics of pressure are discussed, individually and sequentially, with respect to their amenability to the single point modeling paradigm and a set of optimal compromises is constituted within the form and the scope of the model. Thence, this framework is utilized to formulate an illustrative model. The predictions of this model are compared to numerical and experimental data while being contrasted against other popular modeling paradigms. Finally, as a *caveat emptor*, the zones of applicability of this model are clearly delineated for different mean flows.

4.2 Introduction

Diverse applications require accurate predictions of complex turbulent flows. These range from flows over aircraft and inside turbomachinery, atmospheric flows for weather prediction and through the heart for cardiac auscultation, etc. Due to the disparate character of these flows, predictive methods must be robust, so as to be easily applicable for most of these cases, yet possessing a high degree of accuracy in each. Furthermore, as the processes of analysis and design involve repeated iterations, the predictive method must be computationally economical. In this vein, the Second Moment Closure approach to modeling is of great engineering utility as it is

less computationally expensive than numerically intensive methods like Direct Numerical Simulation or Large Eddy Simulation. Yet, this approach is more accurate and robust as compared to one or two-equation models.

The Second Moment Closure methodology is based on the Reynolds Stress Transport (RST) equations:

$$\begin{aligned} \frac{dR_{ij}}{dt} &= P_{ij} - \frac{\partial}{\partial x_k} T_{ijk} + \pi_{ij} - \epsilon_{ij}, \\ \text{where, } R_{ij} &= \sum_{\kappa} \langle u_i u_j \rangle, \\ \pi_{ij} &= \left\langle p(\frac{\partial u_i}{\partial x_j} + \frac{\partial u_j}{\partial x_i}) \right\rangle, \\ \epsilon_{ij} &= -2\nu \left\langle \frac{\partial u_i}{\partial x_k} \frac{\partial u_j}{\partial x_k} \right\rangle, \\ \text{and } P_{ij} &= -R_{jk} \frac{\partial U_i}{\partial x_k} - R_{ik} \frac{\partial U_j}{\partial x_k}. \end{aligned} \tag{4.1}$$

Herein, the convection and production terms adjust to inertial phenomena via the addition of scale factors or Coriolis terms; hence models based on this paradigm lead to better descriptions of complex flows. Furthermore, due to the presence of the terms representing the convection and diffusion of the Reynolds stresses, this approach is potentially able to account for the non-local and history effects. However, due to the lack of closure in the Reynolds stress transport equations, models must be incorporated for the higher order or non-local terms. These include transport, dissipation and the pressure-strain correlation terms. The ability of any turbulence model to describe the flow physics depends on the accuracy of the model expressions utilized therein.

Of these terms, the pressure strain correlation, embodying the action of pressure is regarded as the most important (Sagaut & Cambon, 2008). The evolution of the fluctuating velocity field in an incompressible, turbulent flow is determined by

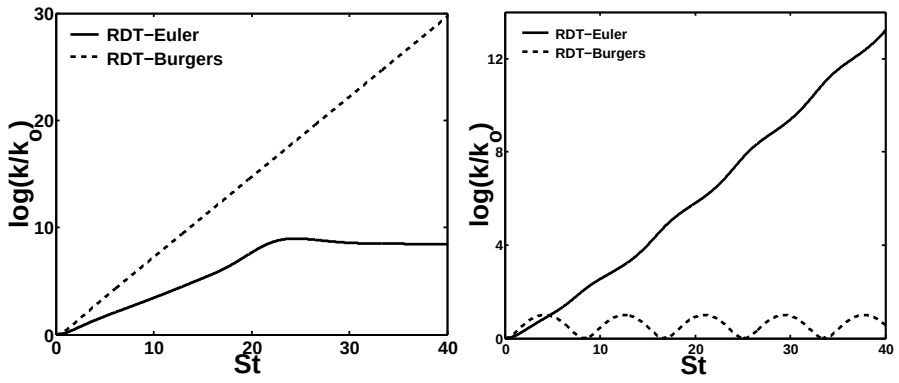

Figure 4.1: Evolution in the Navier-Stokes system contra the Burgers system, for the case of (a)a representative hyperbolic flow, (b)a representative elliptic flow.

the balance between inertial, pressure and viscous effects. The inertial effects deform the fluctuating velocity field without any regard to the incompressibility requirement. The viscous effects are dynamically passive and do not change the dilatation state of the velocity field. It is the function of pressure to modify this inertial deformation, so as to render the velocity field divergence free. Thus, *the pressure effects are omnipresent*.

Additionally, *the action of pressure is highly complex*. The key issues that compound the complexity of turbulence are the non-linearity and the non-locality of the phenomenon (Tsinober, 2009; Pope, 2011). However, the "pressure-released" Burgers turbulence, that embodies much of the non-linear character of turbulence, has been much better understood (Sagaut & Cambon, 2008) in contrast to its Navier-Stokes analogue. Consequently, the complex action of pressure is the key toward understanding the complicated nature of turbulent flows.

Finally, *the action of pressure is critically important in the evolution of turbulent flows*. As illustrated in figure 4.1, in different regimes of quadratic flows, the pressure effects either suppress (hyperbolic flow) or engender and sustain flow instabilities

(elliptic flows). Thus, this term determines the central characteristics of turbulent flows and consequently, its accurate modeling is highly exigent.

The foundations for pressure strain correlation modeling were established in landmark papers by Chou (1945) and Rotta (1951). In single point closures the classical formulation attempts, via rational mechanics, to express the pressure strain correlation as a function of tensors that can be measured in an engineering context such as the Reynolds stresses, dissipation, mean gradients, etc. In this vein, it represents the only modeling approach with the requisite measure of *engineering applicability*. However, this approach illustrates the schism between the engineering limitations and the requirements dictated by physics. The set of tensors that can be used in an engineering perspective does not constitute a complete basis to model the pressure strain correlation. According to the axioms ordained by physics in dealing with incompressibility, pressure is governed by an elliptic Poisson equation. Pressure reacts instantaneously to any changes in the entire velocity field and is thus, a non-local variable. An attempt to develop one-point (or local) models for such non-local behavior is inherently encumbered by a deficiency in required information (or, an incomplete basis for this reconstruction). Two-point models do not have to make such sacrifices regarding the physical description. They are able to represent the physics of turbulence more realistically, especially regarding the non-local nature of the pressure fluctuations. However, at this juncture, multi-point approaches are not robust and computationally expensive and consequently, they are not practical for engineering applications. Thus at present, single-point closures represent the only viable engineering recourse. However, this approach has to make concessions in the modeling procedure as the information available to it is limited. Such an encumbrance leads to limitations in the features of the pressure strain correlation that the classical modeling formulation is capable of reproducing. In light of these limitations,

the pertinent questions involve the degree to which we can replicate these phenomena and the levels of certitude associated with these predictions.

In this context, various pressure strain correlation models have been developed. The nominations available and popular at present, like those by Speziale *et al.* (1991), Launder *et al.* (1975), Johansson & Hallback (1994) etc, are limited in their robustness and scope. In regimes like elliptic flows, the predictions of said models are not satisfactory. Such regimes of flow are fundamentally important to problems such as those regarding wingtip vortices and wake turbulence. Thus, these models are of limited engineering utility for a wide variety of pressing problems. Per contra, there are models like the PRM of Kassinos & Reynolds (1994) that are able to give moderately accurate predictions for a larger set of flows. However, the engineering applicability of these models is limited as they require basis tensors that cannot be measured in an engineering context. Accordingly, there exists a pressing need for a robust yet austere closure for the pressure strain correlation.

This investigation aims to address these issues, systematically and sequentially. We outline a paradigm to formulate models for the rapid pressure strain correlation that possess a very high degree of agreement with linear physics and yet maintain engineering utility. To this end, the specific issues that are addressed include:

1. *Compromises in the scope of the model*: Single-point modeling of the RPSC is an attempt to represent a global phenomenon by the medium of local quantities. Such an exercise is limited in the extent to which it can replicate the dynamics of pressure. Herein, we discuss specific flow features, their import in engineering prediction and their tractability to one-point closure modeling.

2. *Compromises in the structure of the model*: As mentioned, the basis used in single point modeling is incomplete for the purposes of reconstructing the

dynamics of pressure. We discuss the optimal surrogate for this non-local information and the best manner in which to incorporate and actualize this information in the model.

3. *Execution and analysis*: As an illustration, we develop an archetypical model using this paradigm. The predictions of this model are compared to numerical and experimental data while being contrasted against other popular modeling paradigms.

4. *Applicability and extent*: As a clear caveat emptor, we explicitly demarcate the zones of validity of this model for different mean flows.

4.3 Mathematical background

Explicitly, the pressure strain correlation is denoted by:

$$\pi_{ij} = \left\langle \frac{p}{\rho}(\frac{\partial u_i}{\partial x_j} + \frac{\partial u_j}{\partial x_i}) \right\rangle, \tag{4.2}$$

where lowercase symbols represent the fluctuating quantities and $\langle\rangle$ represents ensemble averaging.

$$\frac{1}{\rho}\nabla^2 p = -2\frac{\partial U_i}{\partial x_j}\frac{\partial u_j}{\partial x_i} - \frac{\partial^2}{\partial x_i \partial x_j}(u_i u_j - \langle u_i u_j \rangle). \tag{4.3}$$

With regard to pressure action, by precedent fluctuating pressure is divided into two components, viz. rapid and slow pressure. These are then modeled separately. Mathematically, the terms “rapid" and “slow" refer to the components of pressure arising from the linear and non-linear parts of the source term in the Poisson equation for pressure. The slow component acts to conserve the incompressibility of the velocity field generated by the nonlinear interactions among velocity fluctuations. It is the

function of rapid pressure to impose the divergence free condition on the fluctuating velocity field produced by linear interactions between the mean and fluctuating fields. By their very nature, the non-linear interactions are reasonably independent of the mean velocity field. It is generally accepted that slow-pressure strain correlation tends to isotropize the fluctuating velocity field, irrespective of the mean velocity gradient. In contrast, the action of rapid pressure and consequently, the rapid pressure-strain correlation is highly dependent upon the mean velocity field. Furthermore, it is observed that the rapid pressure evolution is linear with respect to the fluctuating velocity. Thus, the rapid pressure term conserves the number of fluctuating modes.

With respect to the modeling aspect, the RPSC is expressed as a function of measurable tensors.

$$\frac{\pi_{ij}^r}{k} = \sum Q_n T_{ij}^n, \tag{4.4}$$

wherein T_{ij}^n are symmetric, deviatoric tensors and Q_n are the corresponding model coefficients. Due to the linear form of the Poisson equation, the model expression for the RPSC must also be linear. The classical form of such a linear RPSC expression is

$$\begin{aligned}\frac{\pi_{ij}^r}{k} =& Q_1 S_{ij} + Q_2 S_{pq}(b_{ip}\delta_{jq} + b_{jp}\delta_{iq} + \frac{2}{3}b_{pq}\delta_{ij}) \\ &+ Q_3 W_{pq}(b_{ip}\delta_{jq} + b_{jp}\delta_{iq}).\end{aligned} \tag{4.5}$$

In the classical modeling approach, the model expressions are regulated by guidelines based on mathematics and physics, and limitations stipulated by engineering. Categorically, these are:

1. limitation of tensor bases to local, measurable quantities, like the Reynolds stresses, mean gradients, etc;

2. linearity in the Reynolds stresses;

3. linearity in the mean velocity gradient tensor;

4. other ancillary specifications, such as realizability, the Crow constraint, Material Frame Indifference when applicable, etc.

As has been observed in literature, these properties pertain to an ideal model and at present, no model can conform to all these conditions. Thus, the exercise of modeling seeks to develop a “best-possible" model, while observing only select guidelines. In many cases, the individual conditions are antithetical to each other. For instance, it is proved that linear models, obligated by (a), cannot ensure realizable predictions in all regions of the AIM as obligated by (d). Thus, there has been a trend to append non-linear terms to the modeling expression, culminating in the model of Johansson & Hallback (1994) that ensures realizable predictions everywhere.

However, the modeling of the RPSC is tantamount to modeling a fourth order M_{ijkl} tensor. Explicitly,

$$\begin{aligned} &\pi^r_{ij} = 2\frac{\partial U_l}{\partial x_k}(M_{kjil} + M_{ikjl}), \\ &wherein, M_{ijpq} = -\frac{1}{8\pi k}\int \frac{\partial^2 R_{ij}}{\partial r_p \partial r_q}\frac{d\vec{x}'}{r}; \vec{x}' = \vec{x} + \vec{r}. \end{aligned} \tag{4.6}$$

. It is expedient to model this forth order tensor, as just ensuring the adherence of the RPSC model to said guidelines does not lead to a physically consistent expression for the M tensor. Furthermore, the M tensor affords the application of comprehensive realizability conditions.

The most general ansatz for a linear model of M, which has the imprimatur of

the classical framework of pressure strain correlation modeling, is:

$$\begin{aligned} M_{ijpq} =& A_1\delta_{ij}\delta_{pq} + A_2(\delta_{ip}\delta_{jq} + \delta_{iq}\delta_{jp}) + A_3\delta_{ij}b_{pq} + A_3\delta_{pq}b_{ij} \\ &+ A_5(\delta_{ip}b_{jq} + \delta_{iq}b_{jp} + \delta_{jp}b_{iq} + \delta_{jq}b_{ip}). \end{aligned} \tag{4.7}$$

Analogous to the RPSC, certain constraints are obligated upon such a representation. These include:

1. linearity condition, with respect to the Reynolds stress anisotropies;
2. symmetry conditions, with respect to the indices ($M_{ijkl} = M_{jikl}, M_{ijkl} = M_{ijlk}$);
3. continuity condition ($M_{ijil} = 0$);
4. Green's condition ($M_{ijkk} = \frac{R_{ij}}{2k}$);
5. Crow constraint.

$$\begin{aligned} \frac{\pi^r_{ij}}{k} =& \frac{4}{5}S_{ij} - 12A_5S_{pq}(b_{ip}\delta_{jq} + b_{jp}\delta_{iq} + \frac{2}{3}b_{pq}\delta_{ij}) \\ &-\frac{4}{3}(2 + 7A_5)W_{pq}(b_{ip}\delta_{jq} + b_{jp}\delta_{iq}). \end{aligned} \tag{4.8}$$

Thus, adhering to the classical framework and its concomitant constraints, the RPSC model has a single degree of freedom. In the succeeding sections, we shall outline the specification of the same and the rationale underlying this process. For the purposes of the analysis preceding the modeling paradigm, we restrict ourselves to planar quadratic flows (Salhi *et al.*, 1997). Herein, to characterize the applied gradient field, ellipticity parameter, β , is defined as:

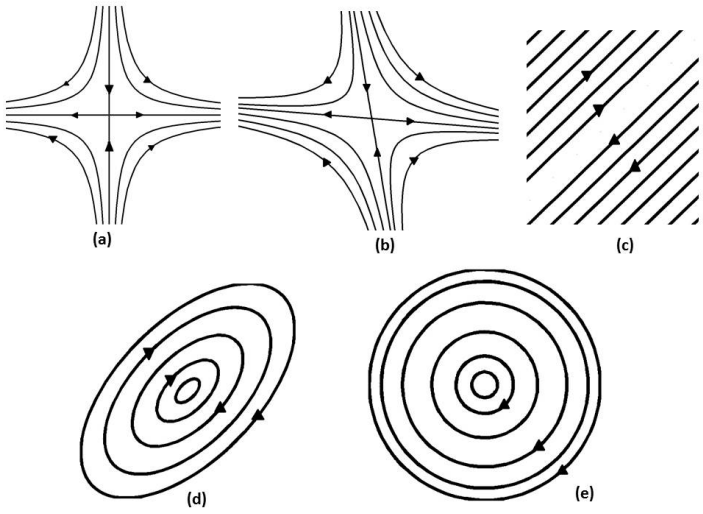

Figure 4.2: The mean flow streamlines as a function of the parameter β. With increment in β, from zero to one, we observe the variation in the mean flow streamlines. (a) and (b) represent hyperbolic flows, where $\beta < 0.5$. (c) represents a pure shear case with β=0.5. (d) and (e) are representative of elliptic flows cases, where $\beta > 0.5$.

$$\beta = \frac{W_{pq}W_{pq}}{W_{ij}W_{ij} + S_{ij}S_{ij}}, \text{where,} \tag{4.9}$$

$$S_{ij} = \frac{1}{2}(\frac{\partial U_i}{\partial x_j} + \frac{\partial U_j}{\partial x_i}), \quad W_{ij} = \frac{1}{2}(\frac{\partial U_i}{\partial x_j} - \frac{\partial U_j}{\partial x_i}). \tag{4.10}$$

W_{ij} and S_{ij} refer to the rate of rotation and rate of strain tensors of the background flow. Planar quadratic flows can be uniquely characterized by the value of β, as exhibited in figure 4.2. For the purposes of the present investigation, the applied gradient field is confined to the 1-2 plane and the figures exhibit the streamlines in this plane. Quadratic flows can be divided into three classes, based on the applied gradient field: hyperbolic (strain dominated or open streamline flows), elliptic (rotation dominated or closed streamline flows) and purely sheared flows. The classification and nomenclature used to differentiate between quadratic flows are outlined

	Range of β	Nomenclature
I.	$[0, 0.5)$	Hyperbolic/Strain-dominated/Open-streamline flow
II.	0.5	Purely sheared/Homogeneous shear flow
III.	$(0.5, 1]$	Elliptic/Rotation-dominated/Closed-streamline flow

Table 4.1: The nomenclature for different regimes of flow and their relation to the ellipticity parameter.

in Table 4.1. The relative strengths of the rate of strain and rotation tensors can be quantified by non-dimensionalizing their norms by that of the mean velocity gradient tensor. In this regard, we define the derived parameters:

$$a = \sqrt{\frac{1-\beta}{2}}, \quad b = \sqrt{\frac{\beta}{2}}. \tag{4.11}$$

Thus, the parameter "a" measures the relative strength of the applied strain and "b", of the applied rotation. In the principal co-ordinates of strain, the requisite mean flow tensors are given as,

$$\frac{\partial U_i}{\partial x_j} = \begin{bmatrix} a & -b & 0 \\ b & -a & 0 \\ 0 & 0 & 0 \end{bmatrix}, \quad S_{ij} = \begin{bmatrix} a & 0 & 0 \\ 0 & -a & 0 \\ 0 & 0 & 0 \end{bmatrix}, \quad W_{ij} = \begin{bmatrix} 0 & -b & 0 \\ b & 0 & 0 \\ 0 & 0 & 0 \end{bmatrix}. \tag{4.12}$$

4.4 The effects of pressure: amenability to single point modeling

In an incompressible flow, pressure has to respond instantaneously to any changes in the entire velocity field. This global nature of the pressure action is reflected in its evolution via a Poisson equation. However, in the context of one-point closure modeling, the action of pressure, embodied in the pressure strain correlation, must be

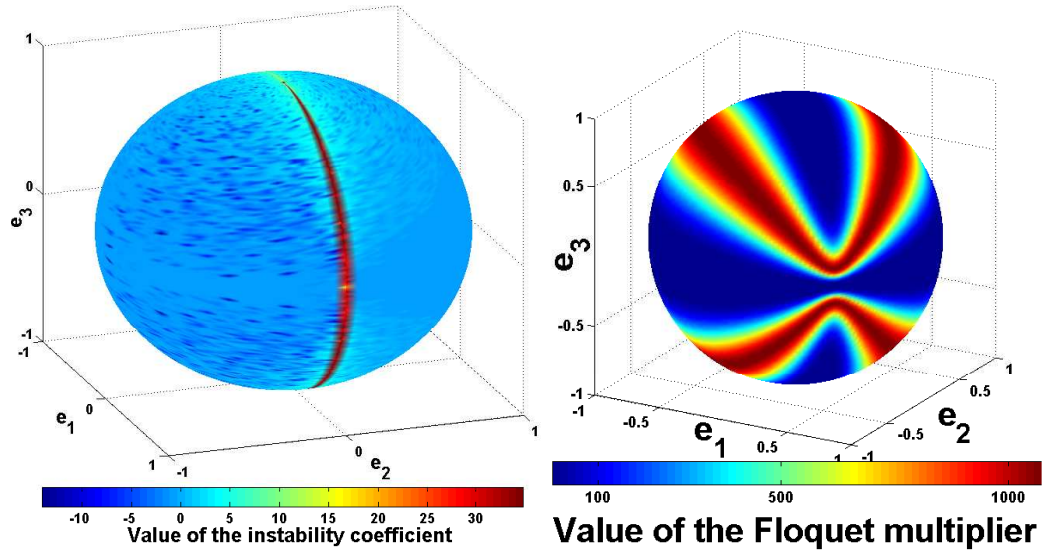

Figure 4.3: The figure illustrates the effect of initial modal alignment on modal stability for (a) a representative hyperbolic flow, and, (b) a representative elliptic flow.

expressed via local tensors which can be measured in an engineering context. Thus, single-point modeling of the RPSC is an attempt to represent a global phenomenon by the medium of local quantities. Clearly, such an exercise will be limited in the scope, to which it can replicate the dynamics of pressure, and the extent, to which it can capture specific phenomena. Herein, we discuss specific flow features and their tractability to one-point closure modeling. These have been examined at length in Mishra & Girimaji (2013). Thence, specific compromises are suggested in the classical modeling formulation to arrive at a "best-possible" formulation.

Flow instabilities: For planar quadratic flows, the inertial effects on a Fourier mode are independent of the alignment of the mode with respect to the eigen-directions of the applied gradient. However, the action of pressure is a strong function of modal alignment. For different regimes of flow, *the pressure effects selectively stabilize or destabilize specific modes, to different degrees, contingent upon the modal*

alignment. This is related to the “structuring effect" of linear physics (Sagaut & Cambon, 2008). Consequently, accurate replication of the action of pressure is highly contingent upon wavenumber space information.

As discussed in Cambon *et al.* (1992); Jacquin *et al.* (1990); Mishra & Girimaji (2013), the pressure effects play a profound role in the inception of the instabilities manifested in planar quadratic flows. Both the elliptic flow instability and the hyperbolic instability are highly dependent on the alignment of specific modes. This is exhibited in figures 4.3(a) and 4.3(b) respectively, where we exhibit the relationship between initial modal alignment in wavenumber space and modal stability. For the hyperbolic flow, only a very small set of modes, aligned with the extensional eigendirection, exhibit prolonged unstable behavior. For pure shear flows, the set of unstable modes is relatively larger. However, only the modes aligned with the “vertical" direction, show significant growth. This scenario is further exacerbated in the case of the elliptic flow instability wherein the effects of pressure initiate and sustain the flow instability. Here, only a narrow “band" of oscillatory modes exhibit unstable behavior. Additionally, the topology of this band of unstable modes is highly dependent on the ellipticity parameter.

Due to the spherical averaging inherent to the Second Moment Closure methodology (Cambon & Rubinstein, 2006), such models are bereft of wavenumber space information. In this light, accurate representation of the flow instabilities is not within the purview of models adhering to this framework.

The oscillatory behavior in elliptic flows: For the regime of elliptic flows, RDT exhibits bilinear oscillations. Consequently, the oscillations have a varying amplitude about a time dependent mean. On the contrary, established models predict linear oscillations, exhibiting a constant mean and amplitude. To reproduce a time dependent mean and amplitude with an incomplete basis, the models would have to resort

to limit cycle oscillations to mimic bilinear phenomena. This would require a rapid pressure strain correlation that is non-linear in the Reynolds stress anisotropies, that would violate guidelines obligated by physics. To completely characterize a state of oscillation, of the generic form $x = Asin(\omega t + \phi)$, one requires three functions, namely amplitude, frequency and phase. The frequency of oscillation is an explicit function of the mean flow topology. However, the determination of the amplitude and the phase require explicit knowledge of the initial conditions of the internal structure of the turbulent flow field. Thus, to approximate the oscillatory behavior shown in elliptic flows, the wavenumber space information needs to be a part of the basis utilized in the model. Prior investigations, such as Sjogren & Johansson (2000), have employed models that are non-linear in the mean gradients to capture said oscillatory behavior. In turbulent flows, the oscillations of flow statistics are caused, primarily, due to the dynamics of the wave-vector and are thus, outside the scope of one-point modeling. No permutations of such local tensors can enable one-point closures to replicate this behavior faithfully.

The bifurcation in the system: In transitioning from hyperbolic to elliptic flows, the system of governing equations undergo a saddle-node bifurcation. Consequently, the evolution of the Reynolds stress anisotropies changes from stationary states to oscillatory solutions. However, this bifurcation is engendered in the wave-vector evolution equation. Thus, popular one-point closure models are not able to capture the location or the nature of this change in the system's dynamics.

Realizability: Schumann (1977) was the first to articulate the realizability constraint for turbulence closures, requiring models to yield a Reynolds stress tensor that is positive semi-definite. It has been pointed out by Shih *et al.* (1990), Cambon & Rubinstein (2006) and Speziale *et al.* (1994) that due to the lack of wavenumber space information in the formulation, models based on the Second Moment Closure

paradigm are limited in their applicability to low to moderate levels of anisotropy. According to Cambon & Rubinstein (2006), this limitation is manifested via realizability violations. It has been proved, analytically (Rubinstein & Girimaji, 2006) and computationally (Lumley, 1978), that linear models cannot ensure physically meaningful solutions for all states of turbulence. This has been one of the principal motivations to append non-linear terms to the model expression. In this vein, the lowest order model that can asservate realizability is the fifth order expression of Johansson & Hallback (1994).

However, in a recent investigation Mishra & Girimaji (2014) have pointed out that even models adhering to these realizability conditions can still predict Reynolds stress dynamics that are completely aphysical. Furthermore, approaches such as those that add higher order non-linear terms to the modeling expression or those that seek to add additional tensors to the basis, manifest larger violations from permissible dynamics for larger regions of the anisotropy invariant map.

This represents a paradoxical scenario for the Second Moment Closure framework. Models adhering to this recourse replicate the dynamics due to unclosed terms in the Reynolds stress transport equations and lead to predictions for the Reynolds stresses. However, to ensure that these predictions are physically meaningful, the models have to resort to measures that engender the Reynolds stress dynamics to be aphysical.

Uncertainty Quantification: The Reynolds stresses express the componentiality of the turbulent flow field and do not provide a complete description of the internal structure of the flow. For the rapid distortion equations, the specification of the Reynolds stresses does not lead to a unique evolution trajectory. Instead of a single unique solution once the Reynolds stress tensor has been specified, there is a range of permissible solutions. In figure 4.4 this range is shown for a representative hyperbolic

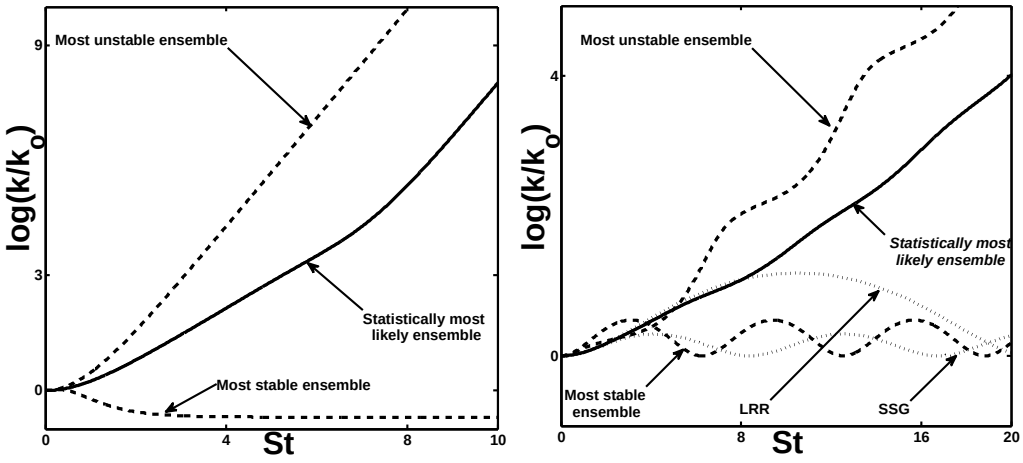

Figure 4.4: The range of permissible behavior for a representative hyperbolic flow, β =0, and an elliptic flow, β =0.64.

flow (plane strain) and an elliptic flow (β =0.64).

In essence, the distribution of the modes accounts for the history of the particular flow. For both these flow regimes, the turbulent kinetic energy evolution is not universal and is notably dependent on the alignments of the modes in the flow. Bereft of wavenumber space information, *high fidelity modeling of such behavior by one-point closures remains infeasible.*

4.5 Single point modeling: compromises and allowances

Building upon the discussion in the prior section, we outline compromises in the scope of the modeling objectives, vis-a-vis their scope. Thence, we delineate modifications in the modeling framework and the rationale underlying the same.

As has been discussed, the oscillatory behavior in flow statistics for rotation dominated flows is not amenable to replication in single point models. However, from an engineering perspective, the dynamics of the oscillatory behavior are relatively unimportant when compared to the evolution of the mean value of the flow statistic. As an illustration, we consider the DNS results of Blaisdell & Shariff (1994) in

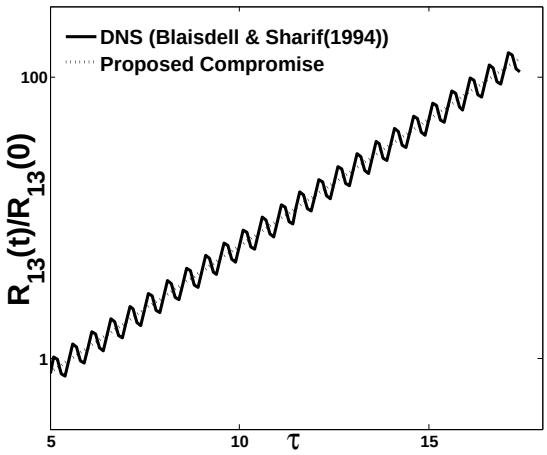

Figure 4.5: Compromise in the scope of the modeling objective.

figure 4.5. As schematically exhibited therein, a model that is able to replicate the evolution on the mean value of the statistic may be of significant engineering utility. Adopting such a simplification in the modeling objective precludes the necessity of considering the bifurcations in the system, as for either variety of flow (strain or rotation dominated), the modeling exercise will predict stationary states.

Considering the issue of realizability, the specification of a model for the pressure strain correlation is equivalent to the ascription of the Reynolds stress dynamics owing to pressure effects. In this regard, it is holistically harmonious to enjoin the Reynolds stress dynamics to be realizable. Furthermore, it has been exhibited that violations in the realizability of the Reynolds stress dynamics precedes and leads to violations in the realizability of the Reynolds stresses. In this light, *it may be expedient for modeling exercises to adopt the process realizability framework* (Mishra & Girimaji, 2014). This approach has two additional advantages, wherein, this framework can explicitly demarcate, a priori, the zones where the model is valid and where it is not applicable, for any and all mean flows. This acts as caveat emptor for engineering applications of any model. Additionally, Mishra & Girimaji (2014)

have outlined an analytical methodology to maximize the zones of validity for any modeling attempt.

Considering the form of the closure expression, the properties that an ideal model for the M tensor should possess are:

1. *The model expression should adhere to a certain functional form.* The specifics of the form of the expression have been discussed in Section II. This form ensures that the modeled M tensor retains the requisite symmetries (that arise due to specific properties of the tensor). Furthermore, this limits the tensor basis to local tensors that can be measured in an engineering context.

2. *The model expression should be linear in the Reynolds stresses.* In this regard, the Poisson equation governing rapid pressure is linear in the fluctuating velocities. Consequently, the rapid pressure strain correlation must conserve the number of Fourier modes in the representation of the fluctuating field. This is often argued via the *superposition principle*, wherein a fluctuating velocity field constituted of uncorrelated fluctuating fields should possess a pressure strain correlation that is the summation of the pressure strain correlations of the individual, uncorrelated constituents (Reynolds, 1976).

3. *The model expression should not be a function of the mean gradient.* Considering the mathematical definition,

$$M_{ijpq} = -\frac{1}{8\pi k}\int \frac{\partial^2 R_{ij}}{\partial r_p \partial r_q}\frac{d\vec{x}'}{r}, \tag{4.13}$$

it is evident that this tensor is not directly affected by changes in the mean gradient field. The dependence of the M tensor on the mean velocity gradient is indirect and arises through the two-point correlation. Consequently, making

the M tensor expression directly dependent on the mean gradient may not possess outright mathematical imprimatur.

It is established that no model can satisfy these properties and yet ensure accurate and realizable predictions for a variety of flows. Thus, different modeling attempts seek to relax some of the aforementioned properties to enable predictions with higher fidelity and realizability. In this regard, it has been established that closures that are linear in the Reynolds stresses are unable to ensure a realizable Reynolds stress tensor in the vicinity of the 2C limit (Lumley, 1978). Furthermore, model expressions that are linear in the Reynolds stress possess only one tunable coefficient. If adhering to all the properties above, this coefficient must be a constant. This hinders the calibration of the model to yield better agreements with experiments for different flows. Consequently, many closure nominations forgo linearity in the Reynolds stresses and incorporate non-linear terms thereof in the closure expression. Adopting nonlinear expressions for the M tensor, allows the model to be realizable in the neighborhood of the 2C limit. Higher degrees of nonlinearity provide additional degrees of freedom in the formulation. This enables the model coefficients to be calibrated for accuracy in certain flows while still maintaining Reynolds stress realizability.

While the relaxation of the linearity requirement represents a pragmatic engineering compromise, this does leads to complications. Nonlinear models of any order cannot ensure a realizable Reynolds stress tensor. Even models satisfying the classical realizability conditions can transition to unrealizable zones near the 1C state (Speziale *et al.*, 1994). Resorting to nonlinear expressions in the Reynolds stresses leads to spurious oscillations in the vicinity of the 2C state (Speziale *et al.*, 1994). In an investigation of modeled Reynolds stress dynamics, Mishra & Girimaji (2014) have exhibited that nonlinear model expressions do not lead to better process realiz-

ability characteristics. In fact, in most cases, as the degree of non-linearity increases, the process realizability characteristics of the closure are progressively undermined. Resorting to modeling expressions that are nonlinear in the Reynolds stresses is equivalent to attempting to use the Reynolds stresses as a surrogate for the missing wavenumber space information. However, the Reynolds stress tensor does not possess this information regarding the internal structure of the flow and consequently, such measures have met with limited success.

As has been exhibited, in homogeneous flows, only small sets of modes from the ensemble exhibit unstable behavior. The flow statistics are determined by the contributions from these modes. The evolution of these modes leads to concomitant ramifications upon the flow statistics. Thus, flow statistics are highly dependent on wavenumber space dynamics. The key hurdle in high-fidelity single point modeling of pressure effects is to reproduce this behavior while bereft of information regarding wavenumber dynamics. However, in a detailed analysis based on Dynamical Systems Theory, Mishra & Girimaji (2010) have shown that due to the invariant sets manifested in the phase space of the wavenumber vector, the wavenumber vector trajectories exhibit universal dynamics. Consequently, after a brief transient, *almost all* modes in wavenumber vector space exhibit similar behavior. The minutiae of this universal behavior are highly dependent on the topology of the mean gradient, that can be characterized via its invariants. Consequently, explicit specification of the mean gradient field in the model for the M tensor can act as a surrogate for the missing wavenumber vector space information. *Thus, inclusion on the mean velocity gradient invariants into the basis for the M tensor, may lead to better fidelity of predictions.*

Considering the issue of realizability, the process realizability approach seeks to ensure that the Reynolds stress dynamics remain physically permissible. Thus, the

model expression should be capable of replicating the dynamics engendered by any set of modes that may constitute the given Reynolds stress tensor. As the dynamics of the modes in the flow are completely dependent on the mean velocity gradient, there is an intimate relationship between the process realizability framework and the mean gradient. As discussed in Mishra & Girimaji (2014), the process realizability constraints are explicit functions of the mean velocity gradient. *Consequently, in lieu of the wavenumber space information, using the mean gradient information in the model for the M tensor would enable better process realizability characteristics.*

Thus, explicit inclusion of mean gradient information in the M tensor expression would lead to models that are capable of better fidelity in the prediction and improved realizability characteristics. Lee (1990) and Sjogren & Johansson (2000) represent the few investigations that have considered such an approach. *Both these models exhibited considerable improvements in predictions.*

Consequently, for the three reasons discussed above, it is suggested that the most optimal recourse may be to make the M tensor expression directly dependent on the mean gradient, while retaining the linearity in the Reynolds stresses. Once this paradigm has been adopted, the next issue to be addressed is how to incorporate this into a model expression. Lee (1990) attempted to utilize this information using the reference logarithmic strain parameter, while Sjogren & Johansson (2000) have used explicit tensor functions of the rate of strain and the rate of rotation. However, the analysis of Mishra & Girimaji (2010) reveals that the dynamics in wavenumber space can be characterized based on the topology of the flow. For the case of planar, quadratic flows, the topology of the mean velocity field can be completely determined by a single scalar parameter. In this light, it may be expedient to make the coefficients, A_i, in the expression for the M_{ijkl} tensor to be explicit functions of this scalar parameter. Explication of this functional dependence, determines the

final model.

In prior investigations, attempts have been made to utilize the conclusions from multi-point theories to develop better single-point models. In Godeferd *et al.* (2001), strategies for such an approach were outlined and discussed. To determine this dependence, it is suggested that explicit numerical simulation under the aegis of the Rapid Distortion Theory be utilized to yield the values of the coefficient. A similar approach has been utilized by Jakirlic & Hanjalic. (2013) to re-examine the values of the coefficients in pressure strain closures. For the purposes of developing an archetypical model to outline this procedure, we use a simple methodology wherein RDT based simulations are carried out with a well distributed modal ensemble. Thus, for this statistical treatment, the initial conditions in Fourier space are chosen to correspond to an isotropic initial state of turbulence representing an unbiased initial state. Herein, velocity fluctuations in all permissible directions are taken to be equally energetic. This ensures that the initial state is not biased and the predilection in the dynamics of the system manifests itself in an unhindered manner. Specific phases, wherein agreement between the simulations and model predictions is essential, are chosen. The details of these phases for different mean flows and the rationale underlying their choice is discussed in extensive detail in Mishra & Girimaji (2010). For these phases, the values predicted by the modes are averaged with over the modes in the ensemble, weighed by the modal kinetic energies, and over the duration of the phase to give the explicit value of the coefficient for the specific mean flow. This leads to a curve determining the value of the coefficient A_5 with respect to the elliptcity parameter, β, as exhibited in figure 4.6.

Despite the severely austere methodology adopted, a few salient features of this functional dependence need to be emphasized. As discussed in Mishra & Girimaji (2013), the predominant energy transfer for hyperbolic flows is from the compres-

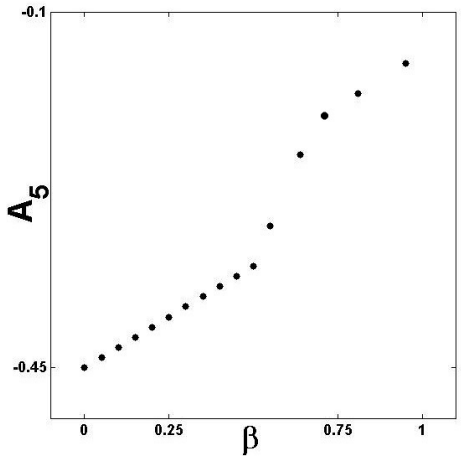

Figure 4.6: The functional relationship between A_5 and the ellipticity parameter, β.

sional eigendirection to the R_{33} component. With increment in the ellipticity parameter, β, these eigendirections shift linearly toward each other. Closures with constant coefficients do not heed this shift and this progressively impairs their ability to mimic the system's behavior in the Rapid Distortion Limit. *The methodology outlined above is able to account for this migration of the eigendirections, manifested in the linear variation of the A_5 coefficient for hyperbolic flows.* Additionally, this modeling methodology ignores the oscillatory behavior for elliptic flows, thus ignoring the bifurcation in the system while transitioning from strain to rotation dominated flows. In spite of this, *the bifurcation in system behavior is accounted for in the A_5 coefficient, wherein the dependence of A_5 changes from a linear to a nonlinear function of β* on transitioning from strain to rotation dominated flows, respectively.

4.6 Model behavior: predictive fidelity

In this section, the predictions of this illustrative model are compared to numerical and experimental data while being contrasted against other popular closures. The popular closures represent different modeling paradigms, with respect to their

adherence to the constraints imposed upon an ideal model, as represented in the schematic.

With respect to the properties obligated upon an ideal closure, the model of Launder *et al.* (1975) adheres to all the three properties obligated upon an ideal model. However, the dynamics predicted by this model are often deficient, especially for the case of rotation dominated flows. The model of Speziale *et al.* (1991) relaxes the condition of linearity in the Reynolds stress tensor. Using an invariant dynamics approach, this model utilizes a closure expression that is quadratic in the components of the Reynolds stress tensor and the coefficients used therein are functions of the invariants of the Reynolds stress anisotropy tensor. This allows the closure to adhere to the weak form of the realizability condition and exhibit better predictions, especially for purely sheared flows (in both inertial and non-inertial frames). However, the dynamics predicted by this model for regimes such as those with rotation are unsatisfactory. The closure suggested by Johansson & Hallback (1994) utilizes fourth order expansions in the components of the Reynolds stress anisotropy tensor. This enables the model to satisfy the strong form of the realizability constraint for all states on the anisotropy invariant map and exhibit improved agreements with experimental data for a variety of flows. However, this model is still deficient for the replication of the dynamics of flows with rotational effects. Due to this unsatisfactory performance of classical pressure strain correlation models, Kassinos and Reynolds(Kassinos & Reynolds, 1994) have attempted to use additional tensors in their modeling framework. Kassinos & Reynolds (1994) have averred that single-point modeling of the dynamics of pressure requires supplementary tensors, such as Dimensionality, D_{ij}, Circulicity, F_{ij} and Stropholysis, Q_{ijk}. For homogeneous

turbulence, these can be defined as:

$$R_{ij} = M_{ijkk}, D_{ij} = M_{kkij}, F_{ij} = \epsilon_{imp}\epsilon_{jrs}M_{psrm}, Q_{ijk} = \epsilon_{ipq}M_{jqpk}. \tag{4.14}$$

The authors then proceed to proffer and test models utilizing this basis. For rotation dominated flows, these models exhibit slight improvement in predictive fidelity and capture more flow features in rotation dominated regimes. However, the improvement in fidelity are not commensurate with the inherent complexity of the model, requiring tensors that are not measurable in a single-point paradigm. Furthermore, the models of Kassinos & Reynolds (1994) are highly susceptible to violations in Reynolds stress realizability. The different paradigms of modeling are contrasted in the schematic given in figure 4.7.

The types of flows utilized in this comparison are discussed in Table 4.2, along with the rationale underlying the choice. The objective of this exercise is to exhibit that the illustrative model developed in the last section is able to exhibit predictions that are at par with other models for the regimes of flow wherein these established models perform adequately. Furthermore, in regimes wherein established models do not exhibit satisfactory performance, the illustrative model is still able to provide predictions of engineering utility.

4.6.1 Performance under the Rapid Distortion assumption

In figure 4.8, the predictions of the illustrative model are compared to RDT simulations and contrasted against other popular models. As can be observed, the new modeling paradigm proffers better agreement with RDT data, as compared to popular closures such as those by Launder *et al.* (1975) and Speziale *et al.* (1991). It is well established that the aforementioned models do not provide satisfactory predictions in the regimes of elliptic flows. For this case, we contrast the new modeling

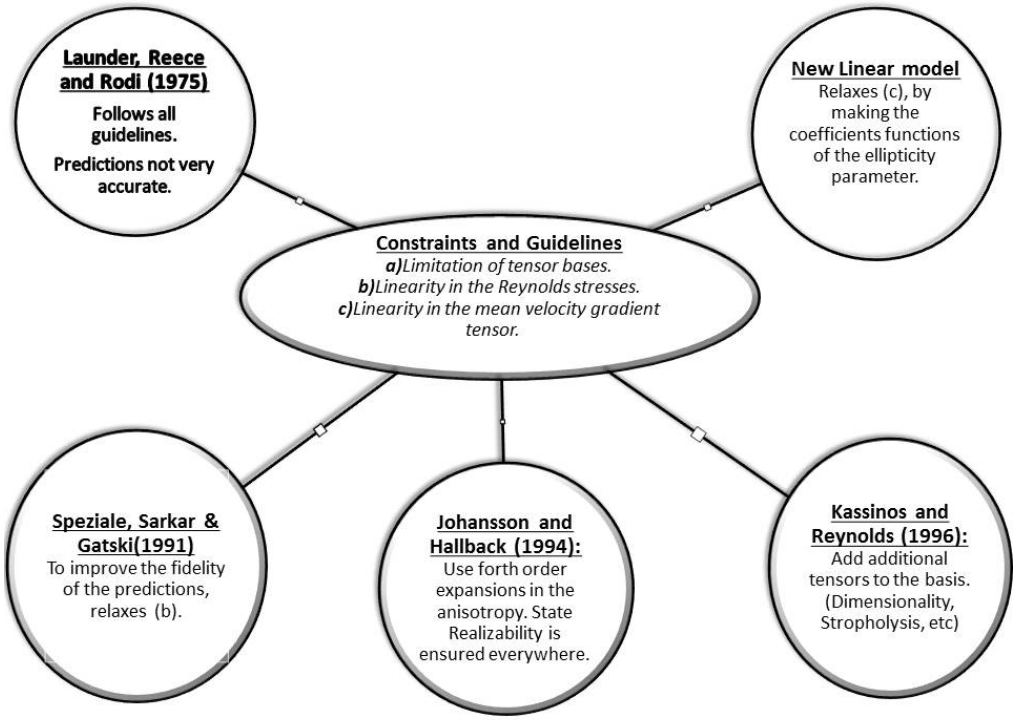

Figure 4.7: Schematic illustration of the different approaches to model the pressure strain correlation.

	Type of Flows	**Rationale**
I.	Under the Rapid Distortion assumption	To test the RPSC model, in isolation.
II.	DNS of hyperbolic flows	Classical benchmarking case.
III.	Axisymmetric Expansion and Contraction.	Performance in non-planar flows.
IV.	Rotating Shear.	Performance in non-inertial frames.
V.	DNS of elliptic flows.	Robustness and applicability.

Table 4.2: The set of cases under consideration and the rationale thereof.

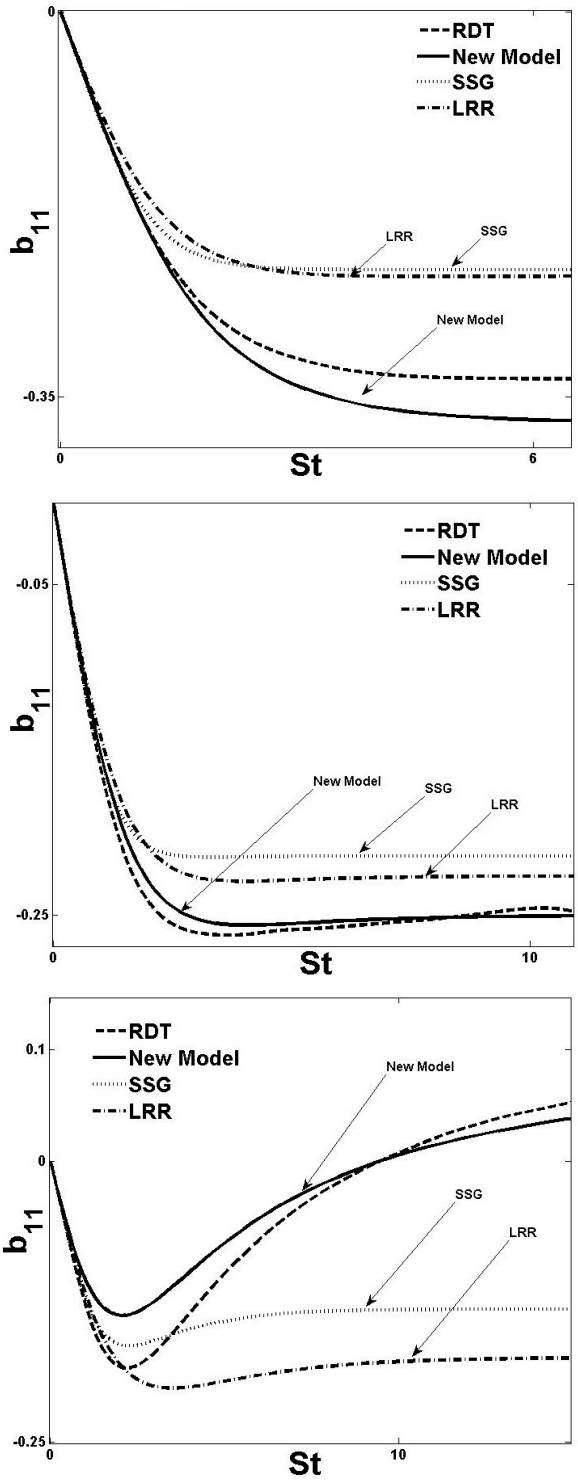

Figure 4.8: Fidelity under the Rapid Distortion assumption. (a)Plane strain, (b)Hyperbolic flow with $\beta = 0.19$, (c)Purely sheared flow.

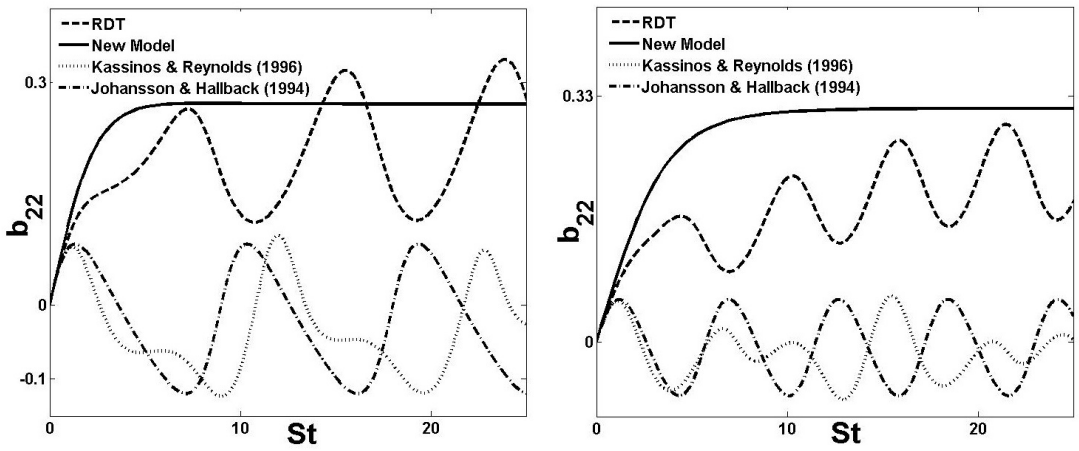

Figure 4.9: Fidelity under the Rapid Distortion assumption. (a)elliptic flow with $\beta = 0.64$, (b)elliptic flow with $\beta = 0.81$.

paradigm against the advanced closures formulated by Johansson & Hallback (1994) and Kassinos & Reynolds (1994). In figure 4.9, it is exhibited that the new modeling paradigm is able to replicate the evolution of the mean of the oscillatory statistic to a satisfactory degree. The models of Johansson & Hallback (1994) and Kassinos & Reynolds (1994) predict oscillatory behavior but the mean of the predicted oscillations is not commensurate to that of the RDT data. Additionally, the nature of the oscillations is markedly different. The RDT simulations undergo bilinear oscillations with an evolving mean and amplitude. The models of Johansson & Hallback (1994) and Kassinos & Reynolds (1994) predict linear oscillations with a constant mean and amplitude. Furthermore, the oscillations predicted by the aforementioned do not possess the correct phase relationship with the RDT data. This underscores the inability of second moment closures to replicate the oscillatory dynamics faithfully.

4.6.2 Performance for hyperbolic flows

In figure 4.10, the predictions of the illustrative model are compared to DNS data and contrasted against other popular models for the case of a plane strain mean

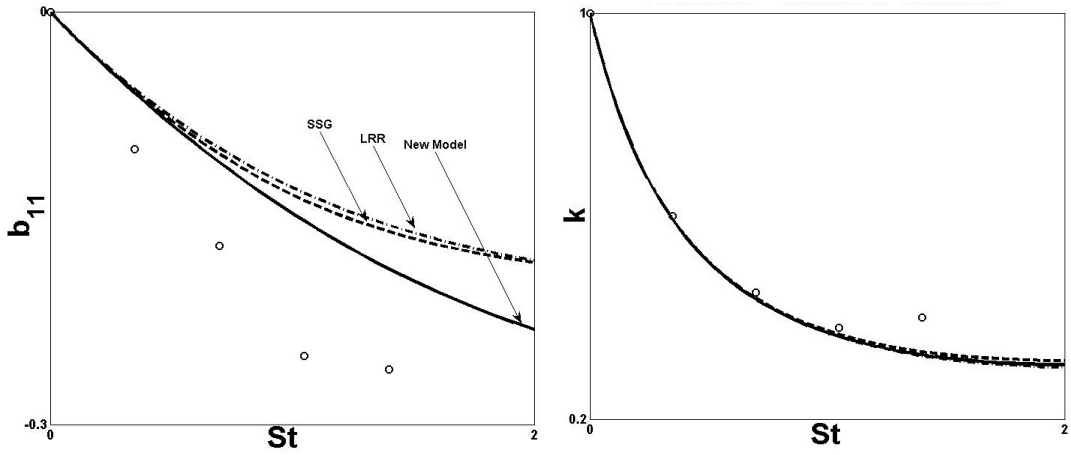

Figure 4.10: Fidelity for hyperbolic flows. (a)anisotropy evolution for plane strain, (b)turbulent kinetic evolution for plane strain.

flow. As can be observed, the new modeling paradigm is able to ensure satisfactory agreement with DNS data, at par with established closures.

4.6.3 Performance for axisymmetric expansion and contraction

In figure 4.11, the predictions of the illustrative model are compared to DNS data and contrasted against other popular models for the case of a mean flow undergoing axisymmetric contraction. As can be observed, the new modeling paradigm is able to ensure satisfactory agreement with DNS data and its predictions are at par with popular closures. Similar behavior can be observed for the case of a mean flow undergoing axisymmetric expansion, as exhibited in figure 4.12.

4.6.4 Performance for the case of rotating shear

In figure 4.13, the predictions of the illustrative model are compared to DNS data and contrasted against other popular models for the case of a shear flow with rotation of the coordinate axes. As can be observed, for moderate values of the parameter $\frac{\omega}{S}$, the new modeling paradigm is able to ensure good agreement with DNS data.

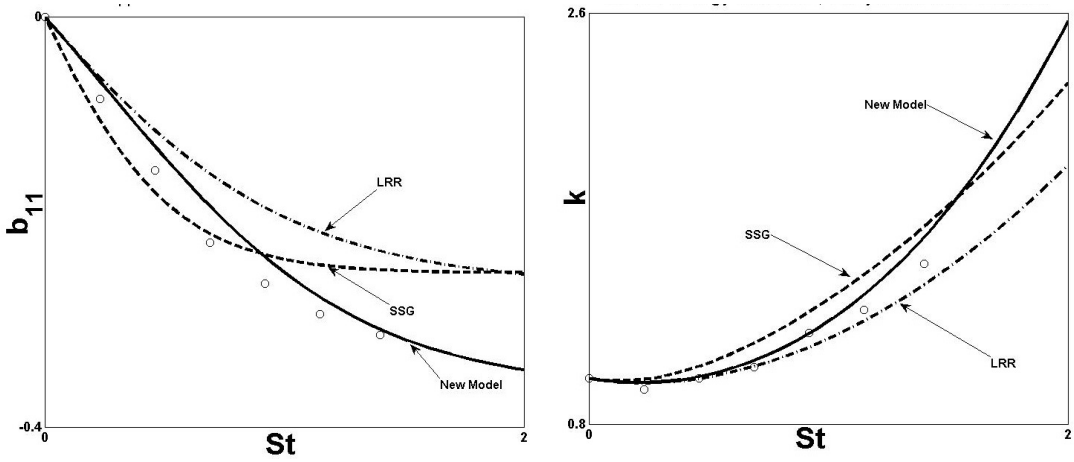

Figure 4.11: Fidelity for Axisymmetric contraction.

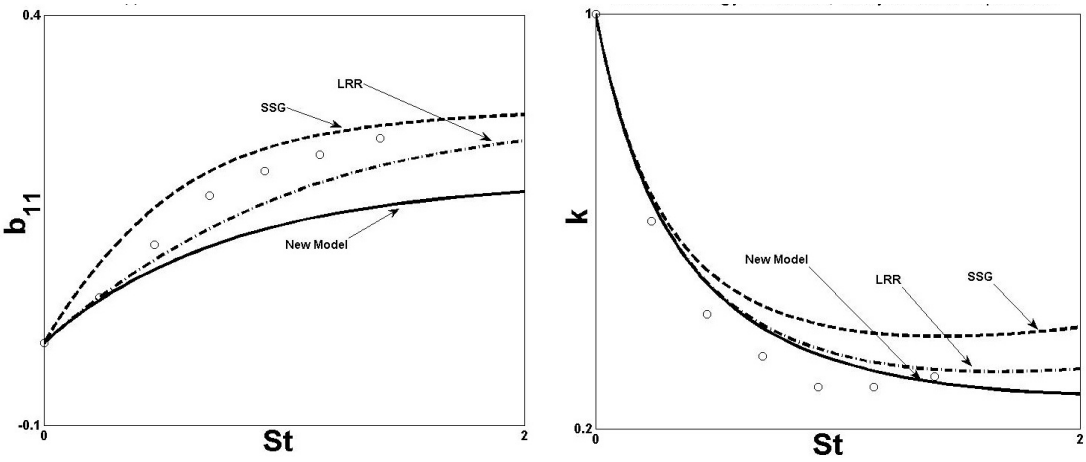

Figure 4.12: Fidelity for Axisymmetric expansion.

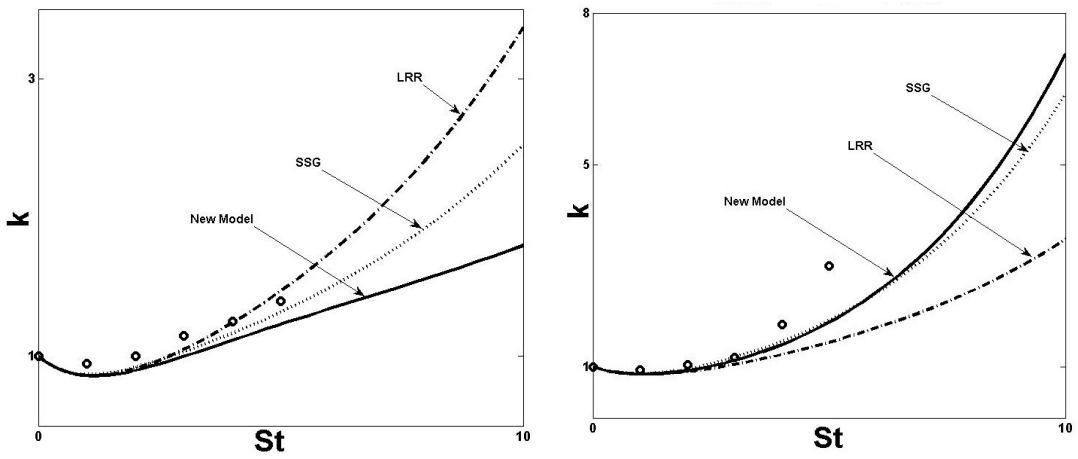

Figure 4.13: Fidelity for the case of rotating shear. (a)$\frac{\omega}{S} = 0.0$, (b)$\frac{\omega}{S} = 0.25$.

4.6.5 Performance for elliptic flows

In figure 4.14, the predictions of the illustrative model are compared to the DNS data of Blaisdell & Shariff (1996) and contrasted against other popular models for the case of an elliptic mean flow ($\beta = 0.74$). As can be observed, the new modeling paradigm is able to give significant agreement for the anisotropy evolution. For the evolution of the turbulent kinetic energy, under the influence of the elliptic flow instability, the new model is able to capture both the existence of unstable behavior as well as the growth rate. As the ellipticity parameter is increased, the predictions of other popular models are exacerbated, as is reflected in figure 4.15. However, even for such higher values, the new modeling paradigm is able to suggest the presence of the instability and predict the evolution of flow statistics.

4.7 Model behavior: realizability of Reynolds stress dynamics

The incomplete basis used in pressure strain correlation modeling leads to the inapplicability of Second Moment closures to higher values of anisotropy(Cambon & Rubinstein, 2006; Sagaut & Cambon, 2008). This is exhibited in the investigation of

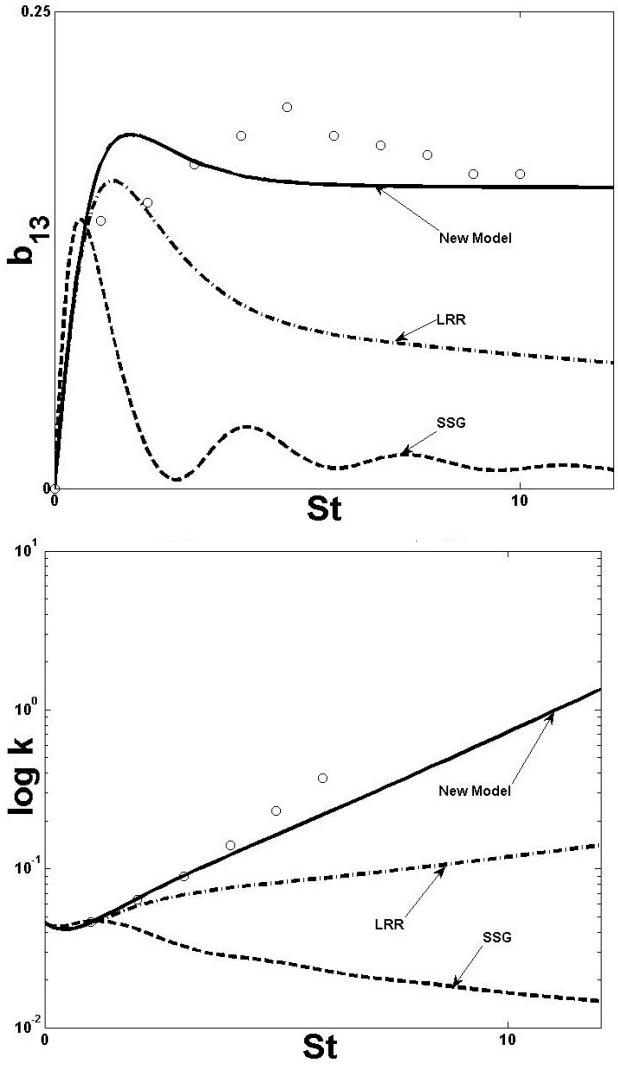

Figure 4.14: Fidelity for the case of an elliptic flow with $\beta = 0.74$. (a)anisotropy evolution, (b)turbulent kinetic evolution.

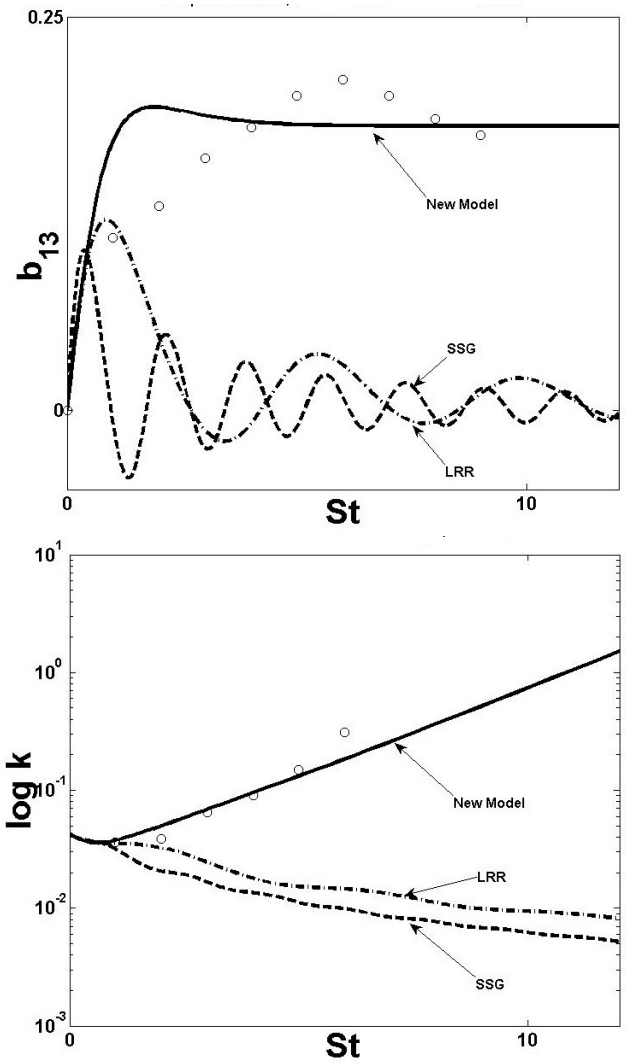

Figure 4.15: Fidelity for the case of an elliptic flow with $\beta = 0.81$. (a)anisotropy evolution, (b)turbulent kinetic evolution.

Mishra & Girimaji (2014), wherein it is shown that most models can ensure realizable predictions only for low to moderate levels of anisotropy. All models have significantly large regions on the anisotropy invariant map wherein they are unable to ensure realizable Reynolds stress dynamics. For this modeling paradigm, we suggest that the process realizability constraints developed in Mishra & Girimaji (2014) be applied to clearly demarcate the states of turbulence wherein the model is able to ensure realizability. Such explicit delineation of the extent of the validity of the closure acts as a caveat emptor in the process of its application to engineering problems.

For the explicit procedure of this demarcation, the reader is referred to Mishra & Girimaji (2014). Herein, we apply the set of process realizability constraints to exhibit the zones of validity of the model for different planar quadratic mean flows, as exhibited in figure 4.16. In line with the limitation discussed earlier, the illustrative model is able to ensure realizable Reynolds stress dynamics for low to moderate levels of anisotropy. However, it must be emphasized that for the case of hyperbolic and purely sheared flows, the model shows process realizability adherence that is at par with other popular models. For the case of elliptic flows, the illustrative model shows process realizability adherence that is better than popular models such as those of Launder *et al.* (1975) and Speziale *et al.* (1991).

4.8 Summary and conclusions

In this investigation, we outline a paradigm toward formulating a pressure strain correlation model that possesses the optimal agreement within the scope of single point closures. The basis of this investigation is grounded in

1. a detailed Dynamical Systems Theory based analysis of modal behavior, and,
2. a analysis of the capabilities of the single-point modeling framework to ensure permissible Reynolds stress dynamics.

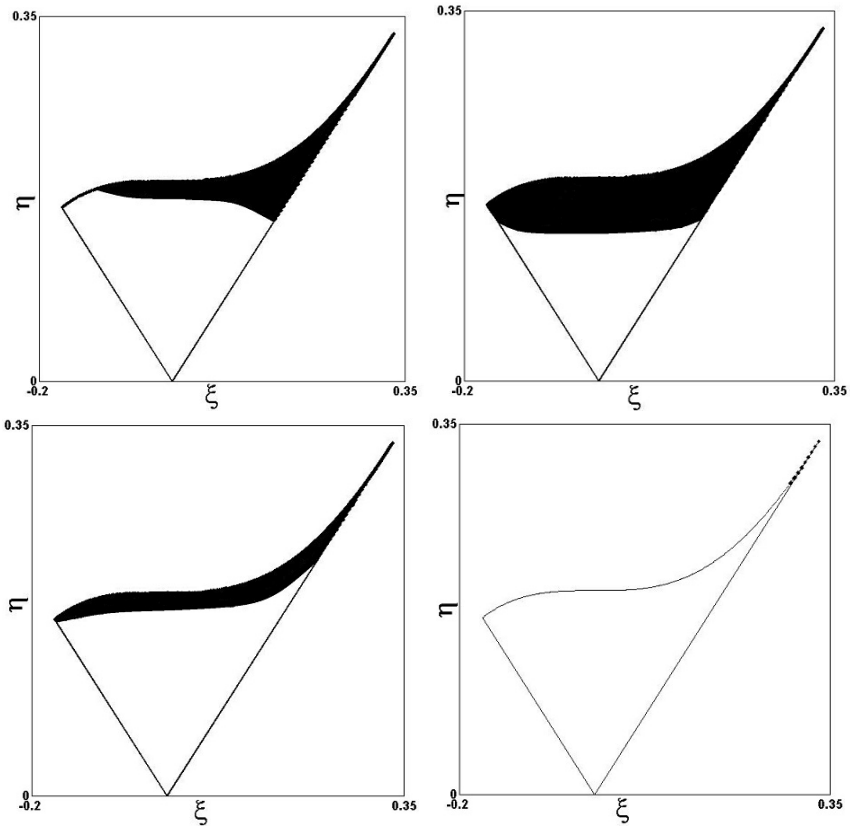

Figure 4.16: Process realizability adherence of the illustrative model for quadratic flows, β=0, 0.5, 0.75 and 1.

Based on these, this paradigm counsels a set of pragmatic compromises with respect to the scope of the characteristics of the turbulent statistics to be modeled and the form of the closure. Thence, this methodology is utilized to formulate an illustrative model. The predictions of this model are compared to numerical and experimental data while being contrasted against other popular modeling paradigms. We exhibit that the illustrative model is able to exhibit predictions that are at par with other closures for the regimes of flow wherein these established models perform adequately. Moreover, in regimes wherein established models do not exhibit satisfactory performance, the illustrative model is still able to provide predictions of engineering utility. Finally, as a *caveat emptor*, the zones of validity of this model are clearly delineated for different mean flows.

5. MANUFACTURED TURBULENCE WITH LANGEVIN EQUATIONS

5.1 Overview

By definition, *Manufactured turbulence*(MT) is purported to mimic physical turbulence rather than model it. The MT equations are constrained to be simple to solve and provide an inexpensive surrogate to Navier-Stokes based Direct Numerical Simulations (DNS) for use in engineering applications or theoretical analyses. In this article, we investigate one approach in which the linear inviscid aspects of MT are derived from a linear approximation of the Navier-Stokes equations while the non-linear and viscous physics are approximated via stochastic modeling. The ensuing Langevin MT equations are used to compute planar, quadratic turbulent flows. While much work needs to be done, the preliminary results appear promising.

5.2 Introduction

Turbulence is an enigmatic mix of *method* (large scale coherent structures) and *madness* (chaotic, small scale motions). While the coherent structures are evidently flow-dependent, the small-scale chaotic motions exhibit a rather surprising level of independence from the large scales (Kolmogorov hypotheses). Arguably, it is the large scale structures that are dynamically important and the role of the small scale motions is merely to provide a means for dissipating the cascaded energy. It is rather interesting that the dynamically decisive large scales are easier to compute and more difficult to model than the small scales which are more onerous to compute but play a more straightforward role. Any attempt at capturing turbulence physics must pay heed to these crucial matters.

Our charge in this work is to develop simple-to-solve equations that mimic physical turbulence, rather than model it. Here we reserve the term *model* to indicate

those attempts to develop closure equations for the moments of the turbulence field. To *mimic* is to yield spatio-temporal realizations of velocity and pressure fields and entire probability distribution functions. We call such a surrogate flow field, *Manufactured Turbulence*(MT). The MT flow-field is intended for use in engineering applications and theoretical analyses as an inexpensive substitute to the Direct Numerical Simulations (DNS) of the Navier-Stokes equations.

In the absence of an analytical theory of turbulence, the computational recourse to turbulence is extensively utilized in industrial and academic applications. Of these, computationally intensive methods like Direct Numerical Simulation and Large Eddy Simulation are limited in their application due to their excessive computational demands. On the other hand, modeling intensive approaches, such as one or two equation models, are encumbered due to their lack of fidelity in many varieties of flows. In this vein, synthetic or manufactured turbulence is a contrivance to generate signals that mimic real turbulent flow fields. Kinematic Simulation (KS) is predominantly used to this end.

An alternative that is popular in the turbulent combustion community is based on the Langevin equation in a Lagrangian framework. Such *Probability Density Function methods* have been extensively applied and have become established in turbulence research (Pope (1985*b*); Pope & Chen (1990)). This work is based, in essence, upon extensions of the simplistic analogy between the motion of fluid elements in a turbulent flow and the motion of gas molecules. Chung (Chung (1969)) used a similar analogy with the motion of fluid elements and Brownian motion, to develop a simplified statistical model for turbulence. Kuznetsov and Frost (Kuznetsov & Frost (1973)) applied a consonant similitude to use a Langevin equation for this purpose. This was extended by Pope and co workers (Haworth & Pope (1986)). In an analogy with the Langevin equation governing the velocity of a particle undergoing Brownian

motion, a linear Markov model for fluid particle velocity was developed in Haworth & Pope (1986). The effects of fluctuating pressure and viscosity are modeled via deterministic drift and diffusion terms. The diffusion term represents a random walk in velocity space. Haworth and Pope (Haworth & Pope (1986)) used the Navier Stokes equation as the starting point for the model formulation, thus adding physical significance to the terms of the Langevin equation and the concomitant coefficients therein. Furthermore, to account for the rapid component of pressure (and specifically, its dependence on mean gradients) an anisotropic drift term was added to the generic Langevin equation.

In this article, we apply a general set of Langevin equations to generate Manufactured Turbulence. It is accepted that linear physics provides a qualitative representation for many features of turbulent flows. However, the exactitude of this linear representation is contingent upon many factors. It is found that the quantitative preponderance of linear theory is highly dependent on the regime of flow. This is explained with respect to the nature of the instabilities manifested in these flows.

5.3 Mathematical formulation and rationale

The essential components of a turbulent flow field consist of:

1. Linear effects, consisting of inertial physics, embodied in production and *rapid* pressure action.

2. Non-linear effects, that include the *slow* pressure action.

3. Viscous effects.

Of these, the linear effects are the drivers of turbulence and engender the variations in different flows. Thus, it is essential to ensure that these are represented as precisely as possible. The non-linear effects are universal and can be modeled statistically.

Based on physics, pressure action can be decomposed into two components, viz. rapid and slow.

$$\frac{1}{\rho}\nabla^2 p' = -2\frac{\partial U_i}{x_j}\frac{\partial u_j}{x_i} - \frac{\partial^2}{\partial x_i \partial x_j}(u_i u_j - \overline{u_i u_j}), \tag{5.1}$$

where the first and second terms on the right, represent the contributions of rapid and slow pressure, respectively. The adjectives rapid and slow refer to the components of pressure arising, respectively, from the linear and non-linear parts of the source term in the Poisson equation for pressure. The slow component acts to conserve the incompressibility of the velocity field generated by the nonlinear interactions among velocity fluctuations. Similarly, it is the function of rapid pressure to impose the divergence free condition on the fluctuating velocity field produced by linear interactions between the mean and fluctuating fields.

Based on established theory, surrogates for the linear and the non-linear effects of pressure can be developed separately. Thence, these can be appended to give a complete, general surrogate for the pressure effects. In contrast to the slow pressure and its universal nature, the action of the rapid pressure effects are a strong function of the mean velocity field and initial flow conditions. In spite of the apparent simplification afforded by linearity, the action of rapid pressure is not straightforward. Depending on the nature of the mean velocity field and initial conditions of the flow field, the effect of the rapid pressure component can be diametric. Furthermore, this action can alter the fundamental nature of the flow. This is best exhibited in the regime of elliptic flows, where it is established that the rapid pressure effects initiate and sustain the elliptic flow instability (Cambon *et al.* (1994*a*)). Most engineering models do not capture the nature of this action and predict a decay of turbulence, contrary to theory and DNS results (Blaisdell & Shariff (1996)). Thus, the linear

pressure effects must be represented as accurately as possible. The import of fidelity to linear dynamics, even in KS has been accepted and attempts have been made to coalesce the knowledge developed via RDT in KS. Nicolleau and Vassilicos (Nicolleau & Vassilicos (2000)) utilized temporal evolution predicted by RDT with the KS velocity field formalism. This was applied and compared contra DNS in Cambon *et al.* (2004). Kaneda and Ishida (Kaneda & Ishida (2000)) used a similar approach to study the diffusion of a passive scalar. Subsequently, this approach of amalgamating RDT with KS has been extended, for instance in Nicolleau & Vassilicos (2008). Under the aegis of RDT, the velocity field can be expressed as a summation of advected Fourier modes. In this formulation, the rapid pressure effects can be represented exactly. To this end, the rapid pressure component of the Langevin set is formulated in spectral space. In spectral space, this formulation can account for the initial conditions accurately and is not hampered by an incomplete basis. The germane equations in this regard are:

$$\frac{d\kappa_l}{dt} = -\kappa_j \frac{\partial U_j}{\partial x_l}, \tag{5.2}$$

$$\frac{du_j}{dt} = -u_k \frac{\partial U_l}{\partial x_k}(\delta_{jl} - 2\frac{\kappa_j \kappa_l}{\kappa^2}), \tag{5.3}$$

and the incompressibility constraint is given by $\mathbf{u} \cdot \boldsymbol{\kappa} = 0$. Herein, $\vec{u}$ and $\vec{\kappa}$, or the Fourier velocity amplitude and wave-vector respectively, are considered random variables and are simulated via Monte Carlo techniques.

With regard to the slow component of pressure, it is established that this has a return to isotropy effect, wherein, the anisotropy of the Reynolds stress tensor is reduced. This, in essence, is a redistribution of the turbulent kinetic energy from any given distribution to an uniform, isotropic distribution. Thus, the slow pressure

effects are represented via a stochastic diffusion form. Explicitly,

$$A_{ij}(u,e)dW_j, \tag{5.4}$$

where A_{ij} is the diffusion tensor and dW is an isotropic Wiener process. Consequently, the representation reduces to

$$de_i = g_i(u,e) + A_{ij}(u,e)dW_j + B_{ij}(u,e)dW'_j. \tag{5.5}$$

$$du_i = h_i(u,e) + H_{ij}(u,e)dW_j + G_{ij}(u,e)dW'_j. \tag{5.6}$$

Constraints are applied to the system to ensure physical fidelity. These are:

1. Ensure that $\vec{e}$ remains a unit vector.
2. Maintain orthogonality of $\vec{u}$ and $\vec{e}$.
3. The PDF of the velocity approaches an isotropic, joint-normal distribution.
4. The evolution of the turbulent kinetic energy is exact in the limit of decaying turbulence.

These ensure realizability of the Reynolds stresses. For details of the derivation, the reader is referred to Slooten & Pope (1997). The velocity evolution equation is represented as a Langevin equation with an anisotropic drift term. Such surrogates can be thought of as bridging methods between one-point closures and multi-point/spectral closures.

The dissipation model is appended to the formulation to complete the basis. This is of the established form:

$$\frac{d\epsilon}{dt} = \frac{\epsilon^2}{k}(C_1\frac{P}{\epsilon} - C_2). \tag{5.7}$$

Consequently, the entire set of equations reduces to:

$$\begin{aligned} du_i = &- u_k\frac{\partial U_l}{\partial x_k}(\delta_{il} - 2e_ie_l)dt - \frac{1}{2}\frac{\epsilon}{k}(1 + \frac{3}{2}a_u)dt \\ &+ \frac{\gamma\epsilon}{k}(b_{ij} - II_b\delta_{ij})u_jdt - \sqrt{a_u\epsilon}dW_i. \end{aligned} \tag{5.8}$$

$$\begin{aligned} de_i = &- \frac{\partial U_m}{\partial x_l}e_m(\delta_{il} - e_ie_l)dt - \frac{1}{2}\frac{\epsilon}{k}(a_e + a_u\frac{k}{u_su_s})e_idt \\ &- \frac{\gamma\epsilon}{k}(\delta_{ij} - 2e_ie_j)b_{jl}e_l - \sqrt{a_u\epsilon}\frac{u_ie_l}{u_su_s}dW_l + \\ &\sqrt{\frac{a_e\epsilon}{k}}(\delta_{il} - e_ie_l - \frac{u_iu_l}{u_su_s})dW'_l. \end{aligned} \tag{5.9}$$

Figure 5.1 exhibits the representation's performance, wherein the predictions are compared against DNS results (Slooten & Pope (1997)).

5.4 Linear physics in planar, quadratic flows

Linear theories such as RDT ignore the interaction of turbulence with itself. This is justified via assumptions regarding the times scales (of mean and fluctuating distortions), a weak turbulence assumption, etc. However, the linear instabilities manifested in RDT obviate these assumptions. With increase in the turbulent kinetic energy, the non-linear effects become more important and thus, linear theory cannot suffice, beyond a very limited time period. In this duration, the linear effects structure the flow field. Thence, non-linear effects modify the evolution of turbulence. This structuring effect of the linear physics is most evident in the instabilities manifested therein, where certain modes are engendered to grow preferentially. Figure

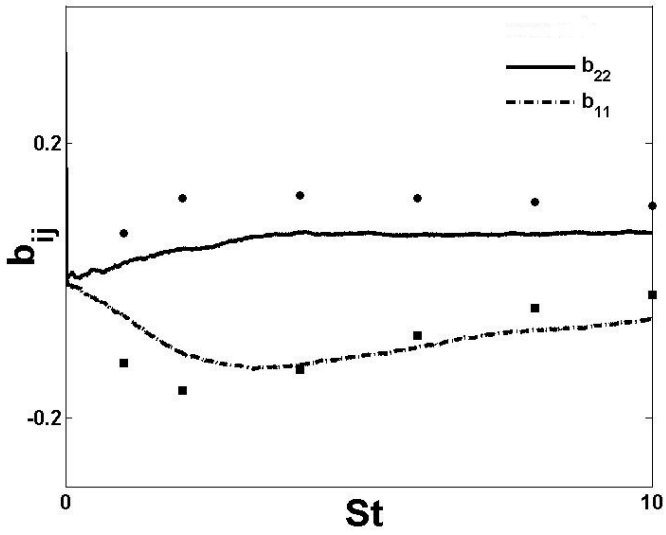

Figure 5.1: Comparison of the predictions against DNS results.

5.2 exhibits the unstable modes, in a representative hyperbolic and an elliptic flow, with respect to their alignment. The figure is motivated by a congruous illustration in Cambon *et al.* (1994*b*).

As can be observed, the unstable modes in an elliptic flow form a continuous band. However, the unstable modes in a hyperbolic flow lie on a set of zero measure. In the hyperbolic case, all other modes are either stable or can undergo some transient growth. Furthermore, this state of alignment for the unstable modes is in itself unstable and these can be forced off this alignment by any perturbations. This is evident in figure 5.3, wherein the hyperbolic flow instability is arrested by the pressure effects. This occurs via the transfer of turbulent kinetic energy out of the plane of applied shear via the pressure strain correlation. The interested reader is referred to Mishra & Girimaji (2010), wherein the linear aspects of this problem are analyzed in detail.

It is observed that this shift is robust and manifests itself for all open streamline

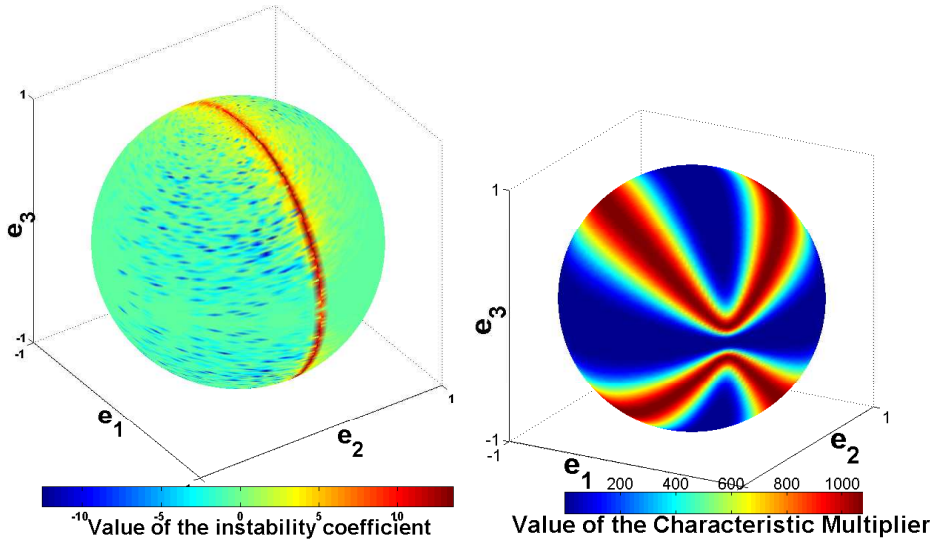

Figure 5.2: The unstable modes exhibited, with respect to their alignment in (a) a representative hyperbolic flow, (b) in an elliptic flow.

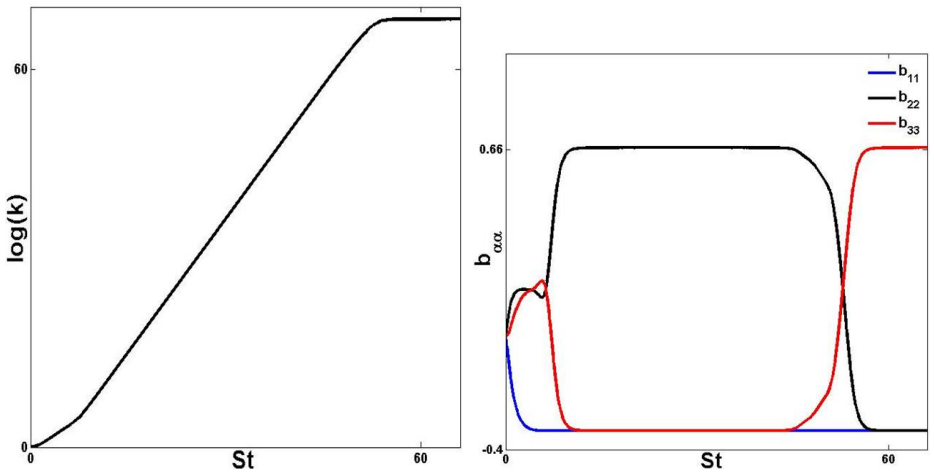

Figure 5.3: The evolution of (a) the turbulent kinetic energy, (b) Reynolds stress anisotropies in a plane strain flow, under the aegis of the Rapid Distortion Limit.

flows, as exhibited in figure 5.4. In this vein, it is pertinent to question the exactitude of the hyperbolic instability, caused by these modes, in regimes where the non-linear effects become more and more significant. Furthermore, this is contrasted against similar comparisons in other regimes of planar, quadratic flows.

The structuring effects of linear physics are most predominant in purely sheared flows. This is evident the large streamwise length scales observed in boundary layers. Furthermore, it has been observed that the evolution of flow statistics is similar in DNS studies, as compared to RDT simulations (Cambon (1999)). This is exhibited in figure 5.5, where the results of the Langevin equation representation are compared to those from RDT based simulations.

Figure 5.6 compares the evolution of flow statistics for elliptic flows in the presence and absence of non-linear effects. As can be observed, the results are very similar in the absence of non-linear effects or when they are of a small finite value. This is due to the finite measure of the set of unstable modes. However, this scenario does not persist for all elliptic flows. For instance, in purely rotating flows, it is known that linear theory is inconsistent with DNS results (Cambon (1999)).

Figure 5.7 compares the evolution of flow statistics in a representative hyperbolic flow as the non-linear effects become more important. It is observed that due to the non-linear effects, the switch in the anisotropy evolution occurs progressively earlier. This is due to the perturbation of the wave-vector due to the non-linear effects, which force modes off the unstable set.

5.5 Conclusions

In this article, we exhibit the application of *Manufactured Turbulence* (MT) to study the linear physics in a planar quadratic flow. The MT equations are exact in the Rapid Distortion Limit and use a Langevin equation to simulate the return to

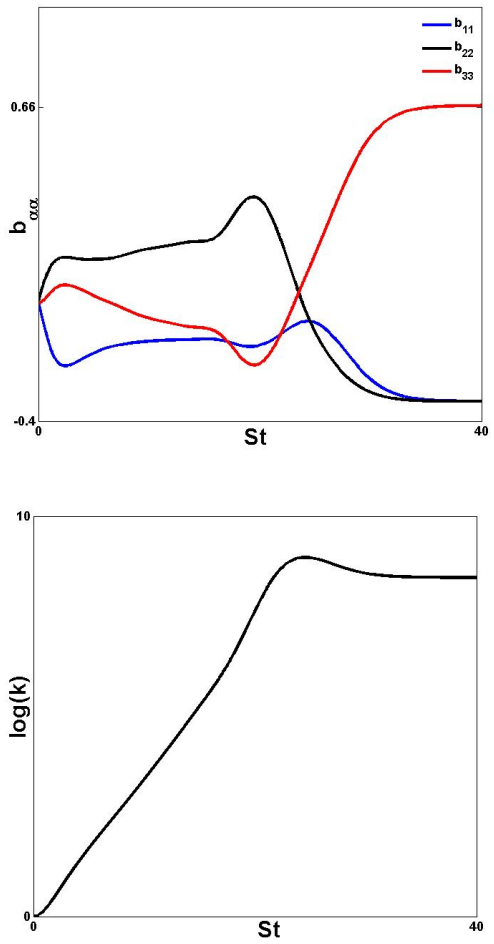

Figure 5.4: The evolution of (a) the turbulent kinetic energy, (b) Reynolds stress anisotropies in a representative open streamline flow, under the aegis of the Rapid Distortion Limit.

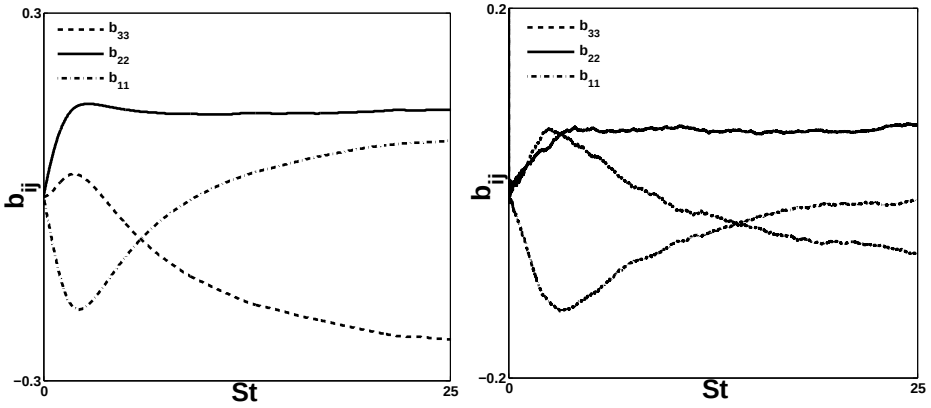

Figure 5.5: Comparison of the evolution of Reynolds stress anisotropies in a purely sheared flow (a) RDT results, (b) Langevin representation with $\frac{Sk}{\epsilon} = 25$.

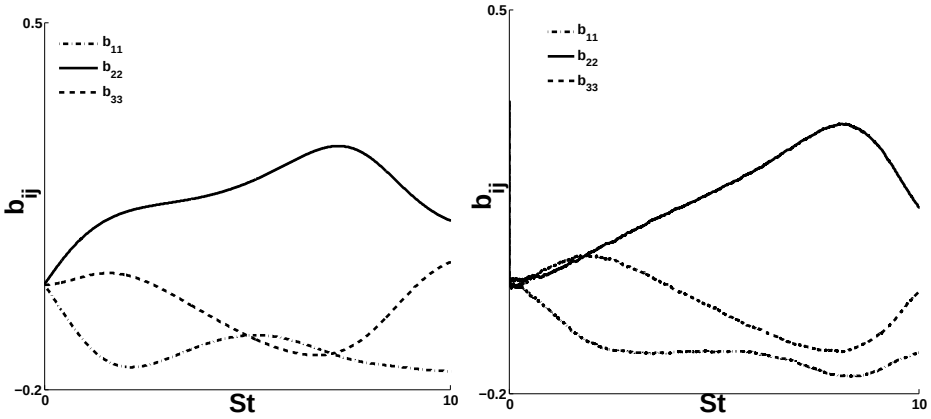

Figure 5.6: Comparison of the evolution of Reynolds stress anisotropies in a representative elliptic flow (a) RDT results, (b) Langevin representation with $\frac{Sk}{\epsilon} = 50$.

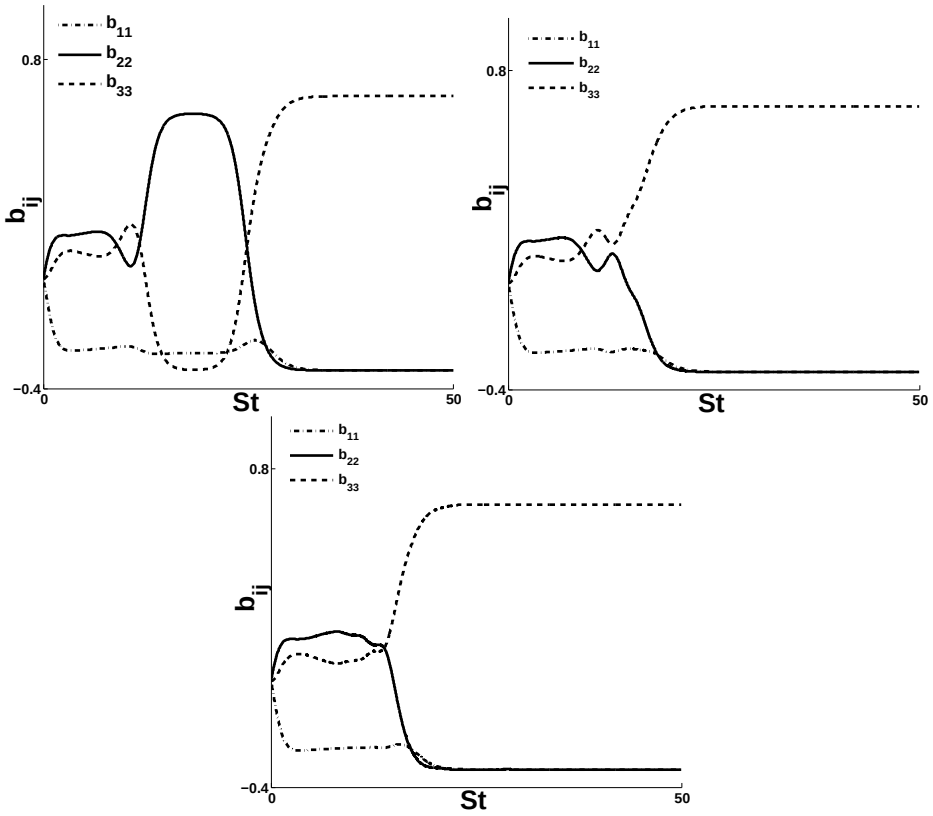

Figure 5.7: Comparison of the evolution of Reynolds stress anisotropies in a representative hyperbolic flow (a) RDT results, (b) Langevin representation with $\frac{Sk}{\epsilon} = 80$, (c) Langevin representation with $\frac{Sk}{\epsilon} = 60$.

isotropy effect of the slow pressure term. Thus, chaotic advection is incorporated using a white noise term. The mathematical formulation of such representations is introduced and the underlying rationale explained.

Thence, this surrogate is applied to study the import of linear physics for planar, quadratic flows. It is found that for purely sheared flows, linear theory provides a very good representation of the evolution of flow statistics, even in the presence of non-linear effects. For general elliptic flows, effects of linear physics are predominant even in the presence of moderate non-linearity. This is due to the banded nature of the instability, where unstable modes lie on a continuous band of finite measure. Thus, perturbations due to the non-linear effects have very little influence on the instability. However, for hyperbolic flows, the linearly unstable modes lie on a set of very small measure. Thus perturbations to these modal alignments may have significant effects on the state of instability and consequently, the evolution of flow statistics. However, only the transient time to reach the asymptotic stage is affected. But the final asymptotic behavior is still as dictated by linear phenomenon. It is observed that linear effects dominate the overall flow behavior, although non-linear aspects can have an important effect on transients.

6. ON THE STABILITY OF GENERAL THREE-DIMENSIONAL FLOWS

6.1 Overview

The stability of homogeneous flows is of considerable importance, vis-à-vis the hydrodynamic stability aspect, as well as for the development of turbulence theory. While the stability of planar flows has been extensively examined and explicated in literature, the case of general three-dimensional flows is not understood as well. This article seeks to address the stability of three-dimensional incompressible, inviscid flows. In addition to the linear stability analysis; we isolate, investigate and enucleate the role of the inertial processes and pressure in the evolution of the perturbation. Based on these analyses, the exact dependence of flow stability, the action of pressure and of inertia upon the flow topology, i.e. the mean flow invariants, is established and explicated.

6.2 Introduction

The stability of incompressible flows with uniform, planar velocity gradients has been extensively studied in literature. These include canonical cases such as the case of a flow under pure rotation, plane strain, pure shear, besides others. This body of flows represents benchmark cases for the purposes of turbulence theory and modeling. Furthermore, this investigation has been rewarding on a purely aesthetic level, revealing fascinating phenomena such as the elliptic flow instability for closed streamline flows.

Apropos the investigations into the stability of such flows, there have been two distinct paradigms that have been followed by different investigators. The geometric approach to hydrodynamic stability was introduced and developed by Arnold (Arnold, 1999). In this regard, Friedlander and co-workers have carried out stability

investigations based on the method of geometrical optics, supplemented by quasi-WKB asymptotics (Friedlander & Vishik, 1991, 1992; Friedlander *et al.*, 1993). This approach avoids the spectral problems associated with the equilibria of the Euler system. Instead, said approach focuses on a purely geometric parameter that provides the lower bound on the growth rate of the linearized Euler operator. Using this technique, Friedlander & Vishik (1991) have proved that all such flows with hyperbolic stagnation points are unstable. It is interesting to note that the system of equations circumscribing the growth rate of the Green's function evolution operator are exactly equivalent to the Kelvin-Moffat system, developed in the linearized analysis carried out under the aegis of the Rapid Distortion Theory. Regarding the investigations carried out under the RDT methodology, Cambon (1982) had discovered and analyzed the instability of elliptic flows. Since then, the stability of planar mean flows with uniform gradients has been extensively analyzed by Cambon and co-workers (Jacquin *et al.*, 1990; Cambon & Jacquin, 1989; Salhi *et al.*, 1997) and additionally, by Mishra & Girimaji (2013). In this regard, RDT based investigations conduct a quasi- stability analysis, in a distorting Fourier space. However, as observed in Cambon (1982), RDT pays heed to both the transients and the asymptotic states for the flow. At the boundary of these two approaches, we find investigations such as those of Craik & Criminale (1986), Waleffe (1990) and Bayly (1986). Herein isolated modes are analyzed for the case of an unbounded flow, which leads, naturally, to a linear analysis as there are no modal interactions.

From the discussion hereto, it is evident that prior investigation have focused on the dynamics of planar flows. However, the case of general three-dimensional flows is not understood as well. In spite of the fact that this classification includes important flows such as axisymmetric expansion and contraction, flows with swirl, etc.; the stability, dynamics and evolution of these flows have not been analyzed as

extensively as planar flows. The primary objective of this study is *to investigate the stability of such general three-dimensional flows*. Furthermore, we aim to *isolate and explicate the role of the inertial effects and that of pressure in the evolution* of the flow. In prior investigations, it has been established that for two-dimensional mean flows, the inertial effects, the action of pressure and the concomitant stability characteristics are clear functions of the invariants of the topology of the mean flow. We investigate if such a scenario persists for three-dimensional flows. Explicitly, we seek *to analyze the dependence of flow stability, the action of pressure and of inertia on the flow topology*, i.e. the mean flow invariants. Additionally, this article investigates if important phenomena from planar flows, such as parametric resonance, persist in three-dimensions.

6.3 Mathematical formulation

As the first step of the analysis, we seek to codify the different varieties of three-dimensional flows. Motivated by the need of a general methodology for categorizing flow topology, Chong *et al.* (1990) proposed a scheme based on the invariants of the velocity gradient tensor, A_{ij}. For an incompressible flow, the invariants are defined as

$$\begin{aligned} P &= S_{ii}(=0), Q = -\frac{1}{2}(S_{ij}S_{ji} + W_{ij}W_{ji}), \\ R &= -\frac{1}{3}(S_{ij}S_{jk}S_{ki} + 3W_{ij}W_{jk}S_{ki}). \end{aligned} \tag{6.1}$$

Here, W_{ij} and S_{ij} refer to the rate of rotation and rate of strain tensors of the background flow. Employing this scheme, the streamline topology of general three-dimensional mean flows can be inferred and categorized, as is exhibited in figure 6.1. The relevant cognomen are chosen to be in harmony with the behavior and precedent. Expansion and Contraction flows are topologically homeomorphic to their

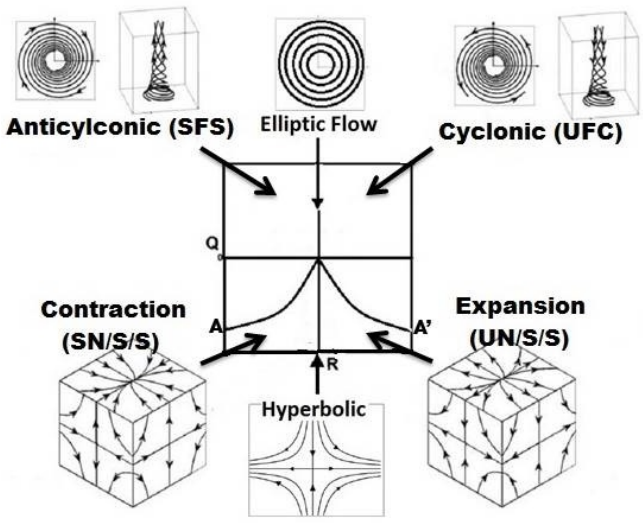

Figure 6.1: Schematic representation of the different regimes of flow and their locus with respect to the II^{nd} (Q) and III^{rd} (R) invariants.

axisymmetric counterparts. The Cyclonic and the Anticyclonic flows are named thus to reflect the directionality of rotation manifested therein and the established nomenclature in Meteorology (Tannehill, 1934).

The Kelvin-Moffat system in Fourier space is given by:

$$\begin{aligned} \frac{du_j}{dt} &= -u_k A_{lk}(\delta_{jl} - 2e_j e_l), \\ \frac{de_l}{dt} &= -e_m A_{mi}(\delta_{il} - e_i e_l). \end{aligned} \tag{6.2}$$

This is subject to the orthogonality condition, $u_i e_i = 0$. Herein, $\vec{u}$ and $\vec{e}$ represent the Fourier amplitude and the unit wavenumber vectors. For a derivation and detailed discussion of the Kelvin-Moffat system, the interested reader is referred to Sagaut & Cambon (2008). In the co-ordinate system utilized, the requisite mean flow tensors

for Strain and Rotation dominated flows are given by:

$$A_{ij}^{Strain} = \begin{bmatrix} \lambda_1 & 0 & 0 \\ 0 & \lambda_2 & 0 \\ 0 & 0 & \lambda_3 \end{bmatrix}, A_{ij}^{Rotation} = \begin{bmatrix} \sigma & \omega & 0 \\ -\omega & \sigma & 0 \\ 0 & 0 & \lambda \end{bmatrix}. \tag{6.3}$$

To isolate and analyze the role of the different mechanisms in the evolution of the flow, we utilize the technique of Burgulence (Sagaut & Cambon, 2008). Herein, the evolution of the "pressure-released" Burgers system is contrasted against the Euler system to isolate the individual mechanisms. This has been applied in similar problems with success by Salhi *et al.* (1997) and Mishra & Girimaji (2013). Hereon, the analysis considers the dynamics of the aforementioned flow categories, individually and sequentially.

6.4 Stability analysis

Expansion Flows: For the expansion flows, the inertial effects engender a state of exponential instability with the energy resident in the u_3 component. The 1 and the 2-axes have a negative production of perturbation energy while the 3-axis has a positive production. However, for this variety of Strain dominated flows, the phase space of the unit wavenumber vector has two attractors located at the 3-axis. Thus, all modes in the flow are attracted to the 3-axis and assume a state of alignment perpendicular to the 1-2 plane, as is observed in figure 6.2. Consequently, the inertial effects produce energy for the u_3 component and the modes are aligning with the 3-axis, thus, $e_3 \to 1$. This represents a stretching of the hypothetical fluid particle along the 3-axis that would cause the velocity gradients along this direction to be unbounded. This would be in violation of continuity. In this scenario, the pressure effects transfer perturbation kinetic energy from the u_3 component to the u_1 and

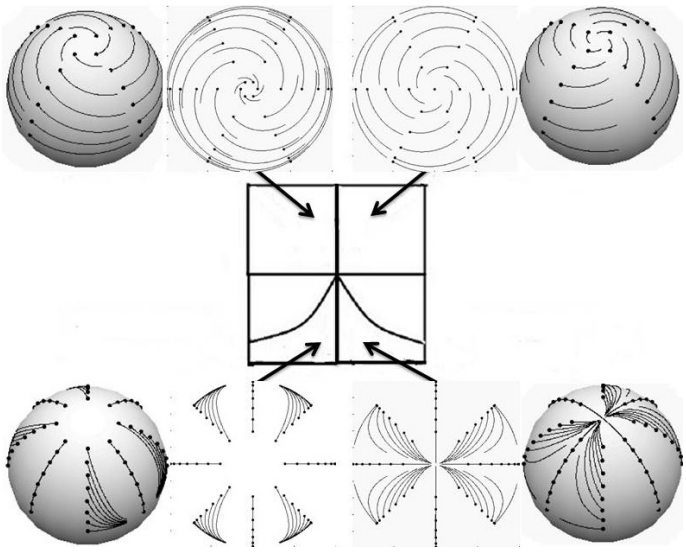

Figure 6.2: Representation of the dynamics of the unit wavenumber vector with respect to the II^{nd} (Q) and III^{rd} (R) invariants. The dark circles mark the initial alignment of the mode.

u_2 components. This energy redistribution arrests the positive production along the 3-axis. The transferred energy is consumed by negative production along the 1 and the 2-axes. This leads to the perturbation kinetic evolution observed for the Euler system, where the pressure effects lead to a state of asymptotic stability, as can be observed in figure 6.3.

Cyclonic Flows: For the Rotation dominated case of Cyclonic flows, the inertial effects lead to a state of exponential instability. Similar to the case of expansion flows, the 1 and 2-axes have a negative production of perturbation energy while the 3-axis has a positive production. Thus, perturbation kinetic energy is resident in the u_3 component. Considering the phase space of the unit wavenumber vector, we see that the shift from a Strain dominated to a Rotation dominated system has lead to a bifurcation in the invariant sets. The attracting fixed points at the poles are no longer extant and have been replaced by a pair of limit cycles. The limit cycle along

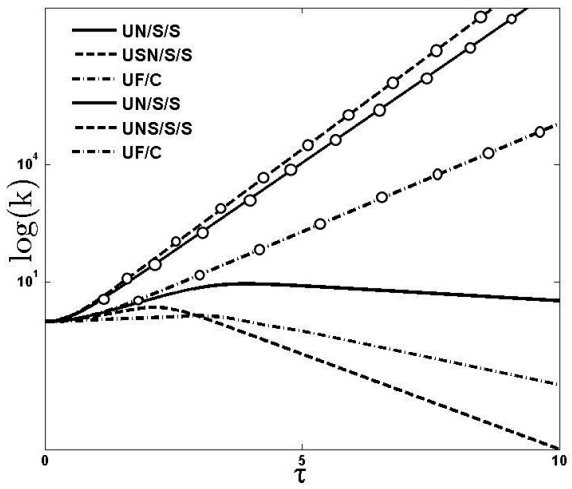

Figure 6.3: Comparison of the perturbation kinetic energy evolution for the Burgers and the Euler systems, for flows where $R > 0$. The trajectories for the burgers system are marked by circles.

the 3-axis is attracting while the limit cycle in the 1-2 plane is repelling. Thus, all the modal alignments are attracted to the $e_3 = 1$ point, along helical trajectories, as is observed in figure 6.2. In this scenario, the inertial effects produce energy for the u_3 component and the modes are aligning with the 3-axis, thus, $e_3 \to 1$. Clearly, this represents a state where the perturbation velocity gradients along the 3-axis are increasing to very high levels, in violation of continuity. The pressure effects transfer perturbation kinetic energy from the u_3 component to the u_1 and u_2 components. This energy redistribution arrests the positive production along the 3-axis. The transferred energy is consumed by negative production along the 1 and the 2-axes. This leads to the perturbation kinetic evolution observed for the Euler system, where the pressure effects lead to a state of asymptotic stability, as exhibited in figure 6.3.

Anticyclonic Flows: For the Rotation dominated case of Anticyclonic flows, the inertial effects engender a state of exponential instability with the perturbation kinetic energy resident in the u_1 and u_2 components. Considering the invariant sets

in the phase space of the unit wavenumber vector, the limit cycle in the 1-2 plane is attracting while the point cycle along the 3-axis is repelling. Thus, all the modal alignments are attracted to the limit cycle in the 1-2 plane, along helical trajectories, as observed in figure 6.2. In this state, the perturbation kinetic energy is resident in the fluctuations along the 1-2 plane *and* the unit wavenumber vectors are also being attracted to this plane. Thus, to maintain continuity pressure transfers energy from the fluctuations in the 1-2 plane to the fluctuations along the 3-axis. This transfer is brief and occurs during the migration of the unit wavenumber trajectories to the limit cycle. In Fourier space, the continuity condition is mathematically expressed in the orthogonality of the Fourier amplitude vector and the unit wavenumber vector, explicitly $u_i e_i = 0$. Once the unit wavenumber vector is close to the 1-2 plane, transfer of energy to the fluctuations along the 3-axis is inadequate as the e_3 component for these states is negligible. Thence, to maintain continuity, pressure has to redistribute perturbation kinetic amongst the u_1 and the u_2 components. If the pressure effects are able to completely drain the perturbation kinetic energy from the fluctuations in the 1-2 plane before this state is reached, the mode is stable. Else, the residual perturbations in the 1-2 plane start to grow due to inertial effects and the modal kinetic energy starts to grow. Thus, the instability engendered by the inertial effects is not completely offset by the effects of pressure for *all the modes*. As can be seen in figure 6.4, pressure has a mildly stabilizing effect on the evolution of the perturbation kinetic energy. This effect is manifested during the initial few time steps, while the modal alignments are evolving rapidly. However, after this transient, the inertial effects dominate and flow is still exponentially unstable.

Contraction Flows: For the Strain dominated case of contracting flows, the inertial effects lead to a state of exponential instability with the perturbation kinetic energy resident in the fluctuation along the 1-2 plane. Considering the dynamics in

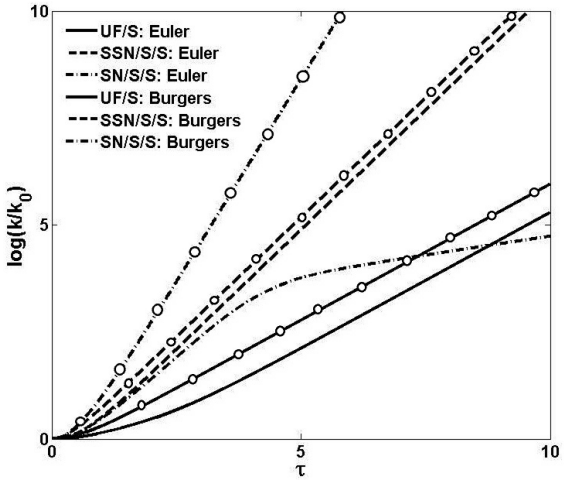

Figure 6.4: Comparison of the perturbation kinetic energy evolution for the Burgers and the Euler systems, for flows where $R < 0$.

the phase space of the unit wavenumber vector, the state of modal alignment perpendicular to the 1-2 plane is repelling (in direct contrast to the case of Expansion flows). All modal alignments evolve to attracting stationary states in the 1-2 plane, exhibited in figure 6.2. In this scenario, the perturbation kinetic energy is resident in the fluctuations along the 1-2 plane and the modal alignments are also being attracted to this plane. Thus, to maintain continuity pressure transfers energy from the fluctuations in the 1-2 plane to the fluctuations along the 3-axis. This transfer is brief and occurs during the migration of the unit wavenumber trajectories to the limit cycle. Due to the transient nature of this energy redistribution, all modes are not stabilized by pressure effects. Pressure has a mild stabilizing effect during this transient stage. After this transient, the inertial effects dominate and flow is unstable, as seen in figure 6.4.

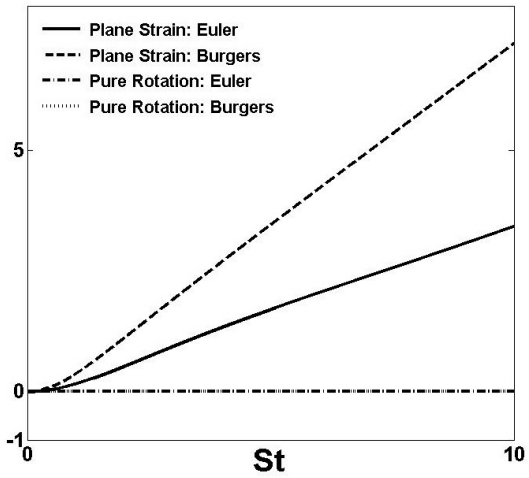

Figure 6.5: Comparison of the perturbation kinetic energy evolution for the Burgers and the Euler systems, for flows where $R = 0$.

6.5 Conclusions

In conclusion, general incompressible, inviscid flows can be classified into two categories based on the dynamics exhibited therein, viz., flows where the flow topology has a positive value of the third invariant ($R > 0$) and flows where $R < 0$. *For either category, the inertial effects are destabilizing* and lead to a state of exponential instability. Furthermore, for *both the classes of flows, pressure has a stabilizing effect.* For flow topologies with $R > 0$*, pressure effects are able to dominate* and lead to flow stability. For flows with $R < 0$*, the inertial effects dominate* and the flow remains unstable.

The cases of planar flows (with $R = 0$) forms the bifurcation boundary in parameter space, separating these behaviors. The dynamics and behavior observed in hyperbolic flows present a natural transition between the dynamics of Expansion and Contraction flows, as observed in figure 6.5. However, the case of elliptic flows has very peculiar dynamics. Unlike all other flows, in elliptic flows the inertial effects

engender a state of neutral stability. Moreover, unlike all other flows, the pressure effects actually initiate and sustain the flow instability herein. Additionally, characteristic phenomena like that of parametric resonance underlying the elliptic flow instability, are found to be completely absent in other Rotation dominated flows. In this vein, the case of elliptic flows represents a singular limit.

7. CONCLUSIONS

As an engineering recourse, one-point closure models are still the workhorse in industrial applications. These have limitations, such as their inaccuracy for flows with large coherent structures. However, with the level of detailed information that these single-point closures provide, at the reasonable computational expense, these are favored over other approaches like LES or DNS. In the context of single point closures, viscosity based models are very simple but have low fidelity and robustness for most flows. Thus, the Second Moment closure paradigm offers the best option. These have under-performed thus far due to the inherent empiricism in the modeling paradigm. In this vein, a better modeling methodology is required. In this investigation, we attempt to develop this, by addressing the key issues of linear stability and realizability. As the non-local action of pressure represents the key hurdle in this modeling framework, we focus on the pressure-strain correlation model. We perform an extensive linear stability analysis based on Rapid Distortion Theory to gauge the Intercomponent Energy Transfer induced by pressure. This is analyzed and explained based on a model analysis. Thence, the statistically most likely behavior is identified, as a guide to model development. We examine the validity and limitations of the one point closure paradigm. This leads to a set of studied compromises in the scope and form of single point closure models. Thence, we discuss the realizability constraints on models. It is exhibited that classical realizability considers only the state of the stochastic process and not the stochastic process itself. Thus, these are insufficient. We develop a set of process realizability constraints to ensure that the Reynolds stress dynamics predicted by models are physically permissible. These are applied to established models and it is shown that even models with adherence to

classical realizability and lead to unphysical Reynolds stress dynamics in the system. Thence, a methodology to ensure optimal process realizability adherence is outlined. Based on the linear stability analysis and the process realizability constraints, we develop a novel modeling methodology. This is applied to develop an illustrative pressure strain correlation model. The predictions of this model are compared to numerical and experimental data while being contrasted against other popular modeling paradigms. It is exhibited that the simple, illustrative model is able to predict the dynamics of the system better than established models. Finally, the zones of applicability of this model are clearly delineated for different mean flows.

The robustness of the linear physics was then checked using stochastic models based on the Langevin equation. These exhibit clearly that the qualitative nature of the dynamics engendered by linear physics are robust under mild non-linear effects.

Having developed a modeling paradigm for planar quadratic flows, we investigate the linear stability of general three-dimensional flows. It is found that the dynamics and the stability of the wave mode are highly dependent on the alignment of the mode, with respect to the strain field, to a degree significantly greater than for planar flow. This suggests that replicating the behavior of general three-dimensional homogeneous flows with single point closures may be prohibitively demanding.

REFERENCES

Arnold, V.I. 1999 *Topological Methods in Hydrodynamics*. Springer (New York).

Bayly, B. J. 1986 Three-dimensional instability of elliptical flow. *Phys. Rev. Lett.* **57** (17), 2160–2163.

Blaisdell, G.A. & Shariff, K. 1994 Homogeneous turbulence subjected to mean flow with elliptic streamlines. *Studying Turbulence Using Numerical Simulation Databases: Proceedings of the 1994 Summer Program* pp. 355–371.

Blaisdell, G.A. & Shariff, K. 1996 Simulation and modeling of the elliptic streamline flow. *Studying Turbulence Using Numerical Simulation Databases: Proceedings of the 1996 Summer Program* pp. 433–446.

Brasseur, J.G. & Lee, M.J. 1987 Local structure of intercomponent energy transfer in homogeneous turbulent shear flow. *Center of Turbulence Research Proceedings of the Summer Program* pp. 165–178.

Brasseur, J.G. & Lee, M.J. 1988 Pressure-strain-rate events in homogeneous turbulent shear flow. *Center of Turbulence Research Proceedings of the Summer Program* pp. 143–156.

Cambon, C. 1982 Étude spectrale d'un champ turbulent incompressible, soumis à des effets couplés de déformation et de rotation, imposés extérieurement. Thèse de Doctorat d'État, Université de Lyon, France.

Cambon, C. 1990 Single and double point modeling of homogeneous turbulence. *NASA Annual Research Briefs (1990)* pp. 135–203.

Cambon, C. 1999 Linear and non-linear models of anisotropic turbulence. *Annual Rev. Fluid Mech.* **31**, 1–53.

Cambon, C., Benoit, J.P., Shao, L. & Jacquin, L. 1994*a* Stability analysis

and large-eddy simulation of rotating turbulence with organized eddies. *Journal of Fluid Mechanics* **278**, 175–200.

Cambon, C., Benoit, J.P., Shao, L. & Jacquin, L. 1994*b* Stability analysis and Large-Eddy Simulation of rotating turbulence with organized eddies: Part ii. *Journal of Fluid Mechanics* **279**, 187–213.

Cambon, C., Godefred, F. S., Nicolleau, F. & Vassilicos, J. C. 2004 Turbulent diffusion in rapidly rotating fows with and without stable stratification. *Journal of Fluid Mechanics* **499**, 231–255.

Cambon, C. & Jacquin, L. 1989 Spectral approach to non-isotropic turbulence subjected to rotation. *Journal of Fluid Mechanics* **202**, 295–317.

Cambon, C., Jacquin, L. & Lubrano, J.L. 1992 Toward a new Reynolds stress model for rotating turbulent flows. *Physics of Fluids* **4**, 812–824.

Cambon, C. & Rubinstein, R. 2006 Anisotropic developments for homogeneous shear flows. *Physics of Fluids* **18**, 1–11.

Cambon, Claude & Scott, Julian F. 1999 Linear and nonlinear models of anisotropic turbulence. *Annual Review of Fluid Mechanics* **31** (1), 1–53.

Chong, M.S., Perry, A.E. & Cantwell, B.J. 1990 A general classification of three-dimensional flow fields. *Physics of Fluids* **2**, 408–420.

Chung, P.M. 1969 A simplified statistical model of turbulent, chemically reacting shear flows . *AIAA Journal* **7**, 91–121.

Craik, A. D. D. & Criminale, W. O. 1986 Evolution of wavelike disturbances in shear flows: a class of exact solutions of the navier-stokes equations. *Proceedings of the Royal Society of London. A* **406**, 13–26.

Crow, S.C. 1968 Viscoelastic properties of fine-grained incompressible turbulence. *Journal of Fluid Mechanics* **33**, 1–20.

Friedlander, S., Gilbert, A. D. & Vishik, M.M. 1993 Hydrodynamic insta-

bility for certain abc flows. *Geophysical And Astrophysical Fluid Dynamics* **73**, 97–107.

Friedlander, S. & Vishik, M.M. 1991 Instability criteria for the flow of an inviscid incompressible fluid. *Phys. Rev. Lett.* **66** (17), 2204–2206.

Friedlander, S. & Vishik, M.M. 1992 Instability criteria for steady flows of a perfect fluid. *Chaos* **2** (3), 455–460.

Germano, M. 1992 Turbulence: the filtering approach. *Journal of Fluid Mechanics* **238**, 325–336.

Girimaji, S.S. 2000 Pressure strain correlation modelling of complex turbulent flows. *Journal of Fluid Mechanics* **422**, 91–123.

Girimaji, S.S. 2004 A new perspective on realizability of turbulence models. *Journal of Fluid Mechanics* **512**, 191–210.

Girimaji, S.S., Jeong, E. & Poroseva, S.V. 2003 Pressure -strain correlation in homogeneous anisotropic turbulence subject to rapid strain-dominated distortion. *Phys. Fluids* **15**, 3209–3222.

Godeferd, F.S., Cambon, C. & Scott, J.F. 2001 Two-point closures and their applications: report on a workshop. *Journal of Fluid Mechanics* **436**, 393–407.

Hanjalic, K. & Launder, B. 2011 *Modelling Turbulence in Engineering and the Environment: Second-Moment Routes to Closure*. Cambridge University Press (New York).

Haworth, D.C. & Pope, S. B. 1986 A generalized Langevin model for turbulent flows. *Phys Fluids* **29**, 387–405.

Jacquin, L., Leuchter, O., Cambon, C. & Mathieu, J. 1990 Homogeneous turbulence in the presence of rotation. *Journal of Fluid Mechanics* **220**, 1–52.

Jakirlic, S. & Hanjalic., K. 2013 A direct numerical simulation based re-examination of coefficients in the pressure strain models in second-moment clo-

sures. *Fluid Dynamics Research* **45**, 126–159.

Johansson, A.V. & Hallback, M. 1994 Modeling the rapid pressure-strain in Reynolds stress closures. *Journal of Fluid Mechanics* **269**, 143–168.

Kaneda, Y. & Ishida, T. 2000 Supression of vertical diffusion in strongly stratified turbulence. *Journal of Fluid Mechanics* **402**, 311–327.

Kassinos, S.C. & Reynolds, W.C. 1994 *A Structure-Based Model for the Rapid Distortion of Homogeneous Turbulence*. Thermosciences Division, Department of Mechanical Engineering, Stanford University, Report TF 61.

Kassinos, S.C., Reynolds, W.C. & Rogers, M.M. 2001 One point turbulence structure tensors. *Journal of Fluid Mechanics* **428**, 213–248.

Kraichnan, R.H. 1959 The structure of turbulence at very high Reynolds numbers. *Journal of Fluid Mechanics* **5**, 497–543.

Kraichnan, R.H. 1971 An almost-Markovian Galilean-invariant turbulence model. *Journal of Fluid Mechanics* **47**, 513–524.

Kuznetsov, V.R. & Frost, V.A. 1973 Probability distribution of the concentration and intermittency in turbulent jets. *Akademiia Nauk SSSR, Izvestiia, Mekhanika Zhidkosti i Gaza* pp. 388–421.

Launder, B.E., Reece, G.J. & Rodi, W. 1975 Progress in the development of a Reynolds-stress turbulence closure. *Journal of Fluid Mechanics* **68** (03), 537–566.

Lee, M.J. 1990 Distortion of homogeneous turbulence by axisymmetric strain and dilation. *Physics of Fluids A* **2**, 630–633.

Lumley, J. L. 1978 Computational modeling of turbulent flows. *Advances in Applied Mechanics* **18**, 123–176.

Malkus, W. 1989 An experimental study of global instabilities due to the tidal (elliptical) distortion of a rotating elastic cylinder. *Geophysical and Astrophysical Fluid Dynamics* **48**, 123–134.

Meyer, C.D. 2001 *Matrix Analysis and Applied Linear Algebra*. Society for Industrial and Applied Mathematics (Philadelphia).

Mishra, A.A. & Girimaji, S.S. 2010 Pressure strain correlation modeling: Towards achieving consistency with Rapid Distortion Theory. *Flow, Turbulence and Combustion* **85**, 593–619.

Mishra, A.A. & Girimaji, S.S. 2013 Intercomponent energy transfer in incompressible homogeneous turbulence: multi-point physics and amenability to one-point closures. *Journal of Fluid Mechanics* **731**, 639–681.

Mishra, A.A. & Girimaji, S.S. 2014 On the realizability of pressure-strain closures. *Journal of Fluid Mechanics (under review)* .

Moffatt, H.K. 1967 The interaction of turbulence with a strong wind shear. *URSI-IUGG International Colloquim on Atmospheric turbulence and radio wave propagation* pp. 139–156.

Nicolleau, F. & Vassilicos, J. C. 2000 Turbulent diffusion in stably stratified non-decaying turbulence. *Journal of Fluid Mechanics* **410**, 123–146.

Nicolleau, F.and Yu, G. & Vassilicos, J. C. 2008 Kinematic simulation for stably stratified and rotating turbulence. *Fluid Dynamics Research* **40**, 68–93.

Orszag, S.A. 1970 Analytical theories of turbulence. *Journal of Fluid Mechanics* **41**, 363–386.

Perot, B. & Moin, P. 1995 Shear-free turbulent boundary layers. part 1. Physical insights into near-wall turbulence. *Journal of Fluid Mechanics* **295**, 199–228.

Pierrehumbert, R.T. 1986 Universal short-wave instability of two-dimensional eddies in an inviscid fluid. *Phys. Rev. Lett.* **57** (17), 2157–2159.

Pope, S.B. 1985*a* PDF methods for turbulent reactive flows. *Progress in Energy and Comustion Science* **11**, 119–192.

Pope, S.B. 2000 *Turbulent flows*. Cambridge University Press (New York).

Pope, S.B. 2011 Simple models of turbulent flows. *Physics of Fluids* **23** (1), 11–30.

Pope, S. B. 1985*b* Pdf methods for turbulent reactive flows. *Prog. Energy Com. Sci.* **11**, 38–79.

Pope, S. B. & Chen, Y. L. 1990 The velocity-dissipation probability density function model for turbulent flows. *Phys. Fluids A* **2**, 163–180.

Reynolds, W.C. 1976 Computation of turbulent flows. *Annual Review of Fluid Mechanics* **8**, 183–208.

Ristorcelli, J.R., Lumley, J.L. & Abid, R. 1995 A rapid pressure covariance representation consistent with the Taylor-Proudman theorem materially frame indifferent in the two-dimensional limit. *Journal of Fluid Mechanics* **292**, 111–152.

Rogers, M.M. 1991 The structure of a passive scalar field with a uniform mean gradient in rapidly sheared homogeneous turbulent-flow,. *Physics of Fluids A* **3**, 144–154.

Rotta, J. 1951 Statistische theorie nichthomogener turbulenz. *Zeitschrift fur Physik* **129**, 547–572.

Rubinstein, R. & Girimaji, S.S. 2006 Second moment closure near the two-component limit. *Journal of Fluid Mechanics* **548**, 197–223.

Sagaut, P. & Cambon, C. 2008 *Homogeneous Turbulence Dynamics*. Cambridge University Press (New York).

Salhi, A., Cambon, C. & Speziale, C.G. 1997 Linear stability analysis of plane quadratic flows in a rotating frame with applications to modeling. *Physics of Fluids* **9** (8), 2300–2309.

Sambasivam, A., Girimaji, S.S. & Poroseva, S.V. 2004 Realizability of the Reynolds stress and rapid pressure strain correlation in turbulence modelling. *Journal of Turbulence* **5**, 126–173.

Schumann, U. 1977 Realizability of Reynolds stress turbulence models. *Journal of*

Fluid Mechanics **20**, 721–725.

Shih, T.H., Mansour, N.N. & Chen, J.Y. 1987 Reynolds stress models of homogeneous turbulence. *Proceedings of the 1987 Summer Program, Center for Turbulence Research, Stanford University* pp. 153–179.

Shih, T.H., Reynolds, W.C & Mansour, N.N. 1990 A spectrum model for weakly anisotropic turbulence. *Physics of Fluids A* **2**, 1500–1502.

Sjogren, T. & Johansson, A.V. 2000 Development and calibration of algebraic nonlinear models for terms in the Reynolds stress transport equations. *Physics of Fluids* **12** (6), 1554–1572.

Slooten, P.R. Van & Pope, S.B. 1997 PDF modeling for inhomogeneous turbulence with exact representation of rapid distortions . *Phy Fluids* **9**, 1085–1105.

Speziale, C.G., Abid, R. & Blaisdell, G.A. 1996 On the consistency of Reynolds stress turbulence closures with hydrodynamic stability theory. *Physics of Fluids* **8** (3), 781–788.

Speziale, C.G., Abid, R. & P.A., Durbin 1994 On the realizability of Reynolds stress turbulence closures. *Journal of Scientific Computing* **9**, 369–403.

Speziale, C.G. & Durbin, P.A. 1994 Realizability of second-moment closure via stochastic analysis. *Journal of Fluid Mechanics* **280**, 395–407.

Speziale, C.G., Gatski, T.B. & Mhuiris, N.M.G. 1990 A critical comparison of turbulence models for homogeneous shear flows in a rotating frame. *Physics of Fluids* **2** (9), 1678–1684.

Speziale, C.G., Sarkar, S. & Gatski, T.B. 1991 Modelling the pressure strain correlation of turbulence: an invariant dynamical systems approach. *Journal of Fluid Mechanics* **227**, 245–272.

Tannehill, I.R. 1934 *Publication No. 197: The Hurricane*. US Department of Agriculture.

Tsinober, A. 2009 *An Informal Conceptual Introduction to Turbulence*. Springer (New York).

Waleffe, F. 1990 On the three-dimensional instability of strained vortices. *Physics of Fluids A: Fluid Dynamics* **2** (1), 76–80.